2009-03-16

Behavior of a Full-Scale Pile Cap with Loosely and Densely Compacted Clean Sand Backfill under Cyclic and Dynamic Loadings

Colin Reuben Cummins
Brigham Young University - Provo

BEHAVIOR OF A FULL-SCALE PILE CAP WITH LOOSELY AND DENSELY COMPACTED CLEAN SAND BACKFILL UNDER CYCLIC AND DYNAMIC LOADINGS

by

Colin R. Cummins

A thesis submitted to the faculty of

Brigham Young University

in partial fulfillment of the requirements for the degree of

Master of Science

Department of Civil and Environmental Engineering

Brigham Young University

April 2009

BRIGHAM YOUNG UNIVERSITY

GRADUATE COMMITTEE APPROVAL

of a thesis submitted by

Colin R. Cummins

This thesis has been read by each member of the following graduate committee and by majority vote has been found to be satisfactory.

Date	Travis M. Gerber, Chair
Date	Kyle M. Rollins
Date	Norman L. Jones

BRIGHAM YOUNG UNIVERSITY

As chair of the candidate's graduate committee, I have read the thesis of Colin R. Cummins in its final form and have found that (1) its format, citations, and bibliographical style are consistent and acceptable and fulfill university and department style requirements; (2) its illustrative materials including figures, tables, and charts are in place; and (3) the final manuscript is satisfactory to the graduate committee and is ready for submission to the university library.

Date

Travis M. Gerber
Chair, Graduate Committee

Accepted for the Department

E. James Nelson
Graduate Coordinator

Accepted for the College

Alan R. Parkinson
Dean, Ira A. Fulton College of Engineering and Technology

ABSTRACT

BEHAVIOR OF A FULL-SCALE PILE CAP WITH LOOSELY AND DENSELY COMPACTED CLEAN SAND BACKFILL UNDER CYCLIC AND DYNAMIC LOADINGS

Colin R. Cummins

Department of Civil and Environmental Engineering

Master of Science

A series of lateral load tests were performed on a full-scale pile cap with three different backfill conditions, namely: with no backfill present, with densely compacted clean sand in place, and with loosely compacted clean sand in place. In addition to being displaced under a static loading, the pile cap was subjected to low frequency, small displacement loading cycles from load actuators and higher frequency, small displacement, dynamic loading cycles from an eccentric mass shaker.

The passive earth pressure from the backfill was found to significantly increase the load capacity of the pile cap. At a displacement of about 46 mm, the loosely and densely compacted backfills increased the total resistance of the pile cap otherwise without backfill by 50% and 245%, respectively.

The maximum passive earth pressure for the densely compacted backfill occurred at a displacement of approximately 50 mm, which corresponds to a displacement to pile cap height ratio of 0.03. Contrastingly passive earth pressure for the loosely compacted backfill occurred at a displacement of approximately 40 mm.

Under low and high frequency cyclic loadings, the stiffness of the pile cap system increased with the presence of the backfill material. The loosely compacted backfill generally provided double the stiffness of the no backfill case. The densely compacted backfill generally provided double the stiffness of the loosely compacted sand, thus quadrupling the stiffness of the pile cap relative to the case with no backfill present.

Under low frequency cyclic loadings, the damping ratio of the pile cap system decreased with cap displacement and with increasing stiffness of backfill material. After about 20 mm of pile cap displacement, the average damping ratio was about 18% with the looser backfill and about 24% for the denser backfill. Under higher frequency cyclic loadings, the damping ratio of the pile cap system was quite variable and appeared to vary with frequency. Damping ratios appear to peak in the vicinity of the natural frequency of the pile cap system for each backfill condition. On the whole, damping ratios tend to range between 10 and 30%, with an average of about 20% for the range of frequencies and displacement amplitudes occurring during the tests. The similar amount of damping for different ranges of frequency suggests that dynamic loadings do not appreciably increase the apparent resistance of the pile cap relative to slowly applied cyclic loadings.

ACKNOWLEDGMENTS

I wish to start by acknowledging my graduate adviser and mentor, Dr. Travis M. Gerber. His support and guidance has allowed me to complete this work in a timely manner. I would also like to thank the other members of my graduate committee, Dr. Kyle M. Rollins and Dr. Norman L. Jones. All members of my committee were willing and able to give me the help and guidance I needed.

The most important thank you goes to my wife, Katrina, and my son, Jackson. Without them, I would not have made it this far in my schooling.

Support for this project was provided by the National Science Foundation under Award Number CMS-0421312 and the George E. Brown, Jr. Network for Earthquake Engineering Simulation (NEES) which operates under NSF Award Number CMS-0402490. This support is also gratefully acknowledged. Additional support for this project was provided as part of a pooled-fund study (Contract No 069148, "Dynamic Passive Pressure of Abutments and Pile Cap") lead by the Utah Department of Transportation (UDOT) with participation by the Departments of Transportation of California, Oregon, Montana, New York and Utah. Mr. Daniel Hsiao served as the project manager for UDOT.

The opinions, interpretations and recommendations in this report are those of the author and do not necessarily reflect those of the sponsors.

TABLE OF CONTENTS

LIST OF TABLES

LIST OF FIGURES

1 Introduction

1.1 Background

Pile group foundations connected by a concrete cap are used in building and bridge structures to increase resistance to lateral loads and overturning moments as well as to decrease lateral displacements. Such loadings and displacements can be induced by wind or earthquakes. The lateral resistance provided by a pile cap foundation comes from both the interaction of the piles and soil beneath the cap and the passive earth pressure from backfill material acting on the sides of the cap.

The ultimate passive pressure of backfill materials surrounding pile foundations can be calculated for static loading conditions using Rankine, Coulomb, or log-spiral theories. However, how passive pressure develops as a function of soil-foundation displacement is less well defined. Some relationships assume a simple linear elastic relationship while others specify non-linear (often hyperbolic) relationships. Unfortunately, nearly all of the existing load-displacement relations for soils are based on static or slowly applied loadings. Under seismic loading conditions, both dynamic and cyclic effects are present which alter the load-displacement relationship. Cyclic loadings will usually reduce the strength of a soil whereas dynamic loading effects tend to produce an apparent increase in soil resistance due to damping. Because there is a lack of well-

defined load-displacement relationships which address the effects of both cyclic and dynamic loading, the engineering community has often applied static load-displacement relationships in seismic design.

1.2 Description and Objective of Research

The research presented in this thesis was undertaken to help quantify the effects of cyclic and dynamic loadings, and develop appropriate load-displacement relationships, for backfill soils. The research consisted of two major parts: performing the field testing, and analyzing and interpreting the test results.

The field testing consisted of laterally loading a full-scale pile cap. The pile cap had one of three different backfill conditions, namely: with no backfill present, with densely compacted backfill in place, and with loosely compacted backfill in place. In these tests, the backfill material was a clean sand. Other tests were also performed during this testing program using other backfill soils; results from these tests will be presented in theses by other students.

Loading was performed using a combination of hydraulic load actuators and an eccentric mass shaker. The actuators were used to slowly push (statically load) the pile cap to incrementally larger target displacement levels. At each displacement level, the actuators were used to cyclically displace the pile cap a small distance and the shaker was used to apply a dynamic loading on top of the static holding force from the actuators.

The analysis and interpretation of the data collected during testing produced various results associated with static, cyclic, and dynamic loadings. The results include horizontal load versus displacement relationships for the pile cap with differing backfill

conditions and earth pressure distributions along the pile cap face. These results also include comparisons between measured and theoretically-based or calculated values. Additional results include descriptions of vertical displacement, horizontal displacement and cracking of the backfill. The stiffness and damping for the pile cap for the different backfill conditions were also determined for both cyclic and dynamic loading conditions.

1.3 Organization of Thesis

This thesis is organized as follows. Chapter 2 provides a review of literature pertinent to this research. The literature includes reports from similar testing conducted at Brigham Young University and other universities. Chapter 3 is a discussion of the test site, the materials and equipment used and the general test procedures. Chapter 4 discusses the methodologies used in analyzing the field testing data. Chapters 5 through 7 discuss the results from the pile cap tests with three different backfill conditions, namely no backfill present, densely compacted clean sand backfill in place, and loosely compacted clean sand backfill in place. The results from the different backfill conditions are further compared in Chapter 8, followed by a summary of conclusions and recommendations in Chapter 9.

2 Literature Review

2.1 Introduction

The following sections will provide a discussion of previous research pertaining to the measurement and quantification of passive soil resistance when subjected to lateral loads from foundations. The first section will discuss the results from previous tests that have been performed to determine the contribution of passive soil resistance on laterally loaded pile caps. The second section will discuss methods used to predict the passive resistance of soils surrounding pile caps or abutments. The final section will discuss methods of determining soil stiffness and damping.

2.2 Lateral Resistance of Backfilled Pile Caps

Mokwa and Duncan (2001)

Mokwa and Duncan (2001) report the results of lateral load testing conducted on three full scale pile caps that were imbedded in the native soil. The initial tests were conducted by laterally loading the pile caps in the native soil which consisted of sandy lean clay and sandy silt. The pile caps were then retested with the native soil being excavated to determine the resistance provided by the piles alone. The final tests were

conducted with compacted sand, loose sand, and compacted gravel to determine the resistance provided by different backfill materials.

The tests showed that the pile caps provided between 40% and 50% of the total resistance. The tests also showed that the removal of the native soil increased the deflections upwards of 500% at a given load. The load deflection curves for the native soil and excavated cases are shown in Figure 2.1. The placement of different backfill material showed that the cap resistance is dependent on the stiffness and strength of the soil surrounding the cap. Two main conclusions were found from these tests. First, lateral resistance increases with increasing backfill strength and stiffness. Second, increasing cap depth or embedment decreases lateral movement at a given load.

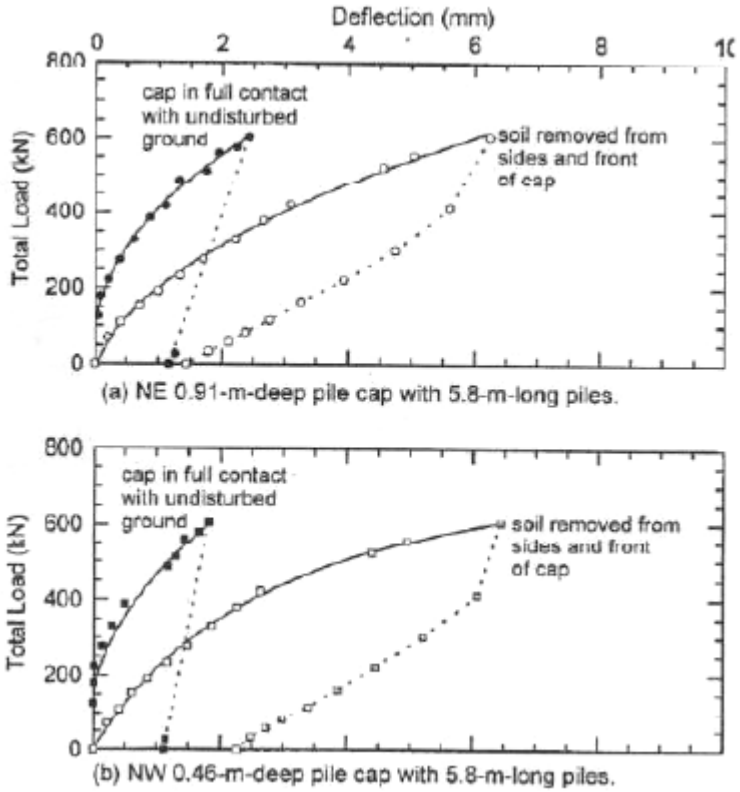

Figure 2.1 Pile cap resistance results (Mokwa and Duncan, 2001)

Cole (2003), Cole and Rollins (2006), Rollins and Cole (2006)

Cole (2003) performed seven full scale tests on a pile cap system consisting of a 5.18 x 3.05 x 1.12 m (length x width x height) concrete cap connecting 12 steel piles in a 4 x 3 configuration. Four of the tests had different backfill materials (silty sand, clean sand, coarse gravel and fine gravel) compacted next to the cap. The remaining three tests included two with no backfill and one with a trench excavated in the backfill material next to the cap face. The tests were performed by cyclically loading the pile cap to increasing displacement levels. The key findings of the research were that "the peak passive force contributed between 33% and 47% of the total pile cap resistance" (Rollins and Cole 2006), "observed sliding surface geometry was in good agreement with that predicted by the log spiral theory" (Rollins and Cole 2006), the ultimate resistance is best predicted using log-spiral theory, and that the hyperbolic model best predicted the load displacement curve (see Figure 2.2 and Figure 2.3).

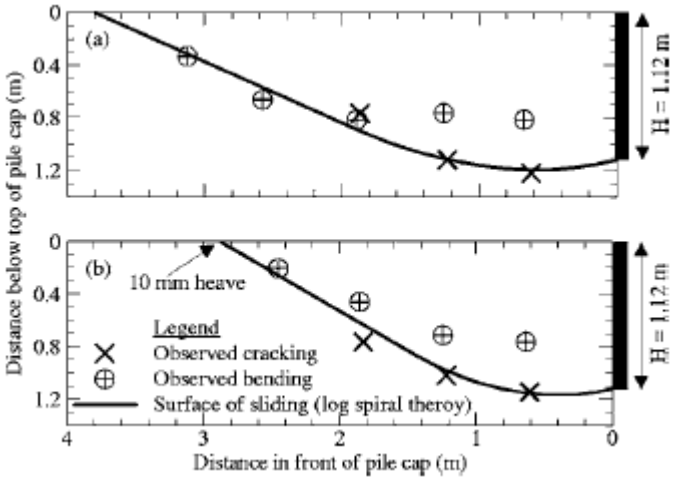

Figure 2.2 Comparison of observed and predicted failure surfaces (Rollins and Cole, 2006)

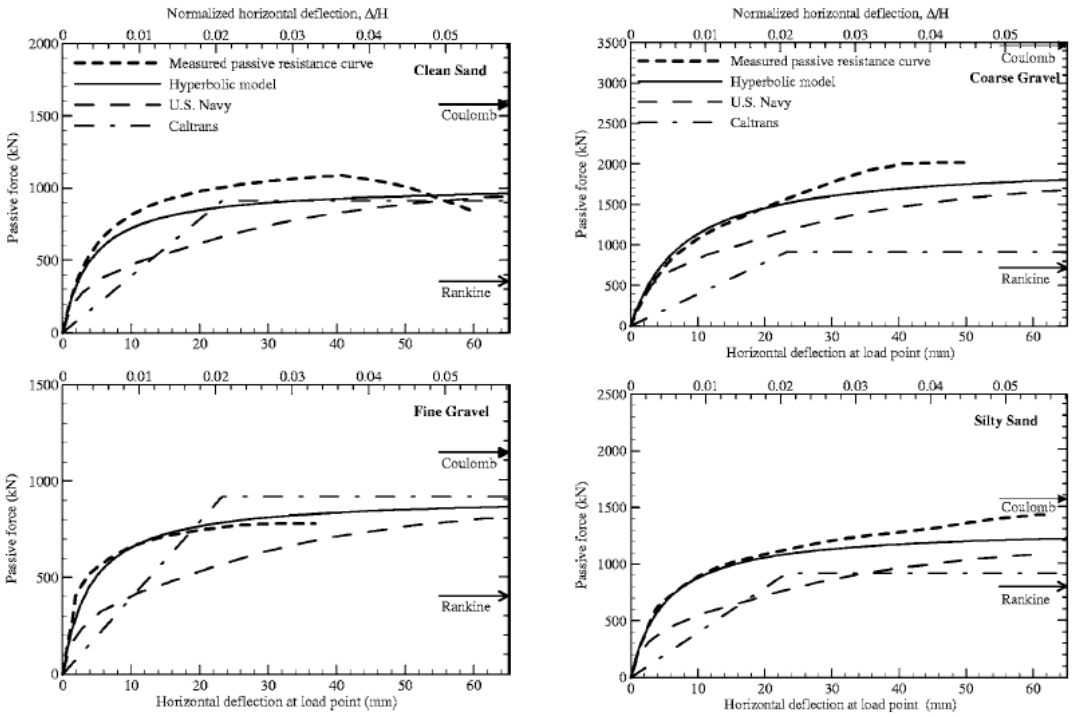

Figure 2.3 Comparison of measured passive resistance curves to predictive methods (Cole and Rollins, 2006)

Valentine (2007) and Runnels (2007)

Valentine (2007) and Runnels (2007) report the results of static and dynamic load tests conducted on a full scale pile cap system consisting of a 5.18 x 3.05 x 1.12 m (length x width x height) concrete cap connecting 12 steel piles in a 4 x 3 configuration; this is the same pile cap used by Cole (2003). The tests involved the use of a mass shaker to provide dynamic cyclic loading to the system. Valentine (2007) compares the static and dynamic responses of the pile cap without backfill and with a densely compacted silty sand backfill. Runnels (2007) compares the static and dynamic responses of the pile cap without backfill and with a loosely compacted silty sand backfill. The silty sand was similar to that used by Cole, but compared to different densities. By subtracting the response of the pile cap system with no backfill, the researchers were able to isolate the

stiffness and damping provided to the pile cap system by their respective backfills. The results indicate that both backfills provide significant increases in stiffness and damping with the densely compacted sand backfill providing more stiffness and damping than the loosely compacted sand backfill.

2.3 Methods of Predicting Passive Earth Pressures

Douglas and Davis (1964)

Douglas and Davis (1964) discuss the mathematical theory behind the displacement and rotation of embedded footings experiencing moments and horizontal loads. The distribution of pressure against the footing was calculated as an intermediate step in their numerical computations. Figure 2.4 shows the solutions to the two basic scenarios: uniform horizontal translation and rotation about the bottom edge of the footing. These two solutions may be added to account for any combination of translation and rotation (Douglas and Davis, 1964). To confirm the theories, several small scale models were created using mediums of gelatin and wax. Comparing the theory with the model results, they concluded that "the experimental results confirm the theory, provided there is full adhesion between plate and medium" (Douglas and Davis 1964). They also concluded that "where this adhesion is doubtful, the theory is still capable of predicting the order of movement" (Douglas and Davis 1964).

Duncan and Mokwa (2001)

Duncan and Mokwa (2001) developed a Microsoft Excel® spreadsheet with Visual Basic programming to numerically calculate the passive force as a function of

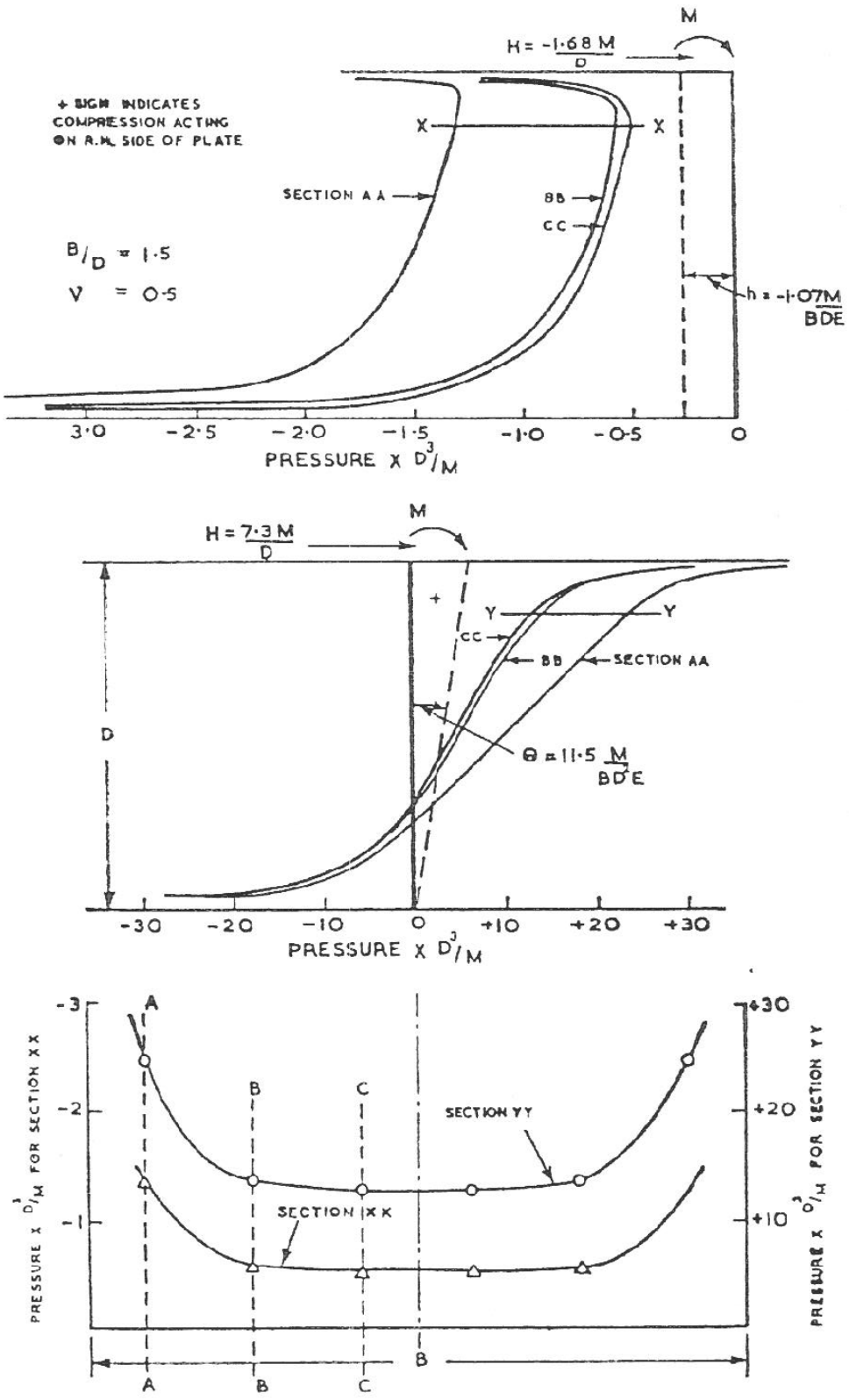

Figure 2.4 Pressure distribution for uniform translation and rotation on footing (Douglas and Davis, 1964)

displacement using the log spiral theory coupled with a hyperbolic displacement model (see Figure 2.5). The solution is solved iteratively by changing the location of the log-spiral center until a minimum passive resistance is found. The spreadsheet includes the Ovesen-Brinch Hansen 3D correction factor to account for the shear plane extending beyond the edge of the pile cap.

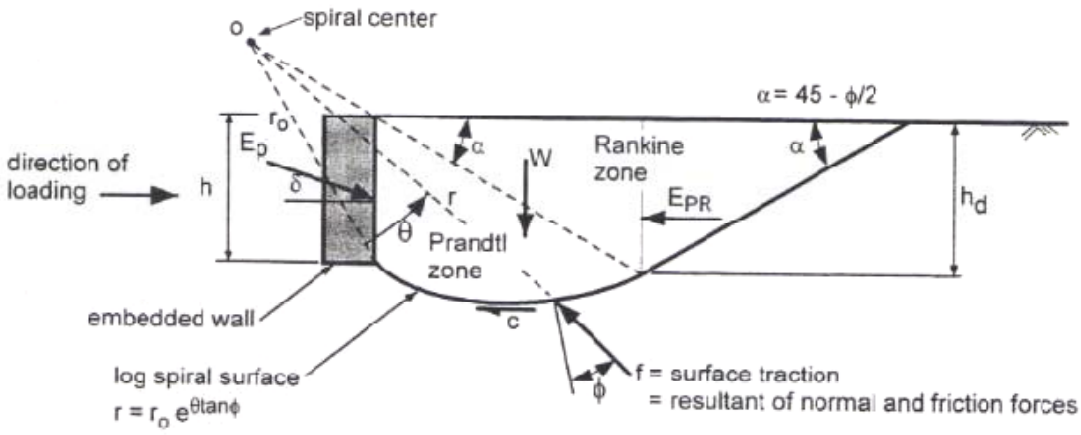

Figure 2.5 Log spiral failure mechanism (Duncan and Mokwa, 2001)

The passive load as a function of cap displacement is calculated using a hyperbolic model shown in Equation 2.1:

$$P = \frac{y}{\left[\frac{1}{K_{max}} + R_f \frac{y}{P_{ult}}\right]} \tag{2.1}$$

where K_{max} is based on the elastic solution from Douglas and Davis (1964), R_f is the failure ratio, y is cap displacement, and P_{ult} is calculated from Equation 2.2:

$$P_{ult} = (E_p)(M)(b) \tag{2.2}$$

where M is the Ovesen-Brinch Hansen 3D correction factor, limited to 2 (Duncan and Mokwa 2001), E_p is the passive resistance per unit length, and b is the structure length perpendicular to the plane of analysis. The R_f value in the hyperbolic model is defined as the failure ratio and is equal to the ultimate load divided by the hyperbolic asymptote value of passive resistance. Figure 2.6 shows the form of the hyperbolic model solution.

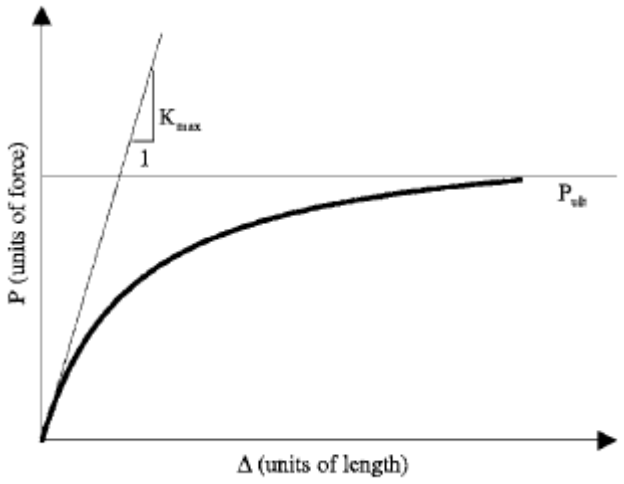

Figure 2.6 Hyperbolic model solution (Duncan and Mokwa, 2001)

Shamshabadi et al. (2007)

Shamshabadi developed a computer program call ABUTMENT that is based on the log-spiral hyperbolic model (LSH) that is presented in Shamshabadi et al. (2007). As the method suggests the ABUTMENT program uses a log-spiral failure wedge and a hyperbolic stress-strain relationship model to estimate the load-displacement curve of a given geometry and backfill soil. The ultimate passive pressure is solved for by dividing the backfill soil into slices and then satisfying force-based, limit-equilibrium equations for mobilized logarithmic-spiral failure surfaces, see Figure 2.7. The method produced a

good comparison to full scale tests that were conducted by Cole (2003). Comparisons of the measured and predicted results are shown in Figure 2.8.

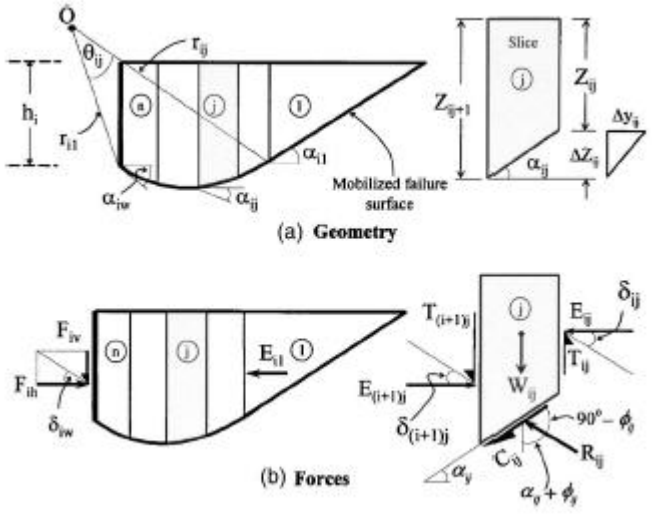

Figure 2.7 Geometry and forces of logarithmic -spiral failure surface (Shamshabadi at el., 2007)

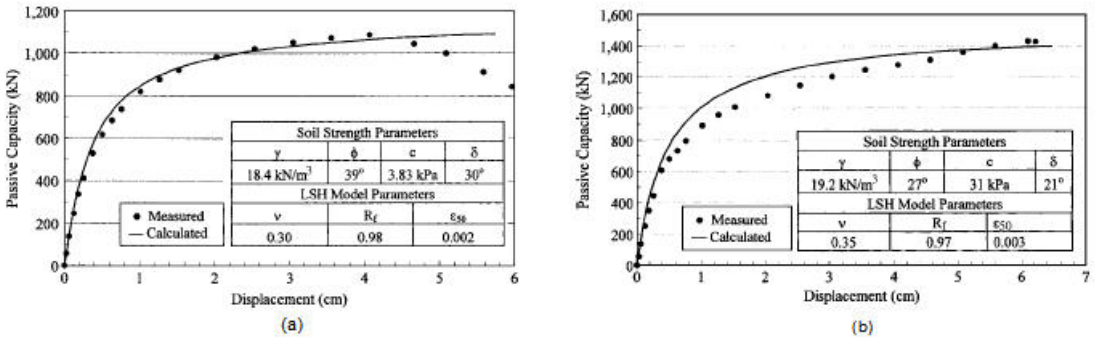

Figure 2.8 Comparison of measured and LSH predicted passive pressure for (a) clean sand and (b) silty sand (Shamshabadi et al, 2007)

Caltrans Method

Based on full scale tests conducted at UC Davis (Maroney 1995) Caltrans developed a method to determine the initial backfill stiffness and ultimate passive

pressure resisting movement for a bridge abutment during an earthquake. The initial stiffness (K_{abut}) and ultimate force (P_{ult}) are calculated using Equations 2.3 and 2.4:

$$K_{abut} = 11.5 \frac{kN/mm}{m} * w_{abut} * \left(\frac{h}{1.7}\right) \quad (2.3)$$

$$P_{ult} = 239\ kPa * A_{abut} * \left(\frac{h}{1.7}\right) \quad (2.4)$$

where w_{abut} is the width of the abutment (m), h is the height of the abutment (m) and A_{abut} is the area of the abutment (m^2). The load-displacement relationship follows the initial stiffness and then goes flat when the ultimate pressure is exceeded. The method scales different abutment heights linearly to the height of the test abutment and does not account of changes in backfill material. In fact, there are not soil properties used in the method.

2.4 Methods of Determining Soil Stiffness and Damping

Dobry and Gazetas (1985)

Dobry and Gazetas (1985) present a series of simplified methods for determining the equivalent dynamic stiffness and damping of different foundation types. The discussed foundations include an embedded foundation, a surface foundation, and a pile foundation. The authors' models are based on basic principles of dynamics and wave propagation and were calibrated by more sophisticated methods. These methods are appropriate when strain levels are relatively small.

In the case of determining the equivalent dynamic stiffness and damping for a pile, the authors present a 3 step method;

1. The horizontal displacement profile and static spring coefficient are obtained for the pile in the given soil profile by any number of accepted methods (i.e., full-scale test, p-y curves, finite element modeling, etc.). The static stiffness is then used with charts to determine the equivalent dynamic stiffness as a function of the forcing frequency.
2. At each depth interval two damping coefficients are calculated that correspond to the material and radiation damping. Both coefficients are functions of the soil. The radiation damping is also a function of depth.
3. The total equivalent damping coefficient is calculated by integrating the sum of the material and radiation damping over the length of the pile.

Figure 2.9 shows a comparison of the simplified method compared to a dynamic finite element analysis. The plots show a good agreement between the two methods with the simplified method generally being lower than the finite analysis and therefore being slightly conservative.

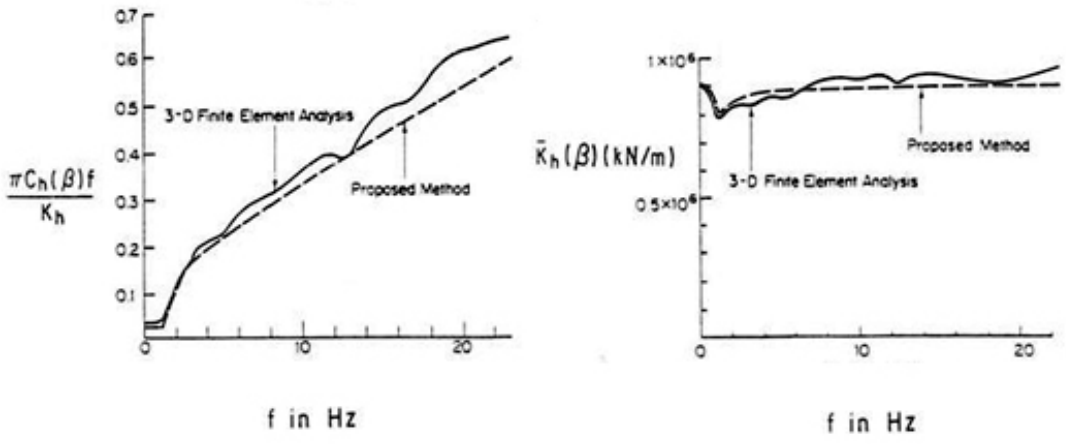

Figure 2.9 Comparison of simplified and finite methods for calculating dynamic stiffness and damping (Dobry and Gazetas, 1985)

3 Testing Methods

3.1 Site Description

The test site used is located approximately 300 m north of the Salt Lake City (SLC) International Airport control tower. The land is an unused portion of the SLC airport. The site is ideal for full scale testing because of its relatively flat topography and openness which allowed for easy access of the large equipment used during the tests. The site has been used for several full scale lateral loaded tests of drilled shafts and driven pile groups (for examples, see Christensen (2006) and Rollins et al. (2005a, 2005b)). An aerial photograph of the test site and the surrounding area is show in Figure 3.1.

The previous tests have provided a large amount of data pertaining to the subsurface conditions of the site. In general, the surface of the test site is covered by approximately 1.5 m of imported clayey to silty sand and gravel fill. Underlying soils consist of multiple silt and clay layers with occasionally interbedded sand layers. For this research, a 1.68 m high pile cap was constructed on an existing pile group such that its top was approximately the same elevation as the surrounding ground surface. Only one face of the cap was in contact with the backfill soil. During the tests, the water table was located approximately from zero to 50 mm above the base of the pile cap.

Figure 3.1 Aerial photograph of test site and surrounding area

3.2 Subsurface Characteristics

As previously mentioned, the test site has been used in several full-scale pile and drilled shaft tests which have provided substantial subsurface soil information. The first extensive subsurface investigation was conducted in 1995 by Peterson (1996). A variety of in-situ tests (such as SPT and CPT) and well as extensive laboratory shear strength and index property testing has been performed. Figure 3.2 shows locations of subsurface tests in relation to the previously existing pile groups and drilled shafts. The pile cap used in this research was constructed on the 9-pile group, but with the middle row of

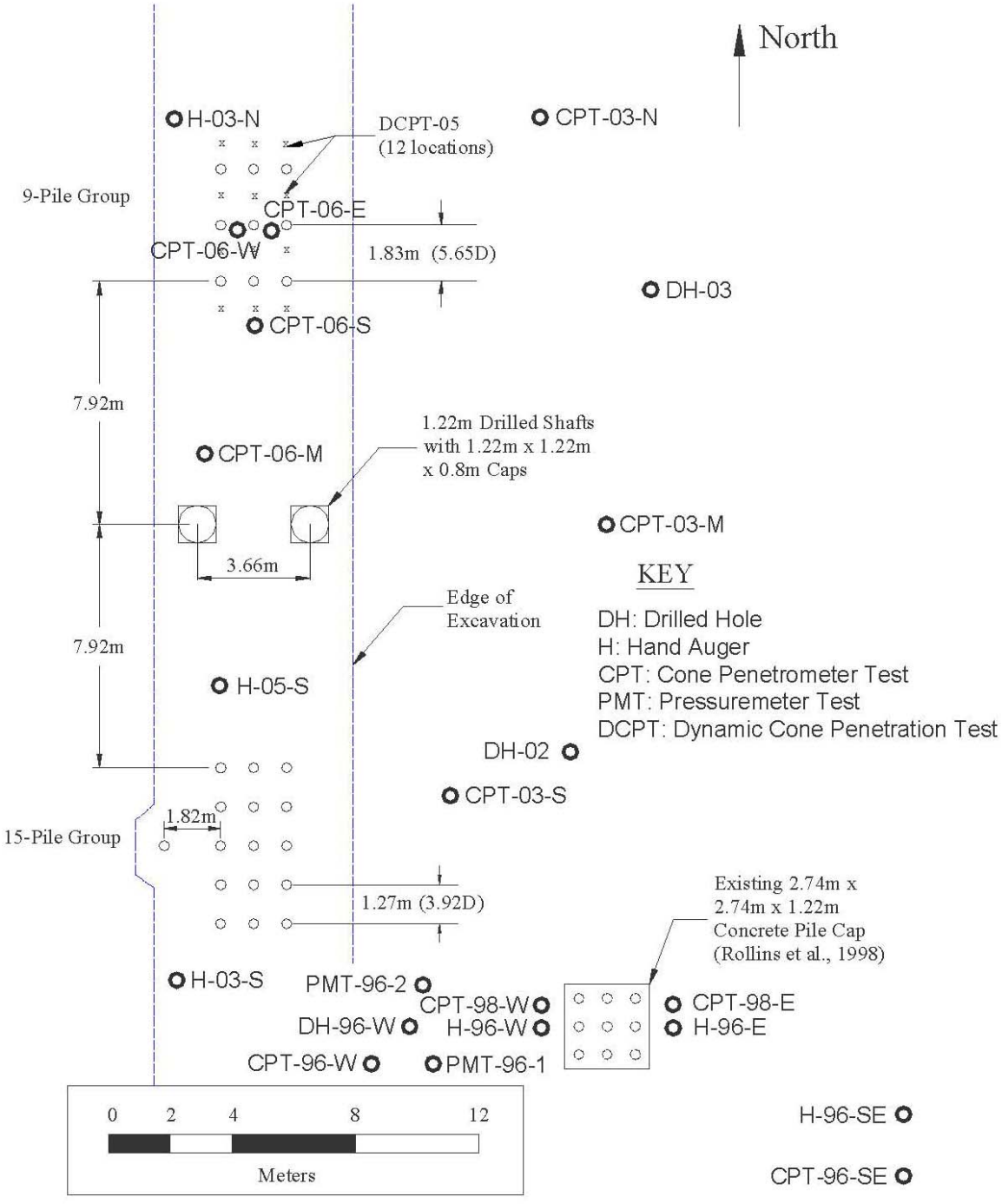

Figure 3.2 Entire test site with locations of subsurface tests (Christensen, 2006)

piles removed. Because this research focuses on the effects of the near-surface backfill, complete data from all previous subsurface investigations focusing on deep foundations will not be presented here, but reference can be made to Peterson (1996), Rollins et al. (2005a, 2005b), Christensen (2006), and Taylor (2006). However, a simplified subsurface profile (largely based on Peterson and presented by Christensen), together with results of a CPT conducted in the vicinity of the pile group upon which the pile cap was built, is shown in Figure 3.3. The layer of clean sand near the ground surface (which replaced previously imported materials) was removed and the piles cut off below the ground surface in order to construct the pile cap. Soils underlying the cap down to a depth of about 10 m consist of various layers of lean clay and sandy silt with two 1.5 to 2 m thick silty sand and poorly graded sand layers. Deeper soils consist of interbedded sandy silts and silty sands.

3.3 Test Layout, Equipment, and Instrumentation

The basic features of the test site consist of a reaction foundation, a test pile cap, and the backfill soil zone. Figure 3.4 shows a plan and profile view of the test site and equipment. Additional views are provided in the photos presented in Figure 3.5.

3.3.1 Reaction Foundation

The reaction foundation was composed of the two existing 1.2-m diameter drilled shafts, spaced 3.66-m center to center, that were buttressed with a sheet pile wall and two reinforced steel I-beams. The top 0.61-m length of shaft above the ground surface are finished as a 1.22-m square cap to facilitate loadings from previous testing. The west and

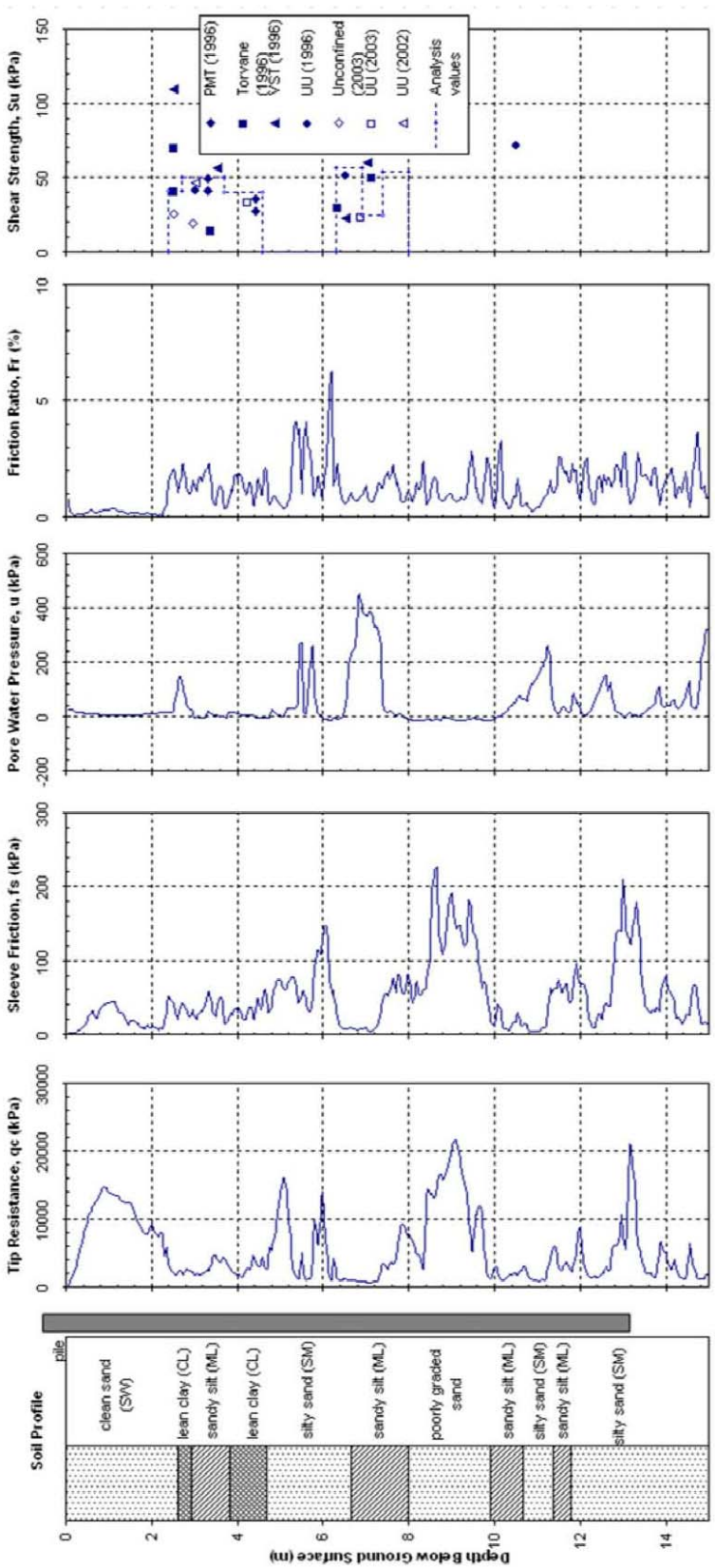

Figure 3.3 Idealized soil profile with CPT data (Christensen, 2006)

east shafts extend to depths of 16.82 m and 21.35 m, respectively. Shaft reinforcement consists of eighteen #36 vertical bars extending to a depth of 10.67 m below ground. These bars are wrapped with a #16 spiral pitched at 75 mm with a 120-mm clear cover of concrete. Half of the vertical bars extend from 10.67 to 16.76 m with a spiral pitched at 300 mm. The average compressive strength of the concrete in the shafts is 41 MPa.

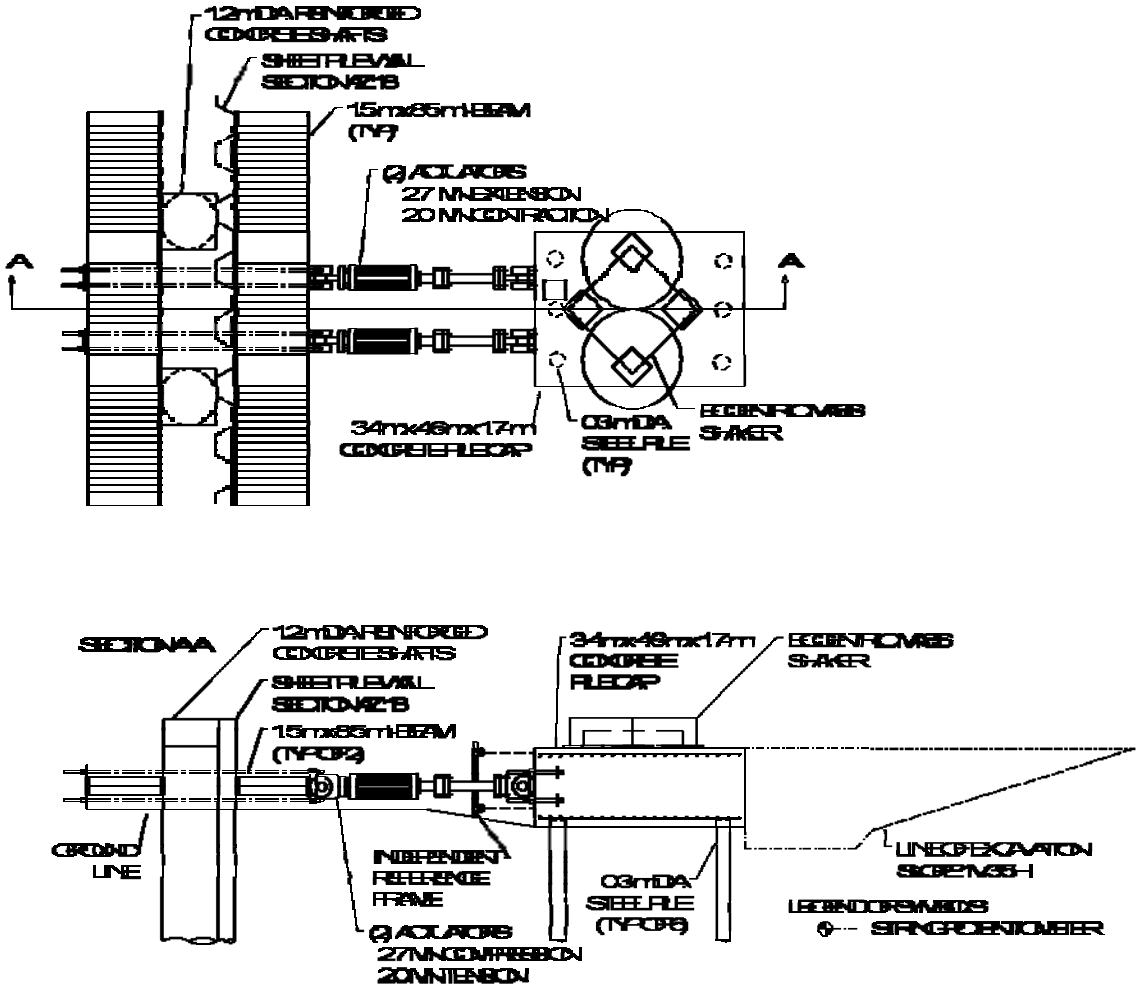

Figure 3.4 Plan and profile view of test setup

To increase the lateral capacity of the shafts being used as a reaction foundation, a sheet pile wall was installed on the north side of the drilled shafts. AZ-18 sheet piling constructed of ASTM A-572, Grade 50 steel was used, being selected from sections readily available in the local area. Installation depth was controlled by the 12.2 m length of the available stock. The piling, as built, extended to depths of 10.24 to 10.85 m below the excavated ground surface. The sheet pile was installed by vibratory hammer, and the sheet piling was kept as vertical and flush with the faces of the shafts as possible.

To help ensure a composite behavior and proper load distribution, two 8.53-m long, 1626- by 406-mm I-beams with numerous stiffeners were placed with the web horizontal on either side of the shafts and sheet piling as shown in Figure 3.4. The reaction foundation was tied together with eight 64-mm high strength treaded bars that were post-tensioned to 45 kN.

3.3.2 Piles and Pile Cap

The previously driven piles are made of ASTM A252 Grade 3 (i.e., 310 MPa minimum yield strength) steel pipe, with an outside diameter and wall thickness of 324 and 9.5 mm, respectively. The piles were driven closed ended to a depth of approximately 13 m (43 ft) below the ground surface. After the removal of three (the middle row) of the original nine piles the remaining piles were spaced 3.66-m center to center in the direction of loading. The tops of the piles were cut-off, leaving an approximate embedment of 150 mm (6 in) into the future cap. The piles were filled with 41-MPa concrete and attached to the cap with a rebar cage consisting of six #25 vertical bars and a #13 spiral at a 152-mm pitch. The 5.49 m long cages extend approximately

1.47 m into the cap and support the upper mat of horizontal reinforcement. Inclinometer tubes and shape array tubes were placed in the center north and center south piles.

Figure 3.5 Photos of test site and equipment setup

The final cap dimensions are 4.57-m long, 3.35-m wide and 1.68-m tall. The concrete used in the cap has a compressive strength of 41-MPa. The cap is reinforced primarily with a mat of transverse and longitudinal reinforcing bars placed in both the top and the bottom of the cap. Each mat consists of #19 bars placed at 203 mm on center, each way. Treaded bars to be used as connectors for the shaker and actuators were into place during construction so as to be integral with the cap.

3.3.3 Loading Equipment

An eccentrically loaded mass shaker was used to provide dynamic loading to the pile cap. This piece of equipment was provided by the Network for Earthquake Engineering Simulation (NEES) equipment site located at UCLA. The shaker was oriented on the pile cap so that the maximum force vector was perpendicular to the reaction frame and parallel to the actuator load. The magnitude of force generated by the shaker is based on Equation 3.1,

$$F = 0.04016 * (WR) * f^2 \tag{3.1}$$

where F is force (kN), WR is the weight-distance (i.e., moment) of the shaker basket (cm-kN), and f is the shaker frequency (Hz). The weight and eccentricity of the shaker baskets can be changed by adding or subtracting 0.04 kN steel blocks which can be variously positioned within the baskets. Equation 3.1 is empirical with unit conversions being covered in the first term of the equation. With the configuration of steel blocks used, the WR parameter was equal to 110.97 cm-kN which gave the shaker capacity of 446 kN of force at a maximum frequency of 10 Hz.

A pair of 2.7 MN (600 kip) capacity hydraulic actuators was used to apply horizontal force to the south side of the pile cap, pushing the cap northward. Each actuator was attached to the reaction foundation system with the threaded bars also used to tie the I-beams together. Each actuator was attached to the test pile cap by four treaded bars embedded in the cap during construction. Both ends of the actuators have free-swiveling heads, providing moment-free loading conditions. Hydraulic pressure was provided by a 227 l/min pumping unit. Load from the actuators was applied at the mid-height of the cap, which corresponds to a depth of approximately 0.84 m below the backfilled ground surface. To help span the distance between the test cap and reaction foundation, 1.22 m (4 ft) long extensions were added to the actuators.

3.3.4 Instrumentation

An independent reference frame was used to provide a non-moving datum for pile cap displacement measurements. The reference frame was located between the reaction foundation and the pile cap. The reference frame was embedded in concrete and tensioned guide cables were used to help reduce movement in the frame.

Four string potentiometers, also referred to as string pots, measured the relative displacement of the four southern corners of the pile cap (the face to which the actuators were attached, two near the top and two near the bottom). An additional seven string pots were mounted on the top of the pile cap near the backfilled face. These potentiometers were attached to metal stakes driven into the surface of the backfill, thus providing a measure of relative movement between the cap and points within the backfill.

Triaxial accelerometers were attached to the top of the cap at each corner and in the center of the northern end. During dynamic loading the reference frame responded

dynamically and therefore the sting potentiometers became unreliable. Displacements during dynamic loadings are based on integration of the measured accelerations, while displacements during static loading and slowly applied cyclic loading are based on the string potentiometers.

Six pressure plates were used to measure the pressure distribution with depth from the backfill material. Their centers were placed at depths of 0.14, 0.42, 0.70, 0.98, 1.26 and 1.54 m in the center portion of the pile cap. These stainless steel pressure cells were designed with a reinforced backplate to reduce point loading effects when directly mounting the cell to a concrete or steel structure. The cells utilize a semi-conductor pressure transducer rather than a vibrating wire transducer to more accurately measure rapidly changing pressures. The cells were cast integrally with the pile cap, with their top surfaces being flush with the concrete face.

To further document changes in the backfill during testing, a 0.61 m square grid was painted on the backfill. After cyclic and dynamic loading at each displacement level, cracking of the backfill was mapped by visual inspection with the aid of the grid. Vertical displacements were measured at grid nodes using traditional surveying equipment at the beginning and end (i.e., at the maximum displacement level) of each backfill test.

3.3.5 Backfill Zone

As shown in the plan view portion of Figure 3.4, the backfill soil zone was approximately 5.2 m wide and 8.5 m long. As viewed in cross-section, the first 2.44 m of the backfill zone was approximately 2.16 m deep, followed by an approximate 3.5H:1V slope to the surface of the existing ground. The dimensions of the backfill zone were

selected to minimize the amount of backfill soil needed while still enclosing the anticipated shape of a log-spiral failure plane in three dimensions. The backfill material was placed and compacted in lifts with thicknesses depending on the desired density. For compaction, a vibrating drum and jumping jack compactors were used. Backfill material was wetted during compaction to facilitate densification. After each lift was compacted, a nuclear density gage was used to determine the relative compaction, wet and dry unit weights, and moisture content. After all of the material was placed, a grid was painted on the top surface that was used as a reference for surveying and visual inspections.

3.4 Backfill Soil

The backfill soil used during testing is classified as well-graded Sand (SW) according to the Unified Soil Classification System (USCS). A particle size distribution chart of the sand is shown in Figure 3.6, with index and compaction properties shown in Table 3.1 and Table 3.2. As a clean, cohesionless material, the moisture-density relationships for this sand backfill are relatively insensitive to the moisture content (i.e., the proctor curves are very flat) and the optimum moisture content is not well defined.

The sand was placed twice in the backfill zone once in a densely compacted state and once in a loosely compacted state. The target density for the loosely compacted state was an average dry density greater than or equal to 90% of the maximum dry density obtained from a standard proctor compaction test (ASTM D 698). The target density for in lifts of approximately 20 cm whereas the densely compacted sand was placed in lifts of 10 cm. In place unit weight histograms actually achieved for the loosely and densely compacted sand backfill are shown in Figure 3.7 and Figure 3.8. The average in place

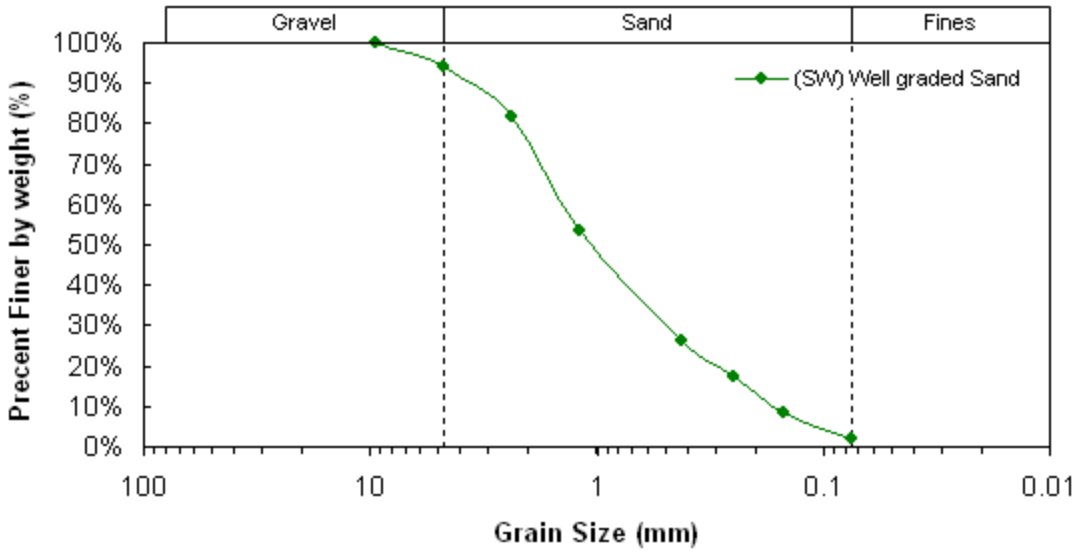

Figure 3.6 Gradation chart of backfill sand

Table 3.1 Summary of clean sand gradation characteristics

Backfill Type	Gravel %	Sand %	Fines %	D_{60}	D_{50}	D_{30}	D_{10}	C_u	C_c
Clean Sand	6%	92%	2%	1.5	1.11	0.56	0.17	8.7	1.21

Table 3.2 Summary of moisture-density relationships of clean sand

Backfill Type	UCSC	Standard Effort		Modified Effort	
		$w_{opt\ SP}$ (%)	$\gamma_{d\ SP}$ (kN/m^3)	$w_{opt\ MP}$ (%)	$\gamma_{d\ MP}$ (kN/m^3)
Clean Sand	SW	17	16.51	15	17.44

dry unit weights of the loosely and densely compacted sand were 15.6 and 16.9 kN/m^3, at 8 and 9% moisture, which correspond to 94% of the standard Proctor and 96% of the modified Proctor values, respectively. Comparing the density values from the proctor tests and the in-place measurements shows for this cohesionless, granular soil shows that it is quite insensitive to moisture content. The densely compacted state was defined as an

average dry density greater than or equal to 95% of the maximum dry density obtained from a modified proctor compaction test (ASTM D 1557). Target densities for the loosely and densely compacted states are thus 14.9 kN/m^3 and 16.6 kN/m^3, respectively.

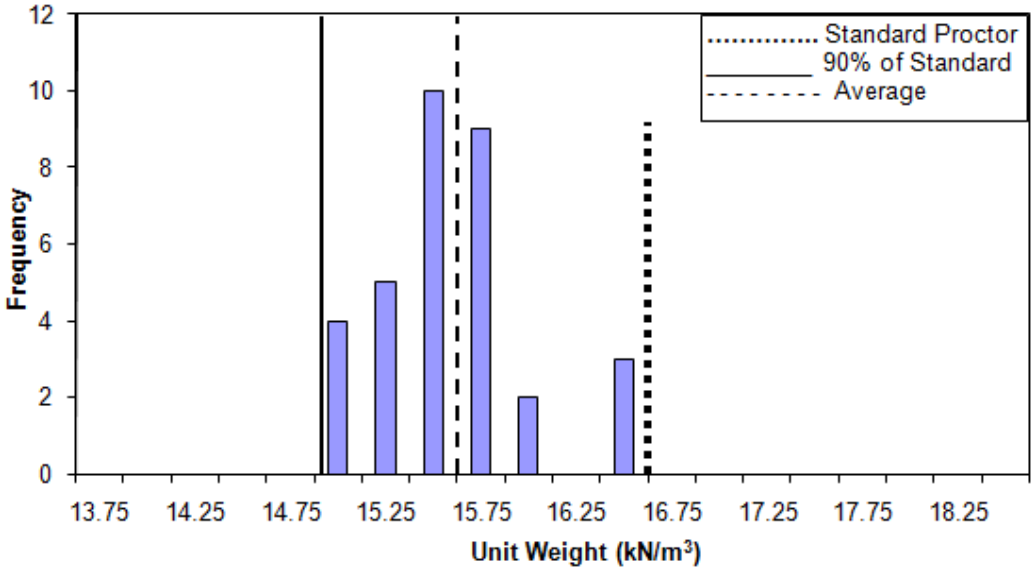

Figure 3.7 Density histogram for loosely compacted sand backfill

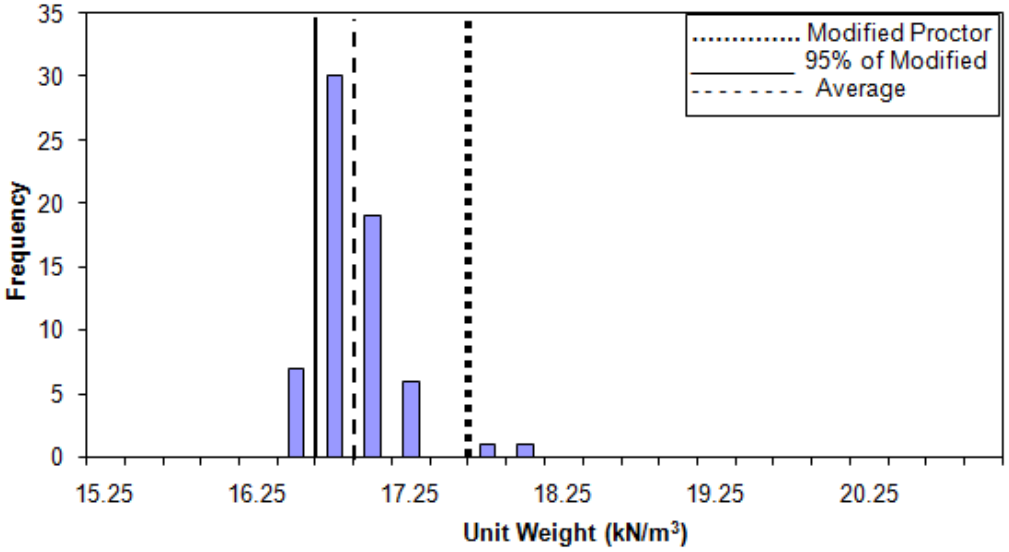

Figure 3.8 Density histogram for densely compacted sand backfill

The clean sand used is similar in gradation to that used by Cole (2003). Based on the similar gradation the maximum and minimum unit weights are assumed to be 17.8 and 13.4 kN/m^3 respectively. Using the maximum and minimum unit weights the average relative densities of the loosely and densely compacted sand were estimated to be 57 and 84%, respectively.

Direct shear tests were performed in the BYU soils lab to define the material's shear strength failure envelope. The direct shear tests were done in general accordance with ASTM D 3080. The normal stress during the tests ranged from 36 to 287 kPa. Figure 3.9 shows the results of the direct shear tests, including both the peak and ultimate failure envelop for both the loose and dense state. The resulting shear strength parameters are summarized in Table 3.3. The similar shear results for the peak and ultimate values of loosely compacted sand are expected because loosely compacted sands do not develop a discernible peak during shearing. The friction angle (φ) and cohesion (c) are based on forcing the failure envelope through the origin.

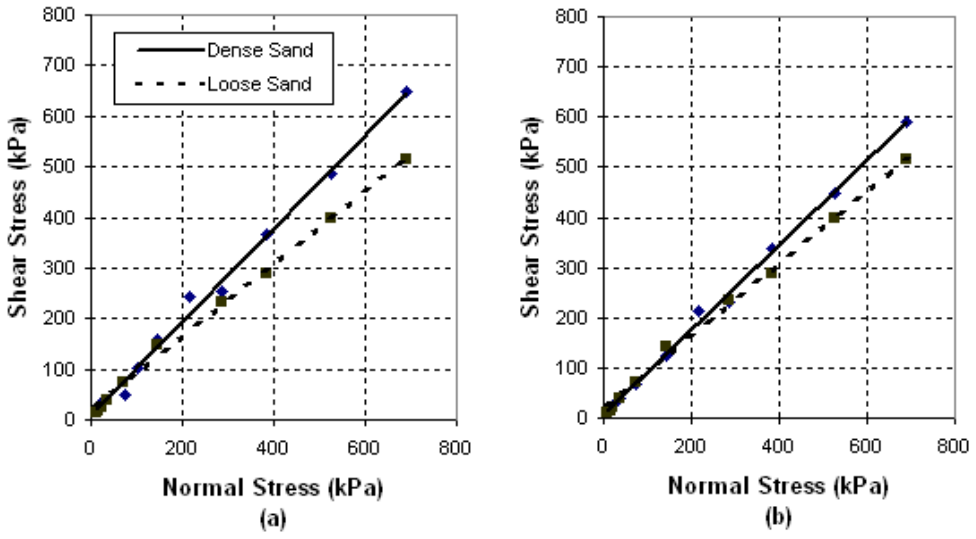

Figure 3.9 Shear strength failure envelopes based on (a) peak values and (b) ultimate values

Table 3.3 Summary of shear strength parameters from laboratory direct shear tests

Density State	Peak Values		Ultimate Values	
	phi (φ)	c (kN/m^2)	phi (φ)	c (kN/m^2)
Loosely Compacted	37.3	0	37.3	0
Densely Compacted	43.3	0	40.5	0

Along with the normal direct shear tests a series of modified tests were performed to quantify the interface friction angle (δ) between the concrete and clean sand in the densely compacted state. The interface friction angle was determined placing a concrete sample of comparable roughness to the face of the pile cap in the field into the bottom half of the shear box. Figure 3.10 shows the results from the interface friction tests for both the peak and ultimate conditions using the densely compacted sand. The interface friction angle was calculated to be 29.4 degrees for both the peak and ultimate conditions when the intercept is set to zero. Using the results for the direct shear tests δ/φ ratios were calculated to be 0.68 and 0.73 from the peak and ultimate strength conditions. The calculated δ/φ ratios from the densely compacted sand were used to calculate the interface friction angle for the loosely compacted sand.

The calculated internal and interface friction angles match reasonable well with those presented by Cole (2003). Cole had an internal friction angle of 39 for his soil and an interface friction angel of 30 degrees, resulting in a δ/φ ratio of 0.77.

3.5 General Testing Procedures

The lateral load pile test were performed using the following procedure was followed during testing. After placement of the backfill material (if any), the hydraulic actuators were used to displace the test cap. The target displacement interval was

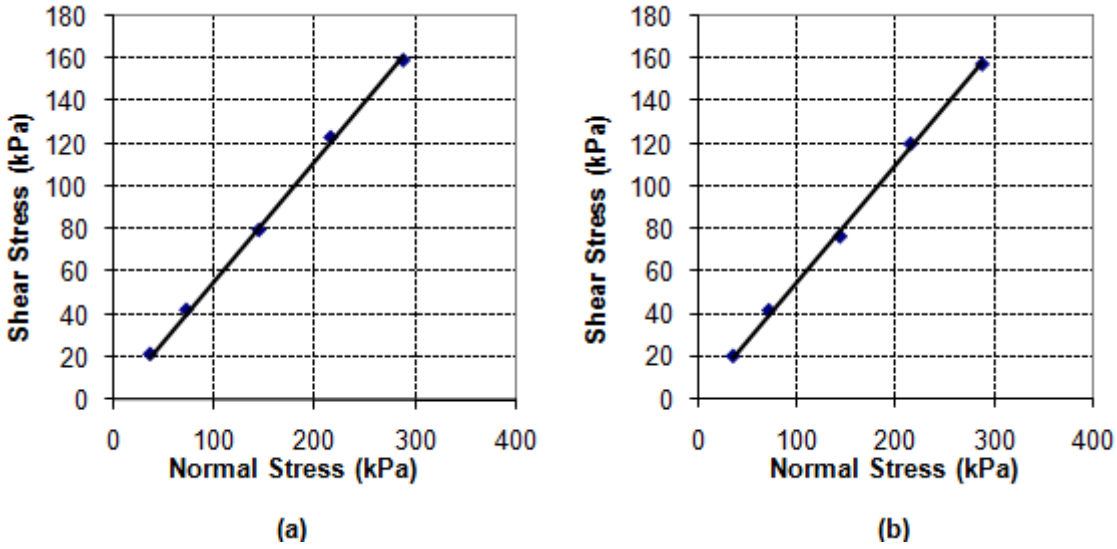

Figure 3.10 Interface shear strength failure envelops based on (a) peak and (b) ultimate values

approximately 6.3 mm. Upon reaching the first displacement level the actuators were programmed to apply a low frequency (0.75 Hz) cyclic load to the cap forward then backward with a target amplitude not exceeding 3 mm. The cyclic loading was applied for 15 cycles. When the cyclic load was completed the actuators were returned to their pre-cycling position and their length was fixed causing them to act as a relatively rigid member (similar to a strut) between the reaction and test foundations. The shaker was then turned on to apply dynamic loads to the cap. The shaker applied a stepped ramped load by dwelling for 15 cycles at each 0.5 Hz from 1 to 10 Hz. After the ramped loading was completed the shaker was ramped down with no dwelling to a stopped position. The entire shaker loading, including ramping up and then back down, lasted approximately 3 ½ minutes.

After the cyclic and dynamic loadings were completed, some data was processed while the backfill material was inspected for cracks. Once all intermediate data was processed and collected the actuators were again used to displace the cap by another

displacement interval. After reaching the next displacement level, the shaker was activated while the actuators were locked in place. After the shaker loading was completed the actuators then applied their cyclic loading. Hence, the order of the cyclic actuator loading and the dynamic shaker loads were alternated between each displacement interval during testing.

The target displacement levels were in 6.3 mm increments. The maximum displacement levels were dependant on actuator and reaction foundation capacity and the functionality of other equipment. Actual actuator displacements were dependant on both the reaction and test foundations stiffness; therefore in order to achieve the target displacements, a knowledge of the relative stiffnesses is needed. Because the relative stiffness was not known for all displacement levels, the actual displacement intervals varied from the target intervals. After the first displacement interval of the no backfill test, two displacement increments were done between the cyclic loading. The double displacement levels were done to insure that the load displacement curve had reached a virgin compression state (i.e., the static loading backbone curve) which was evidenced by the flattening of the load path. Data was recorded at a sampling rate of 200 samples per second (sps). To facilitate data reduction and screening, data files were created at a reduced sampling rate of 1 sps.

After cyclic and dynamic loading at each pile cap displacement interval, the equipment was inspected briefly and manual readings were taken before the cap was pushed to the next target displacement level. During the tests that involved backfill soil, any observed cracking of the backfill soil was mapped with the aid of grid painted on the ground surface therefore, the progression of cracking with increasing pile cap

displacement was captured. Before initially loading the cap, the vertical elevation of the grid nodes were surveyed and inclinometer reading were taken for the center piles in the front and back rows of the pile cap. These measurements were again taken when the cap was at the maximum displacement level. Elevation surveys and inclinometer readings were not taken at intermediate displacement levels because of time constraints, whereas shape array data was collected throughout the test.

As stated previously, the research presented in this thesis is based on a portion of a larger testing program involving many different backfill types. While the focus of this thesis is the behavior of the pile cap with and without clean sand backfill, Table 3.3 lists all of the tests performed in the full testing program.

Table 3.4 Summary of tests conducted

Test Number	Test Date	Backfill Condition
1	18-May-07	Free Response (Condition Cap)
2	25-May-07	Densely Compacted Clean Sand
3	29-May-07	Loosely Compacted Clean Sand
4	1-Jun-07	0.91-m wide Gravel Zone with Loosely Compacted Clean Sand
5	1-Jun-07	No Backfill (Free Response)
6	4-Jun-07	1.83-m wide Gravel Zone with Loosely Compacted Clean Sand
7	6-Jun-07	Loosely Compacted Fine Gravel
8	11-Jun-07	Densely Compacted Fine Gravel
9	18-Jun-07	Mechanically Stabilized Earth (MSE) Wall with Densely Compacted Clean Sand
10	21-Jun-07	Loosely Compacted Coarse Gravel
11	21-Jun-07	No Backfill (Free Response)
12	26-Jun-07	Densely Compacted Coarse Gravel

4 Data Analysis Methods

4.1 Introduction

This chapter will present the methods used to analyze data collected during the pile cap load tests. Subsequent chapters will present the specific results for the three different backfill conditions, namely: with no backfill present, with densely compacted backfill in place, and with loosely compacted backfill in place.

4.2 Determination of Passive Earth Forces from Pile Cap Load-Displacement

The passive earth force from the backfill material can be determined by taking the load-displacement response of the pile cap with the backfill in place and subtracting the response of the pile cap without any backfill. The response of the pile cap without any backfill in place is referred to in this thesis as the "baseline" response of the pile cap. Hence, the baseline response reflects the pile cap resistance provided by pile-soil interaction. The pile cap response with no soil present is shown in Figure 4.1 and is based on the test conducted on June 21, 2007. As shown previously in Table 3.4, there were two other tests conducted without backfill present; however, they were not used as the baseline for several reasons. The first test involved the initial loading of the cap and this initial loading would not be comparable to a reloading of the cap until to softening of

the pile-to-cap connections had occurred after the first few complete load-displacement cycles of up to 90 mm of displacement. In fact, this "conditioning" of the cap was the purpose of the first load test. Later comparisons of the slopes of the load-displacement curves during the pulling of the cap back to its starting position at the end of each backfill test showed generally consistent values, indicating that the cap was well conditioned and that the baseline response of the cap was relatively consistent between tests. The test on June 1, 2007 did not have any dynamic effects in the load-displacement relationship since the shaker had experienced a malfunction; and there were fewer intervals at which cyclic actuator loading were applied. The behavior of the cap suggests that the baseline response is non-linear, with the cyclic and dynamic loadings contributing particularly to this at lower displacement levels.

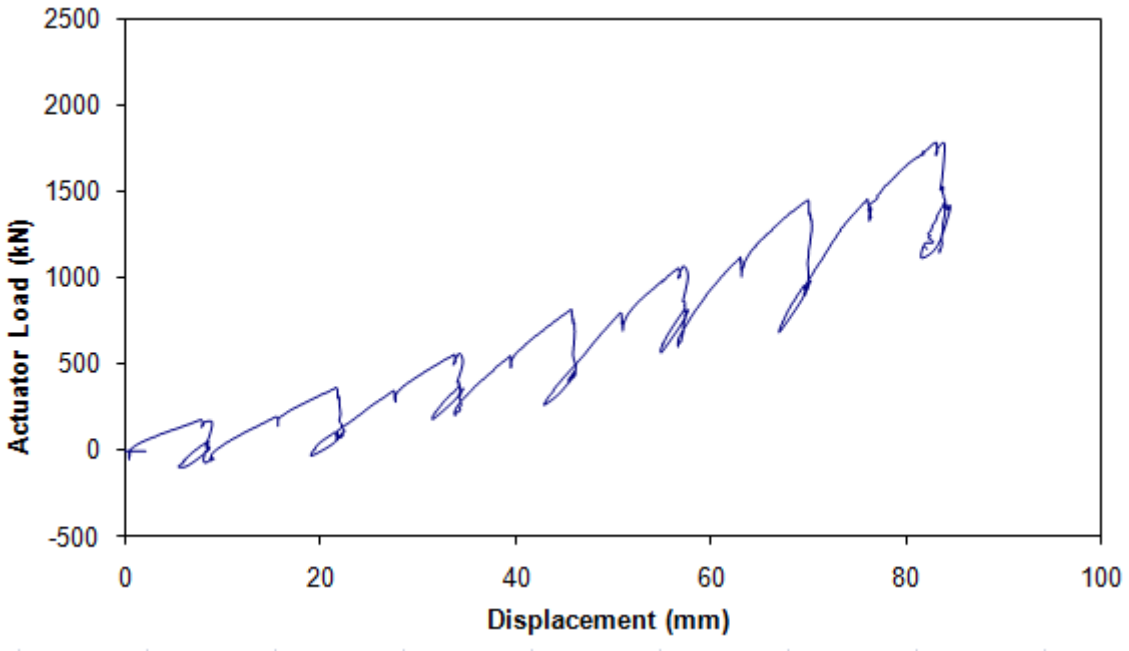

Figure 4.1 Actuator load versus displacement response of no backfill (baseline) test

To account for the non-linearity of the baseline response a fourth order quadratic curve was fit to the peak points of the response (ie the maximum load and displacement before any cyclic loading was applied to the cap). The fitted curve is shown in Figure 4.2 along with the measured response. The equation was used to quantify the baseline response at the peak points of other tests. Due to the high order of the curve , extrapolation beyond the 83 mm maximum displacement level must be done with caution.

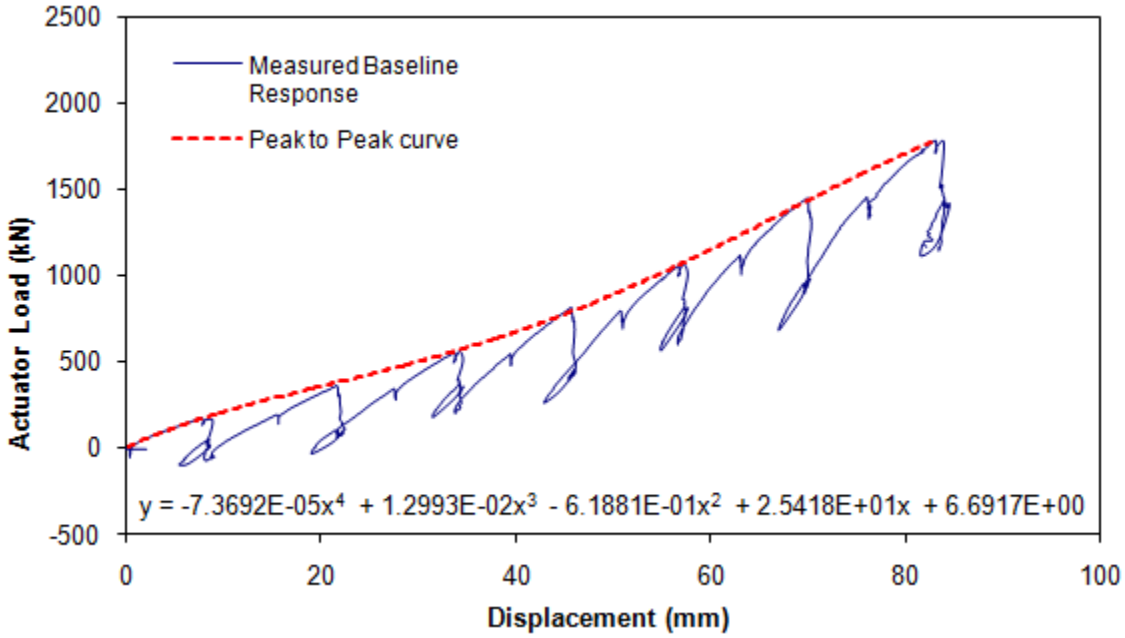

Figure 4.2 Measured baseline response with peak to peak curve

4.3 Calculation of Passive Earth Pressures

Several methods are available to calculate the passive pressure versus displacement relationship for the backfill soils. In this thesis, passive earth pressures were calculated using a modified version of the spreadsheet program PYCAP developed by Duncan and Mokwa (2001), the computer program entitled ABUTMENT which

implements the LSH approach presented by Shamshabadi et al. (2007) and the Caltrans standard design method. Comparisons of these methods to the measured earth pressures will be shown in subsequent chapters.

4.3.1 PYCAP Methodology

The ultimate passive force (pressure) from the backfill is determined using the log-spiral method, the force versus deflection curve is based on a hyperbolic load-displacement relationship where initial loading stiffness (k_{max}) is based on the solution for a laterally loaded plate embedded in an elastic half-space (Douglas and Davis, 1964), and three-dimensional loading effects are calculated using a correction factor, R_{3D}, developed by Brinch-Hansen (1966).

The inputs to this program are soil properties and foundation geometry. The soil properties needed are: internal friction angel (φ), soil cohesion (c), soil-foundation interface friction (δ), initial soil modulus (Ei), poisson's ratio (ν), insitu unit weight (γ), and adhesion factor. The geometry inputs are the foundation height (H), width (b), embedment depth (z), surcharge (q) and failure displacement divided by cap height (Δ_{max}/H). The internal friction angle and cohesion are both peak and ultimate shear strength parameters determined from direct shear testing as discussed earlier. The interface friction angle was determined by correlation as well as the direct shear testing discussed previously. The initial soil modulus, E_i, was found using the loading curve of a one-dimensional consolidation test of the sand. Mokwa and Duncan (2001) provide ranges for the initial soil modulus in terms of density. Table 4.1 shows the suggested ranges for loose, medium and dense sand. Values for Possion's ratio come from common

values, consistent with correlations to the friction angle. The specific values for each parameter used in analyses will be presented subsequently.

Table 4.1 Suggested ranges for initial soil modulus (Mokwa and Duncan, 2001)

Density	Dr	N60	Normally loaded	Preloaded or Compacted
Loose	40%	3	Ei = 9600 - 19200 kPa	Ei = 19200 - 38300 kPa
Medium	60%	7	Ei = 14400 - 23900 kPa	Ei = 23900 - 47900 kPa
Dense	80%	15	Ei = 19200 - 28700 kPa	Ei = 28700 - 57500 kPa

Along with a load-displacement graph of the passive earth pressure, PYCAP has several other outputs, including the soil loading stiffness, the hyperbolic failure ratio (R_f) which is derived from Δ_{max}/H, the three-dimensional shape factor, R_{3D}, and the coefficient of passive earth pressure (K_p) from the log-spiral method of calculating passive soil resistance.

4.3.2 ABUTMENT (LSH Method)

In the ABUTMENT program, the ultimate pressure of the backfill is determined by dividing the backfill soil into slices and then satisfying force-based, limit-equilibrium equations for mobilized logarithmic-spiral failure surfaces. Displacement is determined using a modified hyperbolic stress-strain relationship. The inputs to this program are soil properties and foundation geometry. The soil properties needed are internal friction angel (φ), soil cohesion (c), soil-foundation interface friction (δ), in-situ unit weight (γ), poisson's ratio (ν), and strain at 50% strength (ε_{50}). An additional failure ratio (R_f) parameter must be defined which helps control the sharpness of the hyperbolic curve. Different from the R_f values used in some hyperbolic soil models, this value typically

ranges from 0.95 to 0.98. Output from the program includes the load-displacement relationship and the passive earth pressure coefficient. Most of the soil input parameters were selected in the same way that they were chosen for the analyses using PYCAP. The strain parameter is difficult to precisely define and values shown for similar backfill materials in Shamshabadi et al. (2007) were used in these analyses. Within the computer program, the log-spiral force method of calculation was used with the "composite" option while the stresses and strains were calculated using the "modified hyperbolic" option. Three-dimensional end-effects are treated using an effective foundation width determined using the same Brinch-Hansen (1966) relationships as used in the PYCAP based analyses.

4.3.3 Caltrans Method

The Caltrans method is based linearly scaling the idealized response of an abutment which was tested by Maroney (1995) to the geometry of any other abutment. This scaling is done using Equation 2.3 and 2.4, presented previously. This method does not require any soil properties as input parameters.

4.4 Determination of Stiffness and Damping from Static and Dynamic Loading

During testing, the pile cap was subjected to slow cyclic loadings from the actuators and a cyclically applied dynamic loading from the eccentric mass shaker. The behavior of the pile cap was analyzed by resolving the forces acting on the test cap during testing. The test cap can be isolated from the reaction foundation because the actuator

force is known. Figure 4.3 shows a free body diagram of the test cap and backfill system. Writing the equation of motion for test cap we get Equation 4.1:

$$\boldsymbol{m\ddot{x} + (c_s + c_b)\dot{x} + (k_s + k_b)x = F_a + F_s} \quad \textbf{(4.1)}$$

where x and its derivatives represent displacement, velocity, and acceleration; c_s and c_b are the viscous damping coefficients for the pile cap and backfill; k_s and k_b are the stiffness of the pile cap and backfill; F_a is the externally applied actuator force, and F_s is the externally applied shaker force. Putting the equation of motion in terms of forces and solving for the unknowns we get Equation 4.2;

$$\boldsymbol{F_c + F_k = F_a + F_s - F_I} \quad \textbf{(4.2)}$$

where F_c is the damping force; F_k is the spring force; F_a is the actuator force; F_s is the shaker force; and F_I is the inertial force. Using the actuator and shaker forces that were measured, and the inertia force which could be computed using a constant, single lumped mass for the system and the measured pile cap acceleration, force-displacement loops representing the combined resistance of the piles and any soil backfill were calculated, see Figure 4.4. The lumped mass of the system was estimated using the weights of the test pile cap, shaker, a portion of the piles (the upper eight pile-diameters), one of the actuators, and any backfill that was present. The total weight of the components without any backfill was 707 kN. The mass representing the densely compacted backfill was determined from the log-spiral shape of the failure mass computed using the modified version of the PYCAP program and then adjusted by the three-dimensional factor to account for the fanning of the failure wedge out beyond the edges of the pile cap. For the densely compacted clean sand backfill a mass of 749 kN was used. For the loosely

compacted clean sand backfill where the failure wedge was very poorly defined, half of the densely compacted backfill weight was used.

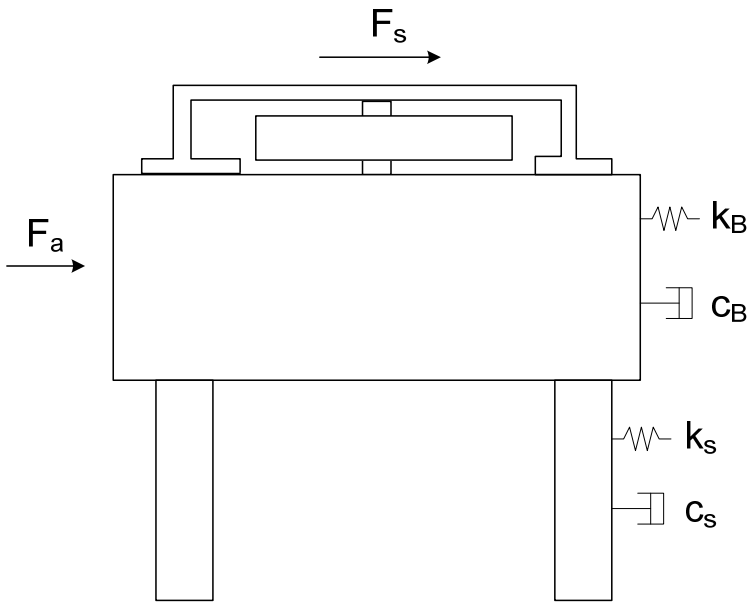

Figure 4.3 Free body diagram of test pile cap

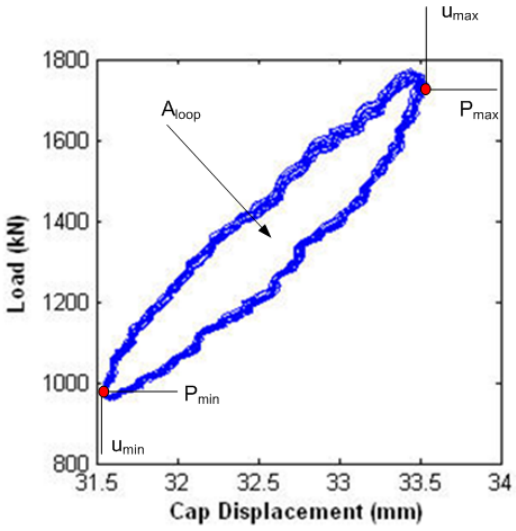

Figure 4.4 Key parameters in load-displacement loop

From the force displacement loops, stiffness was calculated using Equation 4.3:

$$\boldsymbol{k} = \frac{(\boldsymbol{P_{max} - P_{min}})}{(\boldsymbol{u_{max} - u_{min}})} = \frac{\boldsymbol{P_{amp}}}{\boldsymbol{u_o}} \quad \textbf{(4.3)}$$

where u_{max} is the maximum displacement, u_{min} is the minimum displacement, P_{max} and P_{min} are the loads associated with the maximum and minimum displacements, which are not necessarily the maximum and minimum loads during the loop, and P_{amp} is the load amplitude. These parameters are illustrated in Figure 4.4.

From the force displacement loops, damping ratio calculated using Equation 4.4:

$$\boldsymbol{\xi} = \frac{\boldsymbol{A_{loop}}}{\boldsymbol{2 * \pi * k * u_o^2}} \quad \textbf{(4.4)}$$

where ξ is the damping ratio, u_o is the loop displacement amplitude, k is the loop stiffness and A_{loop} is the area of the force-displacement loop . During the dynamic cycles, the pile cap displacement was calculated by using a non-phase shifting filter and double integrating the measured accelerations. Median values of the dynamic properties were calculated from the 15 loops recorded at each dwell frequency ranging from 1 to 10 Hz, at 0.5 Hz intervals.

Determination of damping using the half-power bandwidth approach was also attempted but proved problematic in some instances. In the half-power bandwidth approach, the measured dynamic displacement is plotted versus the frequency ratio, ω/ω_n (where ω is the natural circular frequency of the forcing function and ω_n is the natural circular frequency of the structure). The two frequencies, ω_1 and ω_2 , on opposing sides of $\omega/\omega_n = 1$ whose displacement amplitudes correspond to $1/\sqrt{2}$ times the resonant

displacement amplitude are then selected and used to determine the amount of damping, ξ, by satisfying the Equation 4.5 shown below.

$$\left(\frac{\omega}{\omega_n}\right)^2 = (1 - 2\xi^2) \pm 2\xi\sqrt{1 - \xi^2} \tag{4.5}$$

Often this equation is simplified to the following relationship by the assumption of a small damping ratio, Equation 4.6:

$$\frac{\omega_1 - \omega_2}{\omega_n} \cong 2\xi \tag{4.6}$$

Unfortunately, if damping is large (> 20% is the value typically cited) this latter equation becomes unreliable. It should also be noted that the former equation cannot be used if damping exceeds approximately 38% because with increased damping, the spread between ω_1 and ω_2 increases, and ω_1 would need to be less than zero for that amount of damping to be present. Due to limitations of the testing equipment, the dynamic displacement amplitude versus frequency curves commonly did not extend to a range high enough to identify ω_2. In attempting to use the more rigorous solution with various extrapolations of the measured response curve to estimate ω_2, it was found that the dynamic displacement amplitude versus frequency curves (with displacement amplitude normalized by the net applied load from the shaker and actuator in order to establish a relatively stationary forcing function), exhibited an atypical shape in which ω_2 - ω_n was greater than ω_n - ω_1, thus preventing a solution to Equation 4.5 which was consistent with the measured data. This behavior is attributed to a changing of stiffness and/or damping with respect to shaker frequency because of material non-linearity.

At low frequency levels, the shaker force and resulting pile cap displacement are very small, therefore it was difficult to distinguish between real load and instrumental noise. Because of this, results have not been presented for frequencies less than 4 Hz.

4.5 Horizontal Displacement in Backfill Soil

As mentioned previously seven sting potentiometers were placed on the front of the pile cap and attached to stakes that were driven into the backfill material. By knowing the relative movement between the cap face and the location of the stakes, as well as the absolute movement of the pile cap, plots of both relative displacement of the backfill and strain in the backfill can be computed.

The changes in length recorded by the sting potentiomenters correspond to the total amount of compression between the cap face and any given stake. Negative change in length represented shorting of the string and positive represented lengthening. Movement of the monitoring positions was calculated by subtracting the negative of the string potentiometer change in length from the displacement of the pile cap, effectively subtracting the magnitude of the backfill compression from the maximum total movement. When performed for each monitoring point, this method yielded the net movement of the stake. The data shown in subsequent plots are based on pile cap and stake positions at the end of each displacement interval (i.e., the time immediately after the pile cap had just been pushed to a new displacement level with the actuators).

To calculate the strain in the backfill material, the backfill was segmented into interval bounded by the stakes. This segmenting produced seven intervals, one between the cap face and the first stake and the remaining between any two adjacent stakes. By

normalizing the change in interval length by the initial interval length strains were calculated in each of the seven segments with positive values corresponding to compression.

Paired sets of plots showing the displacement of the backfill (as a function of distance away from the pile cap) and the calculated strains (as a function of pile cap displacement level) are shown for each backfill test. In some cases, small negative displacements or strains (indicative of expansion) may be shown. These values likely result due to the limited precision with which the data could be collected and processed; any tilting of the steel monitoring stakes or differential movement between the far ends of the pile cap along which the different string potentiometers were mounted could result in small errors in the data. Also, in some instances, there were unexplained short-duration jumps in the string potentiometer readings, and these readings were corrected manually by adjusting the affected data to match the data trend before and after the jumps.

5 Pile Cap with No Backfill (Baseline) - Results and Discussion

5.1 Introduction

The June 21, 2007 load test performed on the pile cap with no backfill present was used as the baseline response for the pile cap. This baseline test was used to quantify the response of the pile cap and subsurface material which can then be subtracted out of response from tests performed with backfill present in order to quantify the response of the specific backfill material. No significant deviations from the general test procedure occurred during this test.

5.2 Load-Displacement Results

A summary of test features is presented in Table 5.1. The loads in Table 5.1 correspond to the peak load applied by the actuators at the end of each static push to the target displacement level. The table also specifies the order (first or second) in which cyclic or dynamic loadings from the actuators and shaker, respectively, were applied. A graphical representation of the entire actuator load-displacement history is shown in Figure 5.1 where the static pushes, cyclic actuator loadings, and dynamic shaker loadings are represented by green, blue, and red data points respectively. Due to the dynamic forces from the shaker, the actuators record a decrease in load as the shaker force is

oriented away from the actuators and towards the backfill. Because the net load from the actuators and shaker increases when the force is oriented toward the backfill, displacement of the cap occurs and the load-displacement relationship shown in the figure (which is based on actuator load only) appears to have a reversed slope and the actuator loads can be less than zero. Figure 5.1 shows that the overall baseline response is somewhat non-linear, being concave up (increasing stiffness per loading interval as the pile cap displacement is increased). Slight decreases in load are observable at the intermediate pushes while manual data points were being recorded. The decrease is believed to be a relaxation of the soil acting on the piles and is not due to a decrease in pile cap displacement (pile cap displacement actually increases minutely). These effects are much more pronounced when backfill soils are present and contribute to a larger portion of the overall pile cap resistance.

Table 5.1 Summary of test with no backfill

Displacement Interval	Displacement (mm)	Actuator Load (kN)	Actuator Cycles	Shaker Cycles
1	7.0	178	First	Second
2	16	189	None	None
3	21	365	Second	First
4	27	345	None	None
5	33	553	First	Second
6	39	548	None	None
7	45	815	Second	First
8	50	793	None	None
9	57	1066	First	Second
10	62	1119	None	None
11	69	1448	Second	First
12	75	1454	None	None
13	83	1782	First	Second

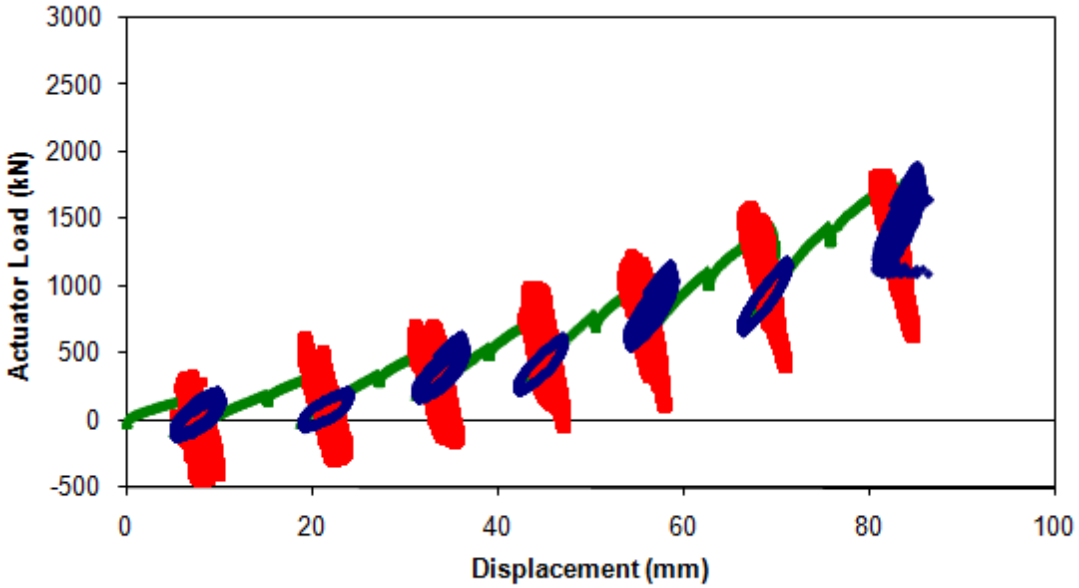

Figure 5.1 Complete load-displacement relationship for pile cap without backfill (baseline test)

5.3 Static Actuator Cycle Results

Figure 5.2 shows the displacement amplitude, stiffness, loop area and damping ratio for the pile cap without backfill as a function of cap displacement. Values are based on the median of the 15 small amplitude cycles performed at each displacement level. Although the displacement amplitude and loop area have little variation, the increase in stiffness with increasing pile cap displacement level causes the damping to decrease from approximately 40% to just under 20% as the cap displacement increases. An interesting trend in the stiffness data is the sawtooth shape of the trend. This shape is caused by the order of the actuator and shaker cycles. The stiffness is higher when the actuator cycles are performed before the shaker cycles because of the softening of the soil during dynamic loading (i.e., when the actuator loading occurs second, the soil has already experienced the dynamic loading from the shaker).

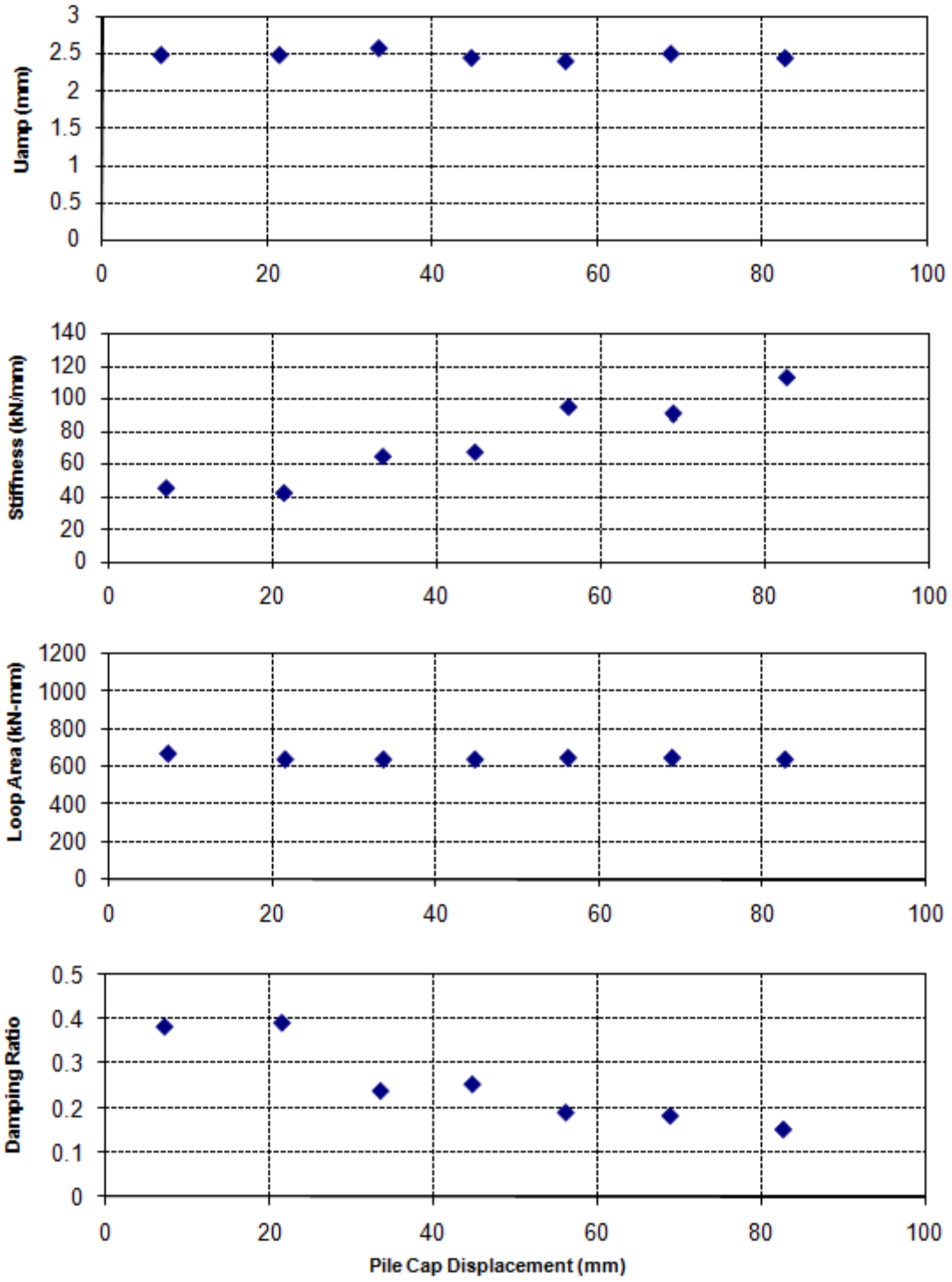

Figure 5.2 Static cycling displacement amplitude, stiffness, loop area, and damping ratio for pile cap without backfill (baseline test)

5.4 Dynamic Shaker Cycle Results

The first row of graphs in Figure 5.3 show displacement amplitude as well as displacement amplitude normalized by the cyclic amplitude of net applied force from the shaker and actuators as functions of the forcing frequency and pile cap displacement level. The second and third rows of graphs show the calculated reloading stiffness and damping, respectively, of the pile cap system. In the left column, these parameters are shown in terms of forcing frequency. If non-linear behavior is present, these properties will also depend on the displacement amplitude; hence, in the right column, these parameters are shown on terms of the displacement amplitude. Based on the data, it appears that both frequency and displacement amplitude must be considered when interpreting test results. The pile cap displacement levels shown in the figures correspond to a cycling phase when the dynamic shaker cycles were applied before the slowly applied actuator cycles.

The peaks in the normalized amplitude graph occur at the damped natural frequency of the system. The damped natural frequency appears to be increasing with increasing pile cap static displacement level. This is consistent with the increasing stiffness with displacement level as also shown on the graph. The damped natural frequency of the pile cap appears to range from 5 to 6.5 Hz. Stiffness generally ranges from between 100 and 200 kN/mm. Calculated damping ratios exhibit a wide range of scatter, varying both with respect to frequency and displacement amplitude. Damping ratios tend to be in the range of 10 to 30% at intermediate frequencies and displacement levels and then increase with increases in those parameters. Interpreting the normalized

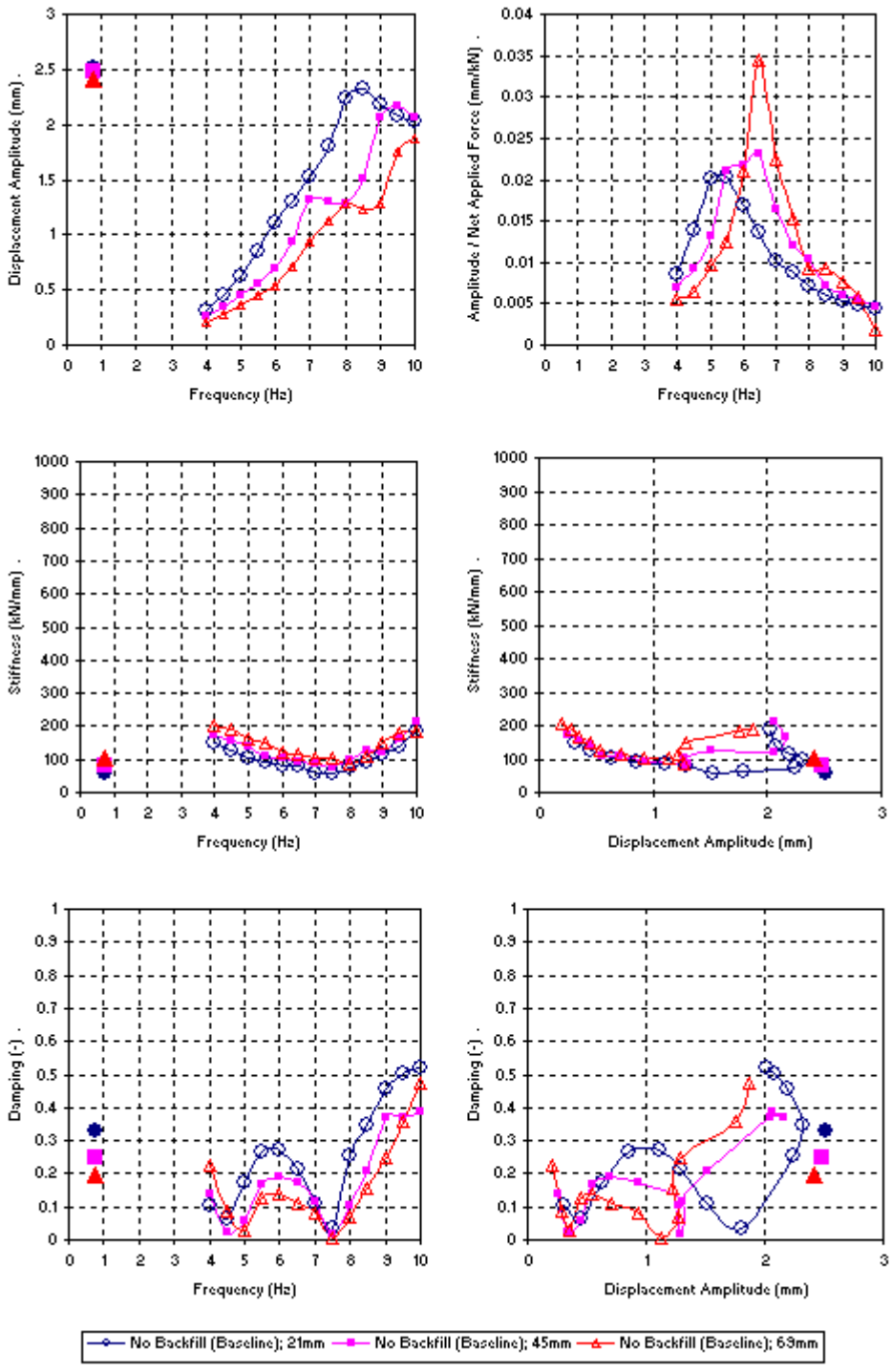

Figure 5.3 Dynamic displacement amplitude, stiffness, and damping for pile cap without backfill (baseline test)

displacement amplitudes using the half-power bandwidth approach yields damping ratios of 18, 17 and 8% for the three pile cap displacement levels shown in Figure 5.3

5.5 Comparison of Static and Dynamic Cycles

Included in Figure 5.3 are displacement amplitude, stiffness and damping ratio calculated from the statically applied cycles from the actuators (~ ¾ Hz) at each represented displacement level (solid points). The values presented are averages of the previous and subsequent actuator cycles. An average value is used to represent stiffness and damping that would have been calculated if the actuator cycles and been performed before the shaker cycles. In terms of frequency, it is difficult to make a comparison between the static and dynamic methods because of the difference in the associated displacement amplitudes (the shaker cannot generate a large force, and hence displacement, at low frequencies). When comparing the values as a function of displacement amplitude, there is somewhat greater consistency between the stiffness and damping ratios determined from the two types of loadings. If one compares the actuator- and shaker-based parameters at similar displacement amplitude of 2 to 2.5 mm, the calculated stiffnesses are quite similar, being on the order of 75 kN/mm. The damping ratios show greater variation, with the shaker-based values of 20 to 50% being higher than the 20 to 30% from the actuator-based load displacement loops. The half-power bandwidth approach gives values slightly lower than those of the actuators. Given the irregularity of the shaker-based damping ratios, it is unclear if this is a real effect or an artifact of the methodology used to interpret the dynamic shaker data. It seems

reasonable, however, to state that the pile cap system has a damping ratio of at about 20% and decreasing somewhat increasing static displacements level.

6 Pile Cap with Densely Compacted Sand Backfill – Results and Discussion

6.1 Introduction

The pile cap with densely compacted clean sand backfill was tested on the 25th of May, 2008. Compaction of the sand material was done on the 23rd and 24th of May. The static and dynamic loading results will be discussed in this chapter. No significant deviations from the general test procedure occurred during this test.

6.2 Load-Displacement Results

A summary of key test features is presented in Table 6.1. The loads in Table 6.1 correspond to the peak load applied by the actuators at the end of each static push to the target displacement level. The table also specifies the order (first or second) in which cyclic or dynamic loadings from the actuators and shaker, respectively, were applied. . Figure 6.1 below shows the entire load verses pile cap displacement relationship, with static pushes, actuator cycles and shaker cycles being represented by green blue and read data points, respectively.

During the loading of the pile cap, a differential in cap displacement was observed between the east and west sides of the cap. The maximum differential, based on the top two string potentiometers, was 4.3 mm, with the west side leading. The differential

displacement can be explained in part by the different stiffness of the drilled shafts used in the reaction foundation. The west shaft is somewhat stiffer than the east shaft (see Taylor, 2006), causing the west side of the pile cap to move more than the east side. We attempted to mitigate this differential movement by applying uneven loads in the actuators, but some differential movement still occurred. The reported pile cap displacements are based on the median displacement measured by the string potentiometers mounted to the pile cap.

Table 6.1 Summary of test with densely compacted sand backfill

Displacement Interval	Displacement (mm)	Actuator Load (kN)	Actuator Cycles	Shaker Cycles
1	2.8	428	First	Second
2	6.6	719	Second	First
3	11	1043	First	Second
4	16	1184	Second	First
5	22	1616	First	Second
6	30	2087	Second	First
7	37	2406	First	Second
8	46	2748	Second	First
9	53	2931	First	Second
10	57	3036	Second	First
11	64	3232	First	Second

6.3 Passive Earth Pressure

Figure 6.2 shows three load-displacement responses (curves) for the pile cap: one for the response with the backfill in place (referred to as the total response), one for the response with no backfill present (referred to as the baseline response), and one showing the passive earth response of the backfill (obtained by subtracting the baseline response from the total response). The curves show that total response and baseline response

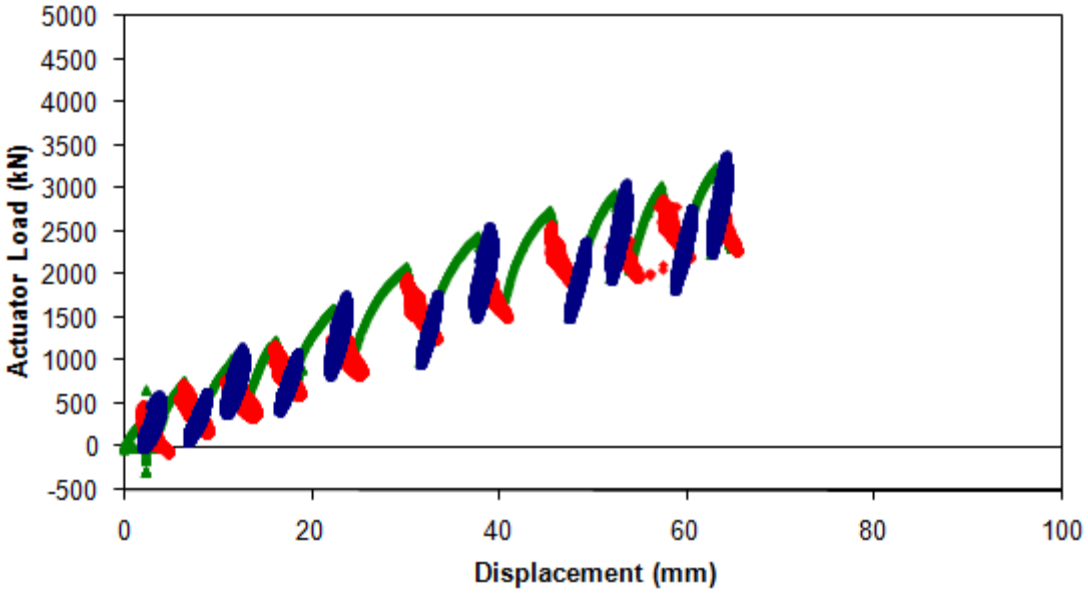

Figure 6.1 Complete load displacement relationship for pile cap with densely compacted sand backfill

increase at different rates until approximately 48 to 50 mm of displacement, depending on visual interpretation). At that point, the backfill response levels off as the baseline and total response increase at approximately the same rate. This leveling off is interpreted as the point when the backfill material is at failure. Hence, the ultimate passive resistance of the backfill is developed at a displacement of approximately 48 to 50 mm, which corresponds to a displacement to wall height ratio (Δ_{max}/H) of 0.029 to 0.03 (say 3%).

6.3.1 Measured versus Calculated Passive Earth Pressure

Passive earth pressures were calculated using the modified PYCAP spreadsheet. Table 6.2 summarizes key inputs and outputs for the three cases analyzed while Figure 6.3 shows the measured and calculated passive earth pressure curves for each case. Case I is based strictly on laboratory-determined ultimate values for shear strength, interface

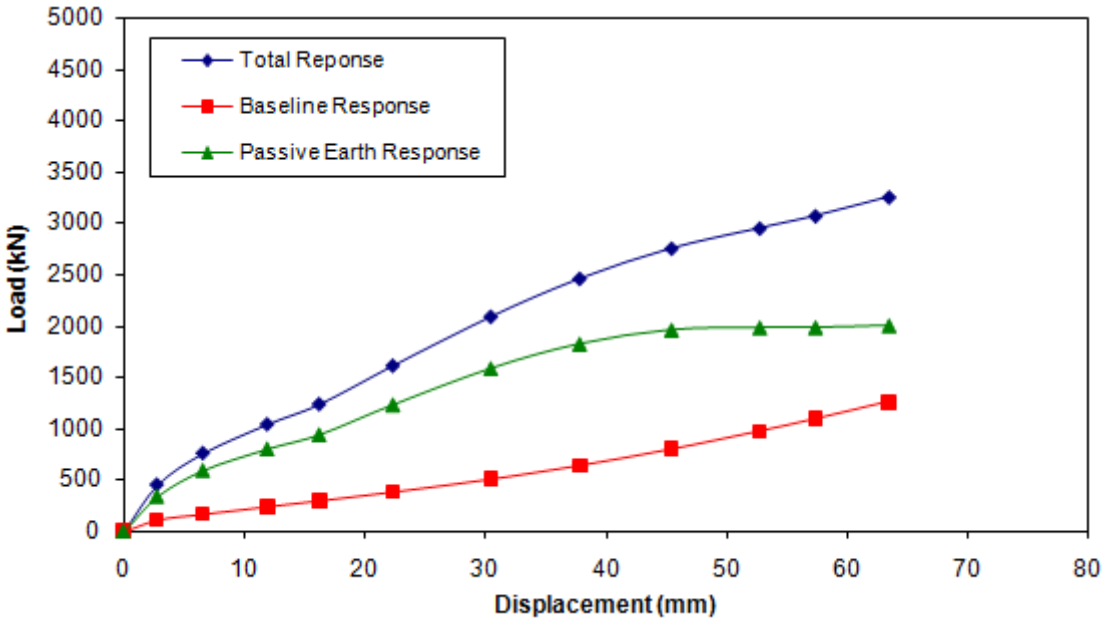

Figure 6.2 Total, baseline and passive earth responses for pile cap with densely compacted clean sand backfill

friction angle and initial modulus. Case II is identical to Case I except that the internal friction angle is the peak value and the interface friction angle is changed by the calculated δ/φ ratio presented earlier. Case III is similar, except an interface friction angle has been changed to match the δ/ φ ratio determined by Cole and Rollins (2006) for a different pile cap using the same type of backfill material and the initial modulus is changed to better fit the initial slope of the measured data. For Case I, the calculated ultimate passive resistance is slightly less than the measured ultimate passive resistance. Case II predicts an ultimate passive resistance 47% greater than Case I. Case III matches the initial slope and the ultimate value of the measured resistance line. Comparing the modulus values with ranges suggested by Mokwa and Duncan (2001), those used in Case I and II are consistent with preloaded or compacted soil, while the modulus value used in Case III is consistent with that suggested for the normal range. Overall the hyperbolic

model used in PYCAP appears to match well with the observed data when ultimate shear strengths and a δ/φ ratio of 0.75 are used.

Table 6.2 Summary of load-displacement analyses using PYCAP for densely compacted sand backfill

Parameter	Case I	Case II	Case III
φ (°)	40.5	43.3	40.5
c (kPa)	0	0	0
δ (°)	29.4	31.9	30.5
γ_m (kN/m3)	18.3	18.3	18.3
E (kPa)	39700	39700	28700
ν	0.26	0.26	0.26
k (kN/mm)	240	240	170
Δ_{max} (mm)	49	49	49
Δ_{max}/H	0.029	0.029	0.029
R_f	0.80	0.76	0.71
R_{3D}	1.83	2.00	1.86
K_p	12.5	16.4	12.5

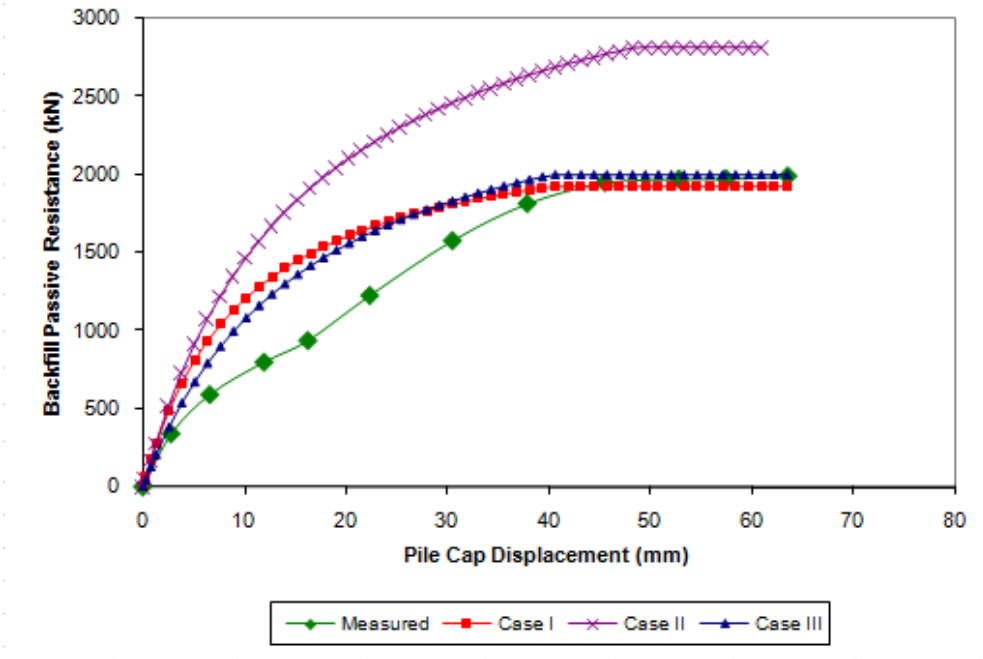

Figure 6.3 Comparison of measured and PYCAP-based calculated passive earth pressure for densely compacted clean sand backfill

Passive earth pressures were also calculated using ABUTMENT and the LSH methodology. Table 6.3 summarizes key inputs and outputs for the cases analyzed while Figure 6.4 shows the measured and calculated passive earth pressure curves for each case. Case I is based strictly on laboratory-determined values for ultimate shear strength and is the same as Case I in analyses performed using PYCAP. Case II is the same as Case I except the peak friction angle has been used. The measured data lies between the two curves. Case III is a result of adjusting Case I to include some cohesion and match the peak resistance. A relatively small amount of 4 kPa was used. This value is interestingly the same value as was used by Shamshabadi et al. (2007) in their analyses of Rollins and Cole (2006) pile cap test results with a similar backfill material. Case IV is the result of doubling the strain parameter to obtain a better match with the initial portion of the curve, but good agreement was not obtained and further adjustments would result in excessive displacement when the ultimate resistance is reached. The best match was obtained in Case III using the ultimate friction angle and a small amount of cohesion.

Table 6.3 Summary of load-displacement analysis using LSH method for densely compacted sand backfill

Parameter	Case I	Case II	Case III	Case IV
φ (°)	40.5	43.3	40.5	40.5
c (kPa)	0	0	4.0	4.0
δ (°)	29.4	31.9	29.4	29.4
γ_m (kN/m^3)	18.3	18.3	18.3	18.3
□$_{50}$	0.002	0.002	0.002	0.004
ν	0.26	0.26	0.26	0.26
R_f	0.98	0.98	0.98	0.98
R_{3D}	1.84	2	1.84	1.84
K_p	10.9	14.1	13.2	13.2

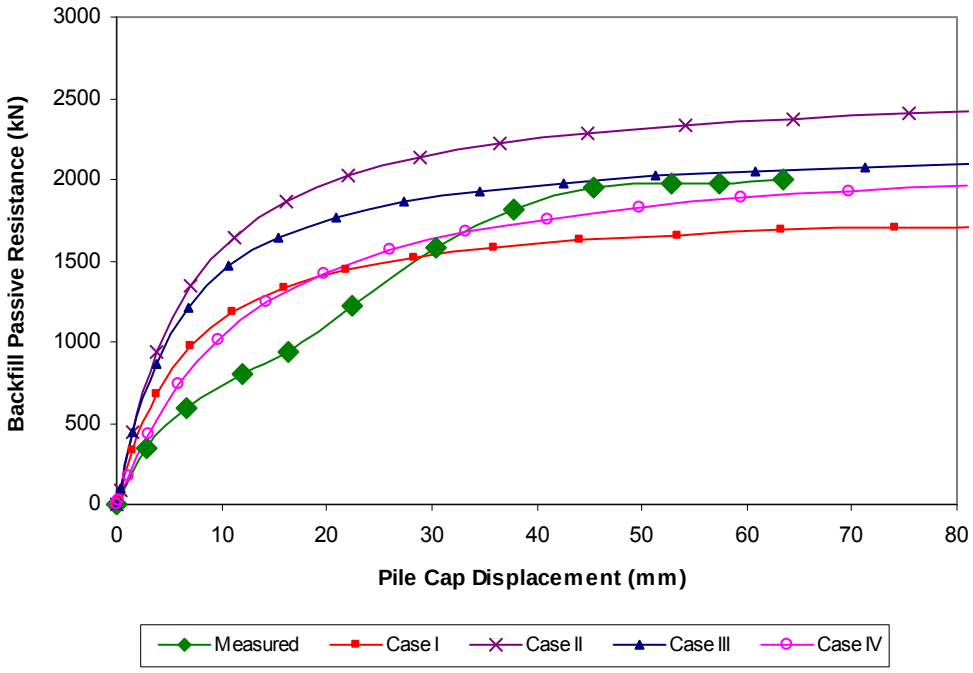

Figure 6.4 Comparison of measured and LSH-based calculated passive earth pressure for densely compacted clean sand backfill

Figure 6.5 shows the measured passive earth pressure compared to the calculated passive earth pressure using the Caltrans method. For the pile cap geometry the initial slope is calculated to be 39.1 kN/mm and the ultimate passive pressure is calculated to be 1381.4 kN. The ultimate passive pressure is under estimated by approximately 31%. The initial slopes of the calculated and measured pressure are comparable, although the calculated pressure in that region is lower than the measured pressure.

6.4 Static Actuator Cycle Results

Figure 6.6 shows the loop displacement amplitude, stiffness, loop area and damping ratio for the pile cap with backfill in place as a function of pile cap displacement

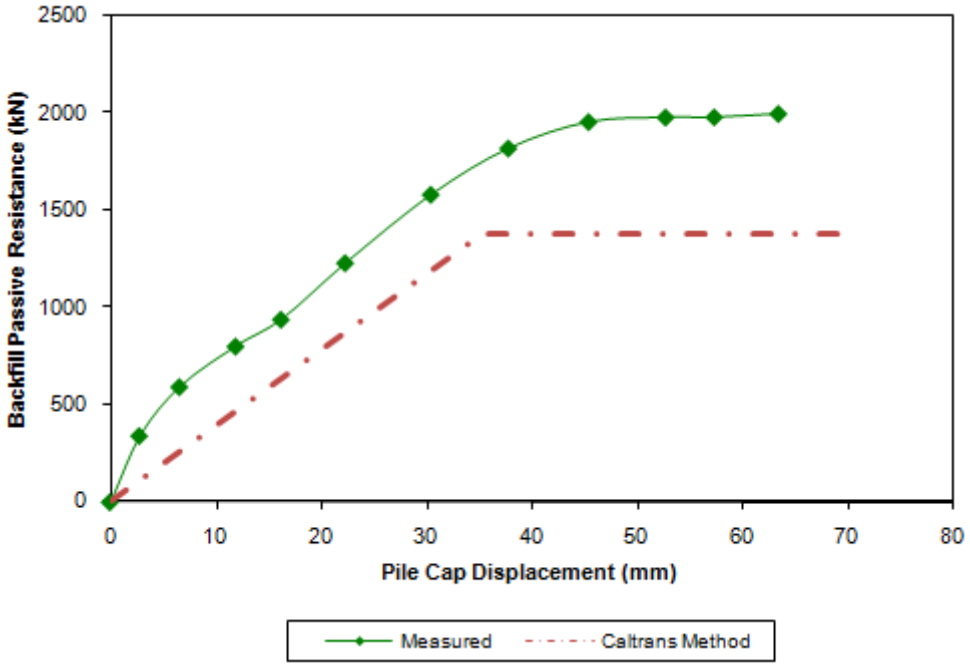

Figure 6.5 Comparison of measured and Caltrans-based calculated passive earth pressure for densely compacted clean sand backfill

for the pile cap with backfill in place. Values are based on the median of the 15 small amplitude cycles performed at each displacement level. The increase in stiffness with pile cap displacement appears to be due to greater mobilization of the backfill soil's passive strength and pile stiffness. The rate of stiffness increase appears to level off in the last several displacement intervals when the ultimate passive resistance of the backfill soil is assumed to be reached. Even with the increasing stiffness and the relatively constant displacement amplitudes and loop areas, the damping remains fairly constant with a median value of 18%.

The stiffness data shows the same sawtooth shape as was seen in the case of the baseline response, due to the order of the static and dynamic cycling phases. Another trend in the test data can be observed in Figure 6.7 which shows typical load-

displacement loops when the actuator cycles are initiated first or second (second meaning that the actuator cycles are performed after the dynamic loading from the shaker). When the static actuator cycles are performed first, there is an increase or drift in the cap's position with little change in stiffness for each progressive loop. However, when the static cycles are performed second after the dynamic shaker loading, no drift is observed. This drift is due to the softening or relaxing of the soil during cyclic loading. Figure 6.7 shows typical actuator loops when the actuator cycles are first and second.

6.5 Dynamic Shaker Cycle Results

The first row of graphs in Figure 6.8 show loop displacement amplitude as well as loop displacement amplitude normalized by the cyclic amplitude of net applied force from the shaker and actuators as functions of the forcing frequency. The second and third rows of graphs show the calculated reloading stiffness and damping, respectively, of the pile cap system. In the left column, these parameters are shown in terms of forcing frequency. If non-linear behavior is present, these properties will also depend on the displacement amplitude; hence, in the right column, these parameters are shown on terms of the displacement amplitude. Based on the data, it appears that both frequency and displacement amplitude must be considered when interpreting test results. The individual line series shown in all of the graphs correspond to different static displacement levels of the pile cap in which dynamic shaker cycles were applied before the slowly applied actuator cycles.

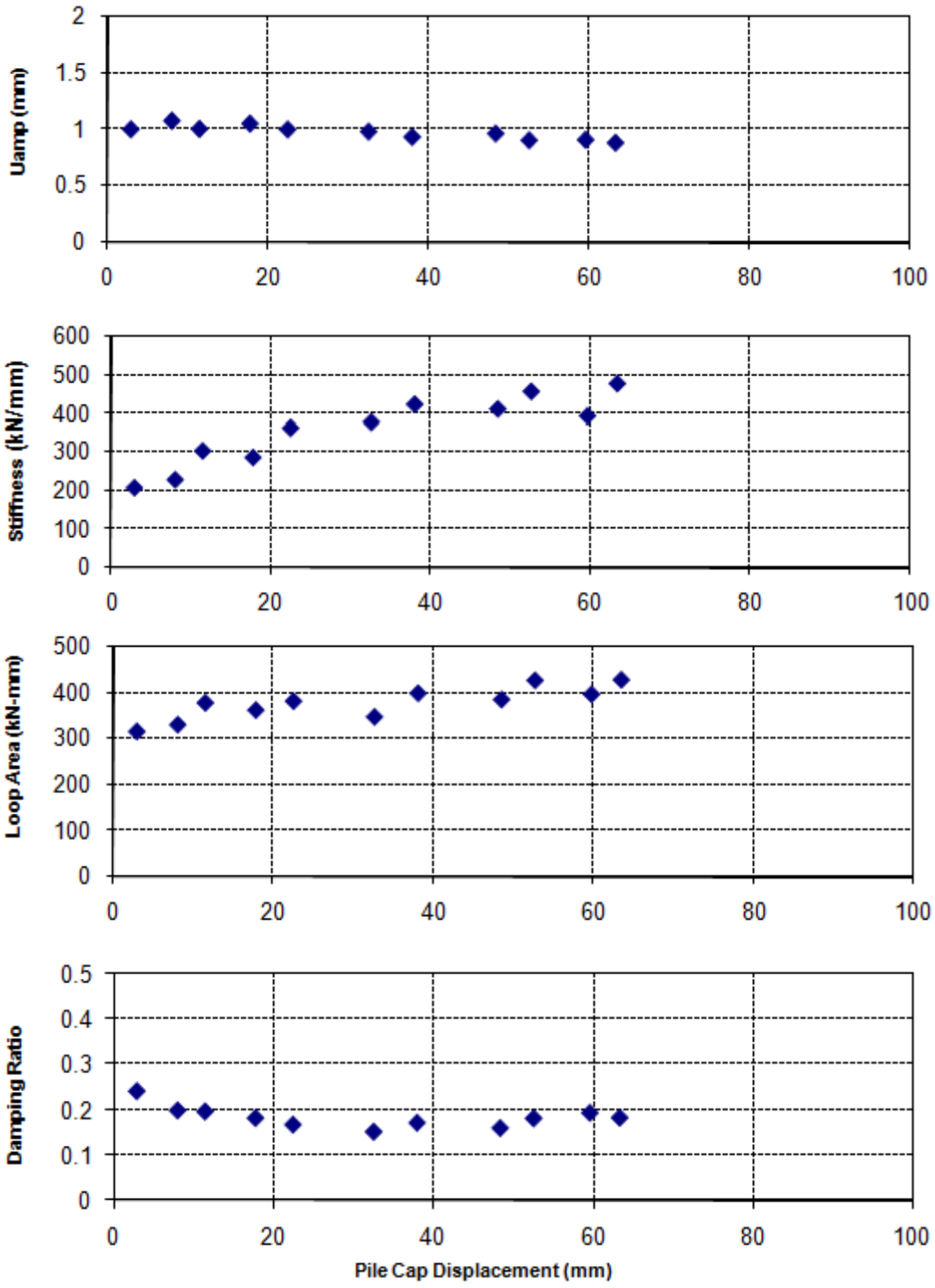

Figure 6.6 Static cycling displacement amplitude, stiffness, loop area, and damping ratio for pile cap with densely compacted clean sand backfill

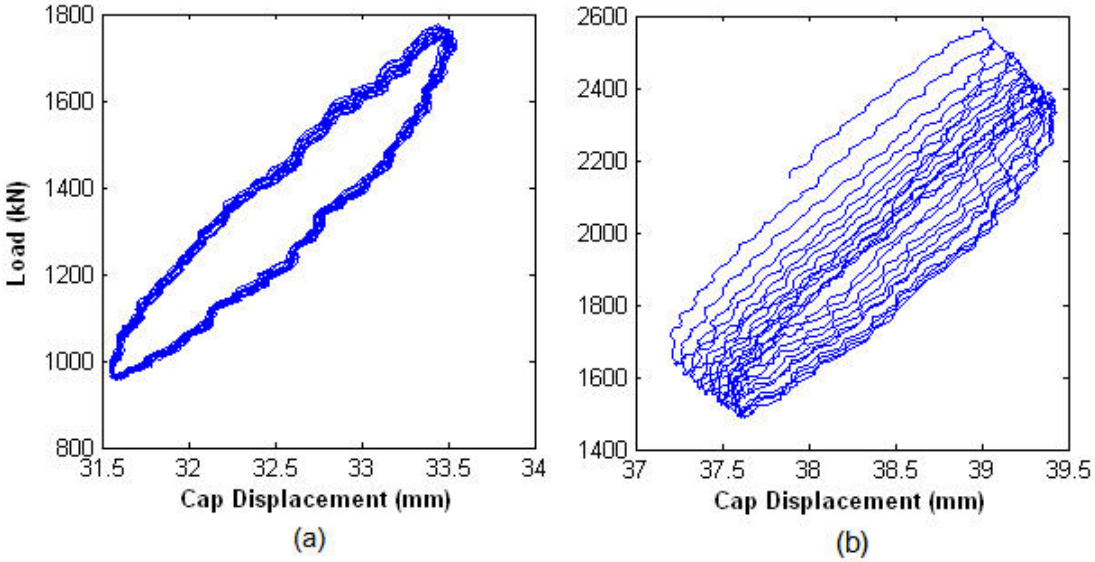

Figure 6.7 Typical actuator loops when actuator cycles are (a) second and (b) first

The peaks in the normalized loop displacement amplitude graph correspond to the damped natural frequency of the system. The damped natural frequency appears to remain fairly constant near 7.5 Hz at all static displacement levels. Reloading stiffness values range from 300 to just over 600 kN/mm, peaking just before the damped natural frequency and dropping afterward. The general trend in the stiffness data shows an increase in stiffness with increasing pile cap displacement level, but there appear to be little difference in the dynamic stiffnesses for the two largest displacement levels of 46 and 57 mm. This is consistent with the concept that at these static displacement levels the backfill soil has already reached its ultimate strength and cannot provide more resistance with increasing pile cap displacement.

Calculated damping values vary greatly with respect to the frequency of the forcing function and displacement amplitude. Damping appears to be a minimum of 5% at about 6 Hz (just less than the damped natural frequency of the pile cap system) and at

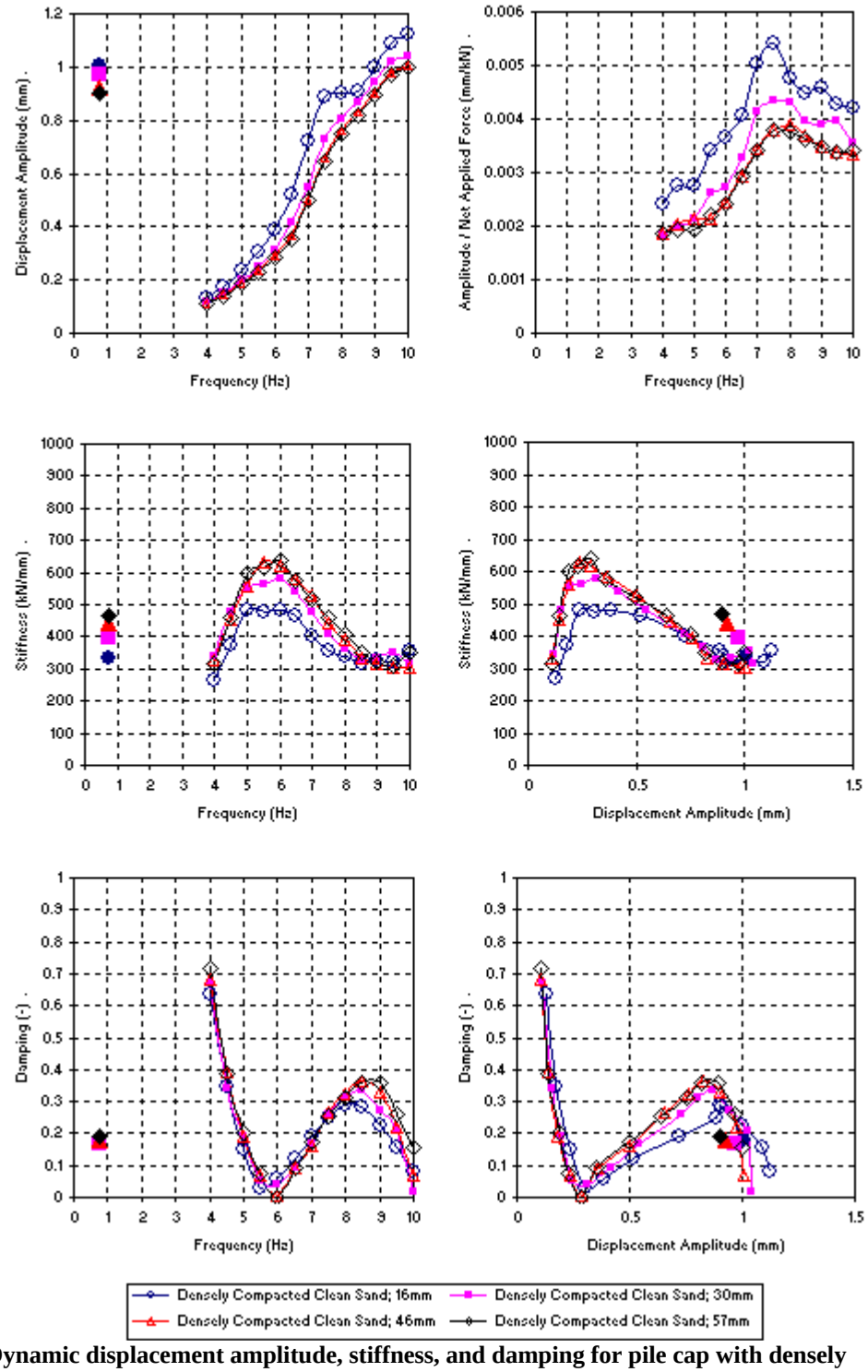

Figure 6.8 Dynamic displacement amplitude, stiffness, and damping for pile cap with densely compacted clean sand backfill

0.3 mm of displacement amplitude. At higher frequencies and displacements, the damping ratio increases up to about 35% (corresponding with the calculated decreasing stiffness) until dropping again at 8.5 Hz (were stiffness reaches a more or less constant value). Unfortunately, the normalized displacement amplitudes were such that the half-power bandwidth approach could not be used. These calculated damping ratios are comparable to those reported by Valentine (2007) for similar test with densely compacted silty sand at another site. His damping ratios ranged from 20 to 40% at frequencies between 4 and 9 Hz.

One of the reasons the stiffness and damping fluctuate in terms of frequency and displacement amplitude is due to the nature of the force displacement loops. As mentioned previously, the shaker was incapable of producing large forces or displacements at low frequencies, therefore causing the load-displacement loops to be influenced by small differences. At about 4 Hz, the load displacement loops become more distinct but their size and orientation change significantly through the remainder of the test. The changes in the load-displacement loops are also significantly affected by the order of the shaker and actuator cycling. Figure 6.9 shows typical load-displacement loops from the shaker cycling.

6.6 Comparison of Static and Dynamic Cycles

Included in Figure 6.7 are displacement amplitude, stiffness and damping ratio calculated from the statically applied cycles from the actuators (~ ¾ Hz) at each represented displacement level (solid points). The values presented are averages of the previous and subsequent actuator cycles. An average value is used to represent stiffness

and damping that would have been calculated if the actuator cycles and been performed before the shaker cycles. In terms of frequency it is difficult to make a comparison between the static and dynamic methods because of the difference in the associated displacement amplitudes (the shaker cannot generate large forces, and hence displacements, at low frequencies).

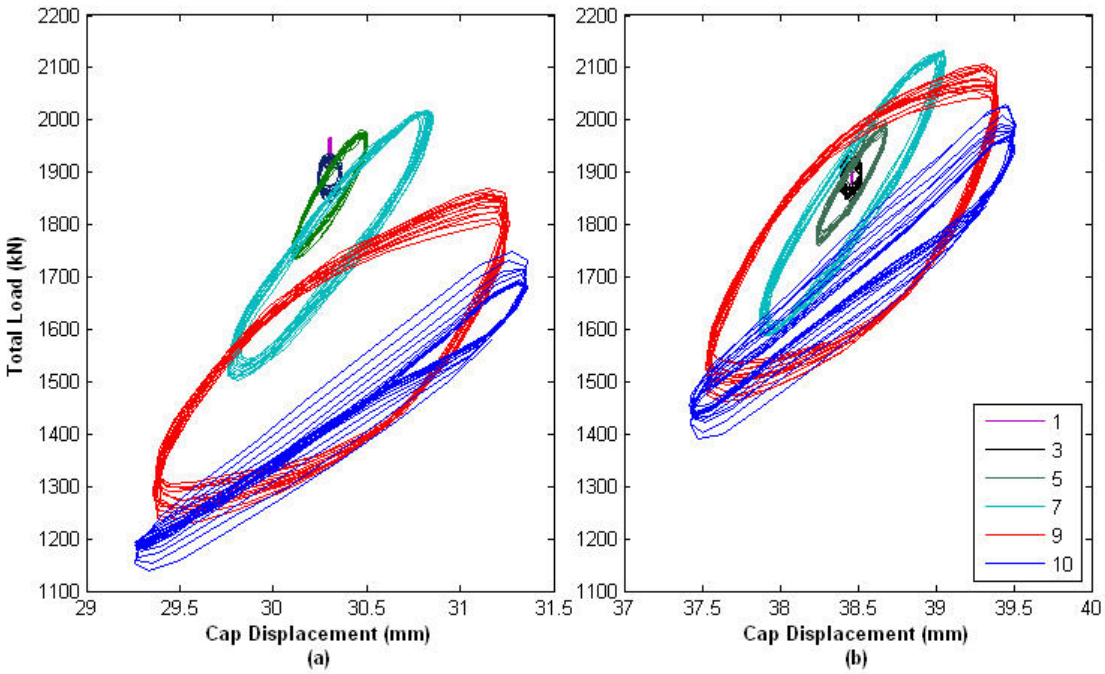

Figure 6.9 Typical load-displacement loops when shaker cycling is (a) second and (b) first

When comparing the values as a function of displacement amplitude, there is somewhat greater consistency between the stiffness and damping ratios determined form the two types of loadings. The dynamic shaker loading as a frequency of 9 Hz resulted in displacement amplitudes (form 0.9 to 1 mm) which are comparable to those produced by the cyclic actuator loading. Comparing the two tests types at this similar displacement

level, the shaker-based stiffnesses are about 325 kN/mm whereas the range of actuator-based stiffness goes higher from 325 to about 450 kN/m. Damping ratios are quite similar, being between 15 and 20%. This similar amount of damping suggests that dynamic loadings do not appreciably increase the apparent resistance of the pile cap relative to slowly applied cyclic loadings.

6.7 Pressure Cell Results

Figure 6.10 shows the pressure measured by the pressure cells with depth at the end of each static push interval. The pressure cells show general trends as expected of increasing pressure with depth and increasing magnitude with increasing pile cap displacement. The bottom pressure cell seems not to follow this trend, with pressure decreasing to near zero after the first two displacement levels. This behavior could result from a rotation of the pile cap or a malfunction of the cell, and this behavior is further discussed later. The top pressure cell also appears to not entirely follow the trend, reaching a plateau at about 125 kPa at a displacement of about 37 mm, and then decreasing slightly in pressure to 110 kPa during the last four push intervals. The peak value in the top pressure cell generally coincides with the displacement level at which the backfill appears to reach its ultimate strength, with the lower cells (excluding the bottom one) showing progressively smaller gains in pressure with increasing displacement.

Figure 6.11 shows the sum of pressure measured by the pressure cells compared to the total and backfill responses. This backfill force was calculated by multiplying each pressure by the respective contributory areas of the pile cap face. This figure suggests that the flushly embedded pressure cells may be under-measuring the soil pressure acting

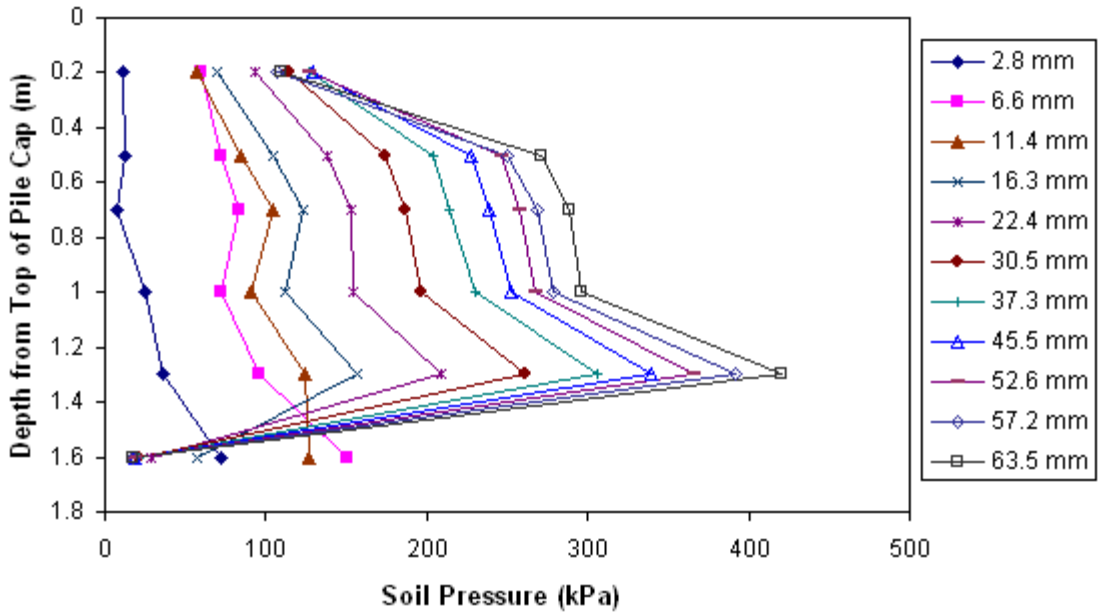

Figure 6.10 Measured pressure on pile cap face with depth at each push interval for densely compacted clean sand backfill

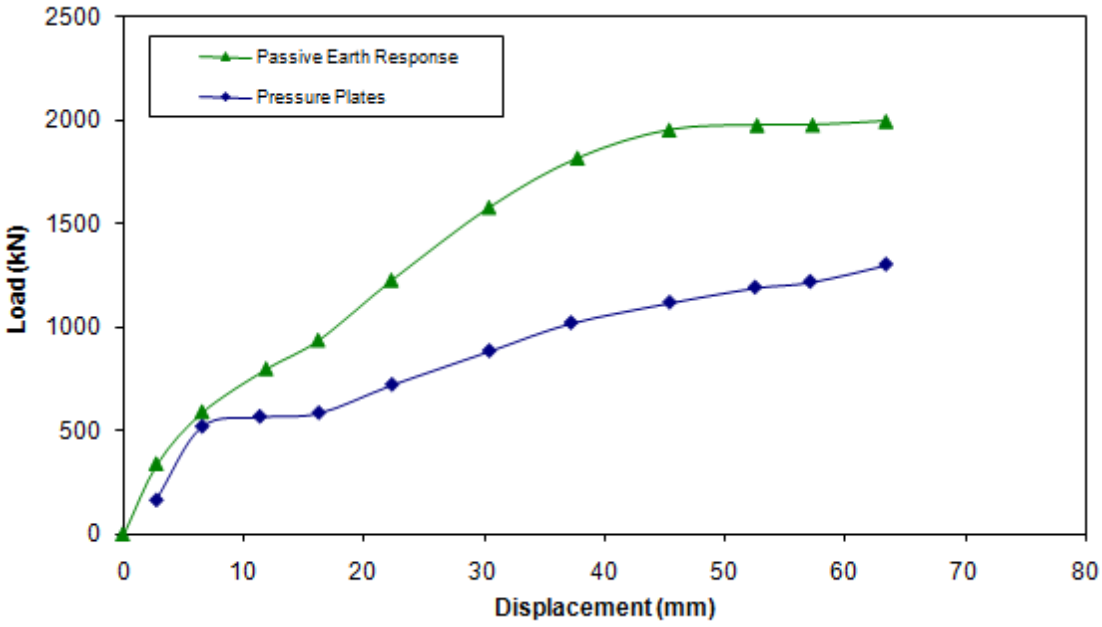

Figure 6.11 Comparison of pressure cell loads to passive earth loads for densely compacted clean sand backfill

on the pile cap. However, the two trends a quite similar in shape. There are several possible reasons for this discrepancy between the two curves, including interface friction differences between soil on the concrete of the pile cap and soil on the steel of the pressure cells, and (much more likely and significantly) three dimensional loading effects where the horizontal fanning of the failure wedge into material beyond the edges of the cap face, and the resulting stress concentrations at those edges, are not fully captured. The elastic stress distribution presented by Douglas and Davis (1964) shows that the pressures on an embedded plate with a horizontal load applied to it are maximum at the edges and minimum in the center. This would be consistent with the data since the pressure cells were located in the center portion of the pile cap. For the geometry of this particular pile cap, Douglas and Davis' solution indicates that a vertical pressure distribution at the center of the pile cap will be approximately 74% of the average pressure distribution acting on the entire loaded face. Douglas and Davis' solution also indicates the amount of pile cap rotation that would be necessary to force the bottom pressure cell to measure negligible pressure is at least an order of magnitude larger than the 2.8 mm (0.1°) maximum rotation experience by the cap. Adjusting the data by Douglas and Davis' ratio of pressure at the center to average overall pressure, there is better agreement between the two curves.

6.8 Cracking and Elevation Change of Backfill

Figure 6.12 shows the visible cracks mapped during the test at each pile cap displacement level. The location of cracks which formed in the backfill material indicates the presence and location of failure surfaces in the material. The cohesionless

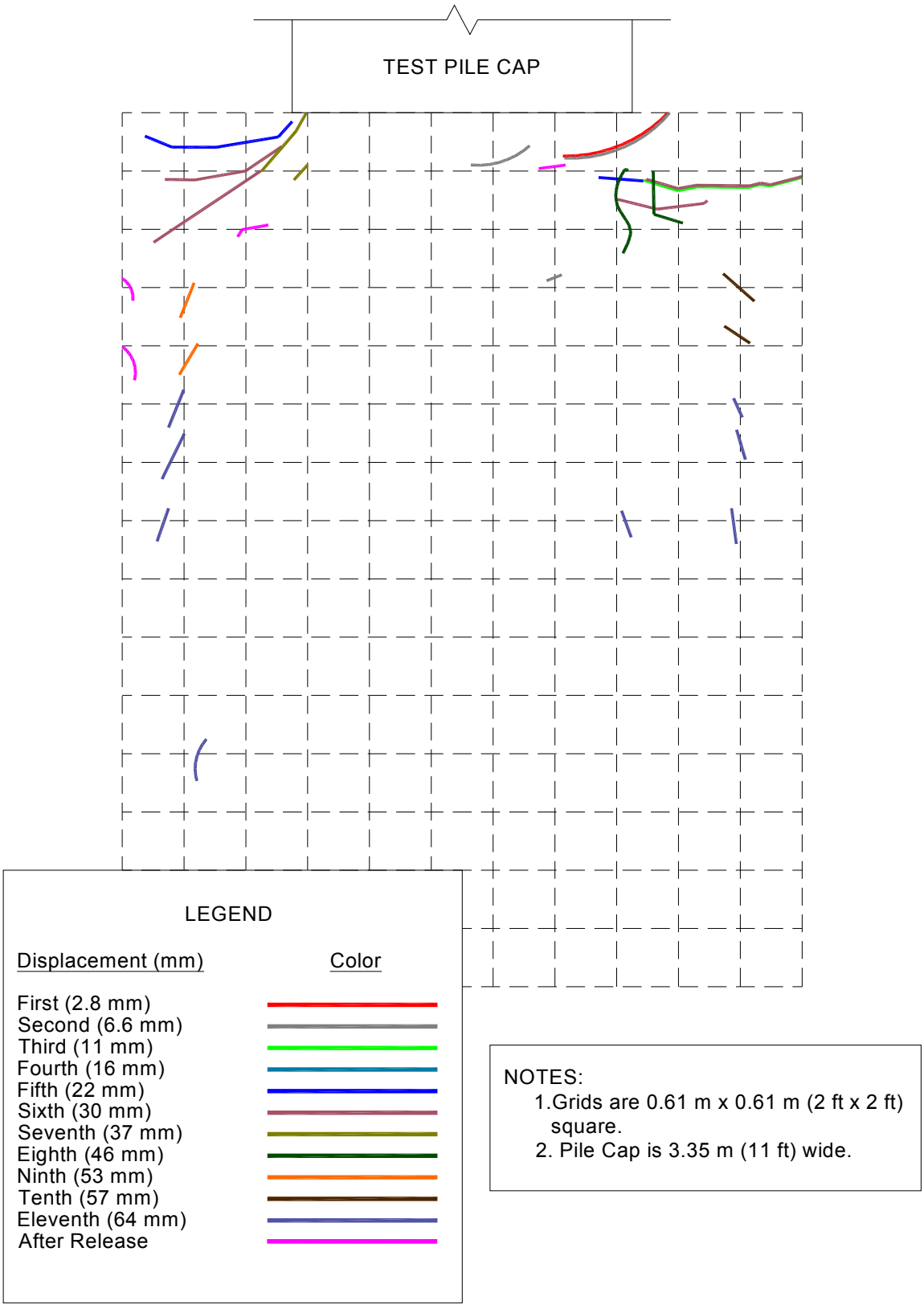

Figure 6.12 Observed cracks in densely compacted clean sand backfill

nature of the backfill material, together with the dynamic vibration due to the shaker, tended to cause the soil grains to shift around during testing, and thus potentially obscuring cracks. The majority of the visibly identifiable cracks are concentrated around the edges of the cap face. These cracks are due to the internal shear stresses radiating out from the cap face and reflected the three dimensional shape of the failure zone. Another distinct set of cracks are the small echelon cracks located approximately 0.6 m from the edges of the backfill zone. The distance between these two sets of cracks is slightly more than 5-½ m, which closely matches the 6 m wide failure wedge calculated using the three dimensional correction factor from the PYCAP spreadsheet program. Unfortunately, cracking potentially suggested the toe of the failure wedge was not observed.

Figure 6.13 shows a contour plot of the change in elevation of the backfill material. The maximum elevation change is 35 mm at 1.83 m from the face of the cap. According to calculations, a log spiral failure surface should daylight at approximately 5.8 m from the face of the cap. Figure 6.13 shows the majority of the of the elevation change occurring within the first 4 m of backfill suggesting the daylighting of the failure wedge just beyond that zone. This is better seen in Figure 6.14 which shows a cross section of the pile cap and backfill zone together with a predicted log-spiral failure surface and the mean heave. The heave data has been multiplied by ten so that it can be seen relative to the geometry of the failure surface. (The coordinate system in the figure is relative to the origin of the log-spiral failure surface). The majority of the measured heave clearly occurs within the zone suggested by the log-spiral failure surface.

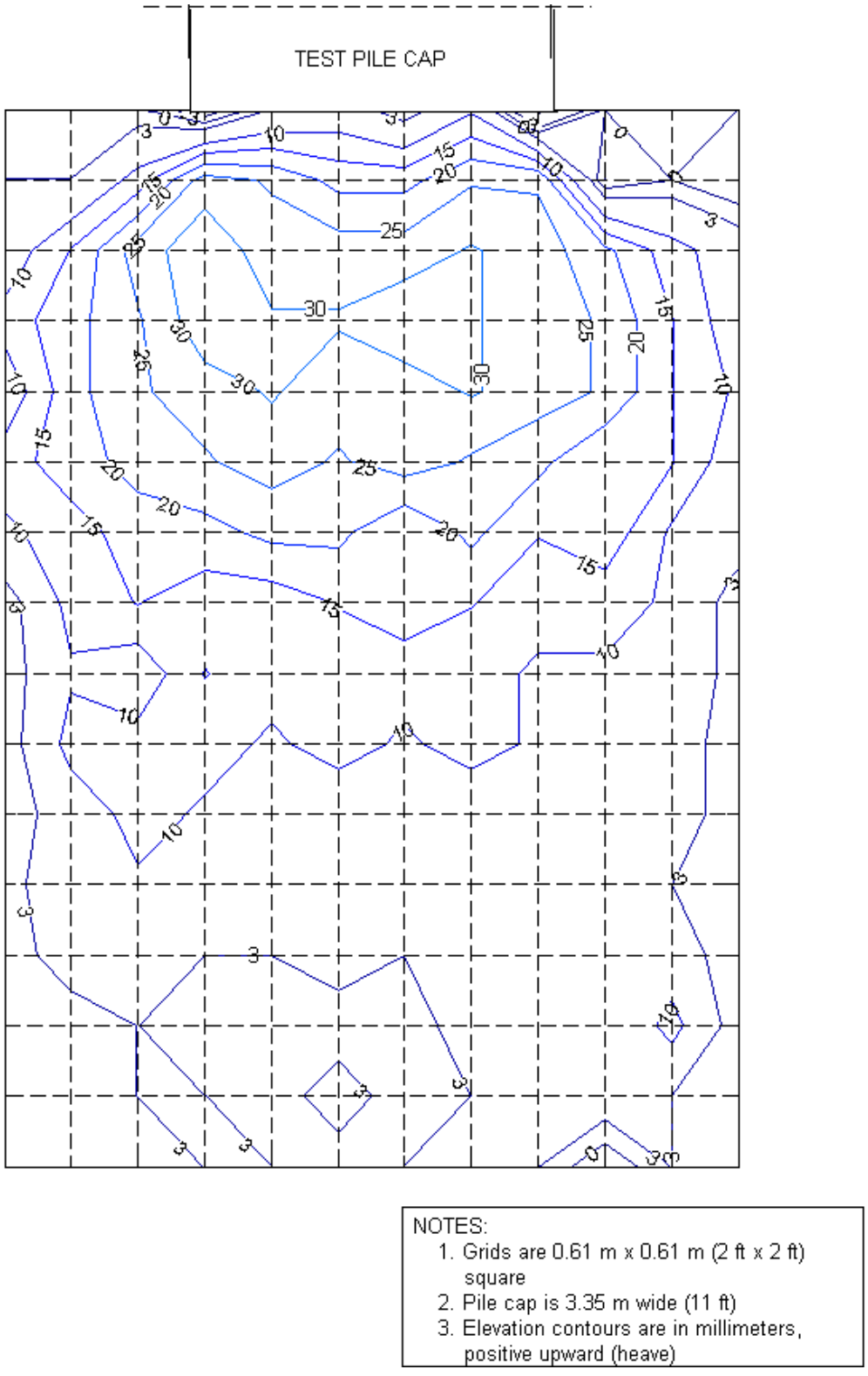

Figure 6.13 Contour plot of elevation change in densely compacted clean sand backfill

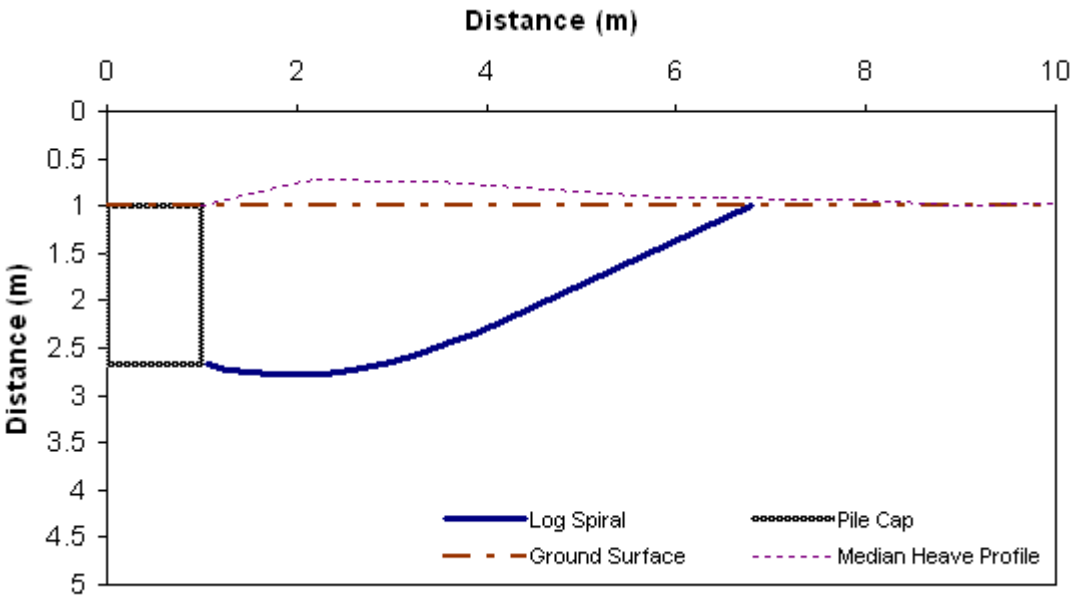

Figure 6.14 Cross-section view of pile cap and densely compacted clean sand backfill

6.9 Horizontal Movement of Backfill Soil

Figure 6.15 and Figure 6.16 show the surface displacement of the backfill and associated calculated strain, respectively. The backfill displacement ranges from 63 mm (100% of cap displacement) at the cap face to 15 mm (24% of cap displacement) at 5.5 m from the cap face. The compressive strain ranges from 0.02 to 0.005 within the backfill zone. The strain distributions is highest at the pile cap face as expected and is relatively uniform with distance away from the cap up to the maximum distance monitored.

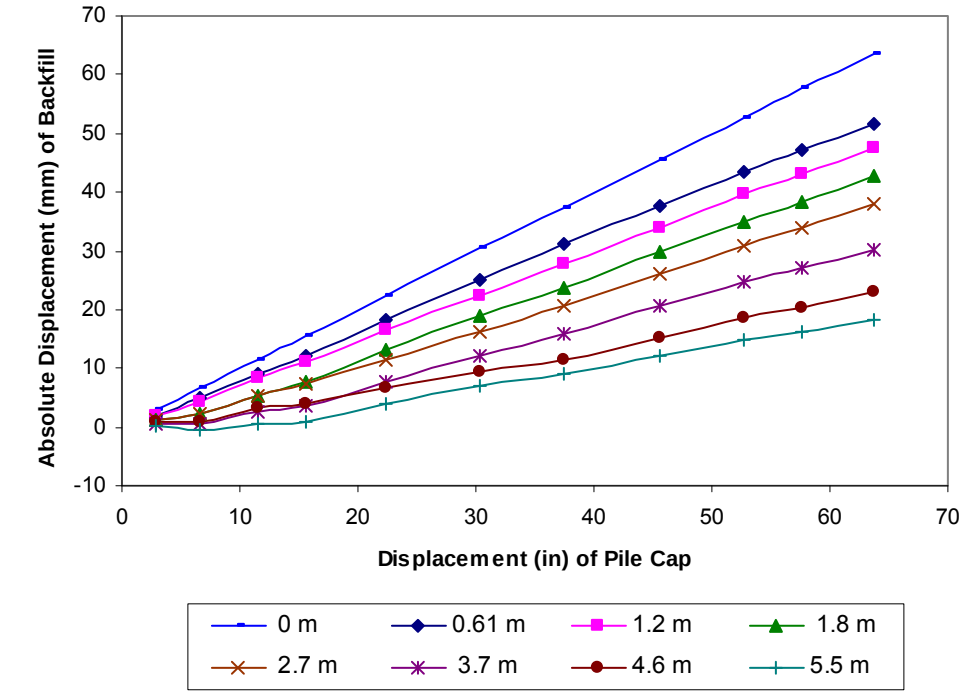

Figure 6.15 Displacement of monitoring points in densely compacted clean sand backfill

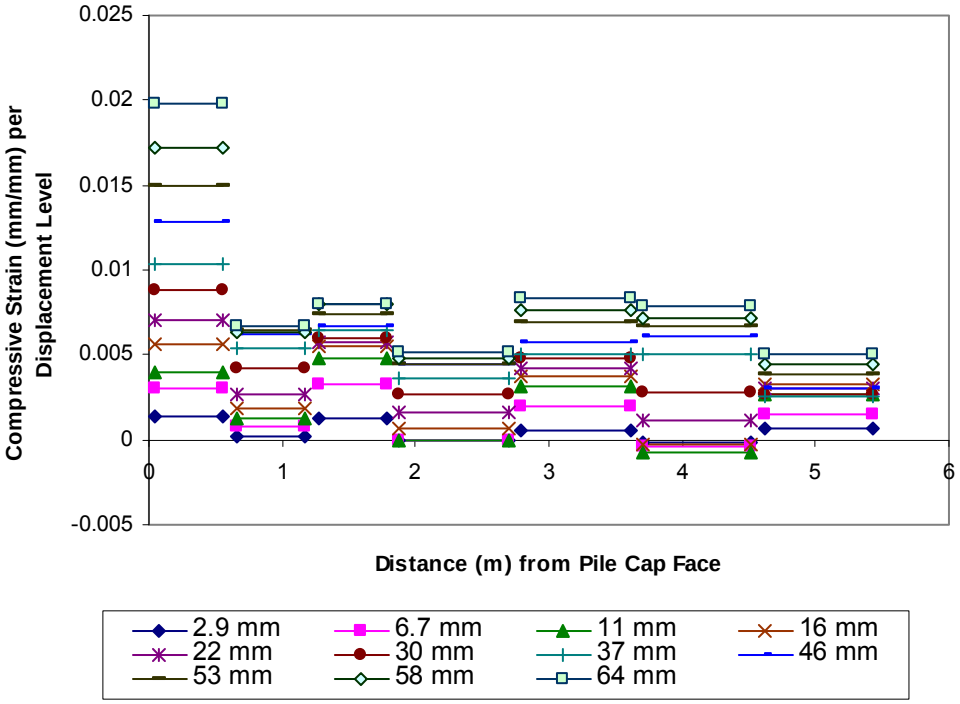

Figure 6.16 Strain per displacement level in densely compacted clean sand backfill

7 Pile Cap with Loosely Compacted Sand Backfill - Results and Discussion

7.1 Introduction

The pile cap with loosely compacted clean sand backfill was conducted on the 29th of May, 2007. The compaction of the sand into the backfill zone was done on the 27th and 28th of May. No significant deviations from the general test procedure occurred during this test, excepting that the test ended prematurely without reaching the intended maximum target displacement because of a mechanical failure in the eccentric mass shaker.

7.2 Load-Displacement Results

A summary of key test features is presented in Table 7.1. The loads in Table 7.1 correspond to the peak load applied by the actuators at the end of each static push to the target displacement level. The table also specifies the order (first or second) in which cyclic or dynamic loadings from the actuators and shaker, respectively, were applied. Figure 7.1 below shows the entire load verses displacement relationship of the pile cap with static pushes, cyclic actuator loadings, and the dynamic shaker loadings being represented by green, blue and red data points, respectively.

Table 7.1 Summary of test with loosely compacted sand backfill

Displacement Interval	Displacement (mm)	Actuator Load (kN)	Actuator Cycles	Shaker Cycles
1	6.0	413	First	Second
2	14	426	Second	First
3	21	599	First	Second
4	28	779	Second	First
5	35	951	First	Second
6	41	1071	Second	First
7	46	1197	First	Second

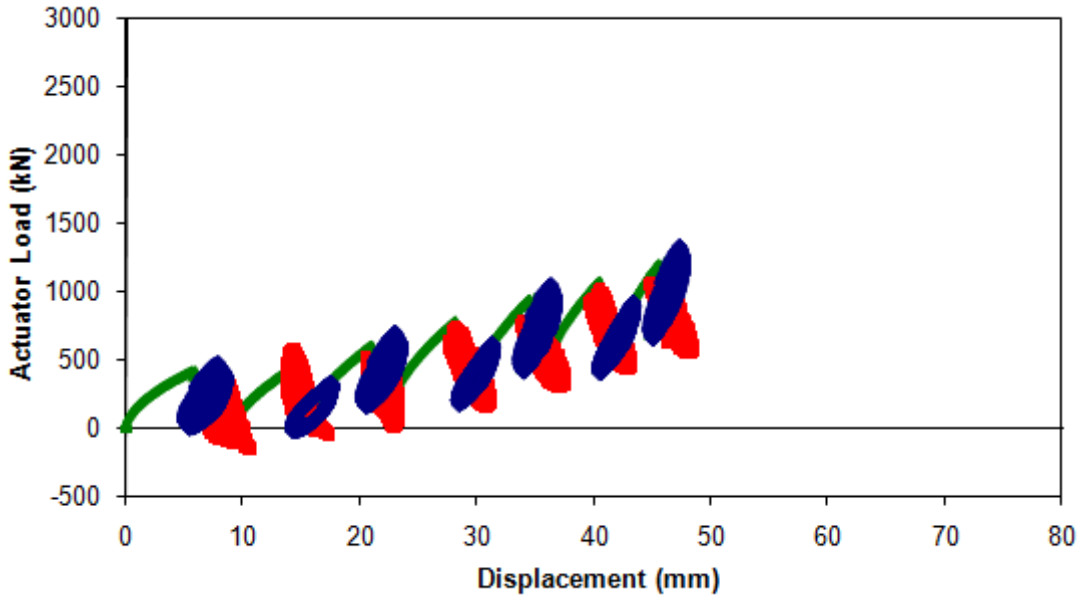

Figure 7.1 Complete load displacement relationship for pile cap with loosely compacted sand backfill

During the test with loosely compacted clean sand backfill, the first static and dynamic cycles seem to have softened the soil to the point that very little increase in load was required to push the pile cap to the second target displacement level. This significant loss in resistance was experienced to a lesser degree at later pile cap displacement levels as well. Inspection of the static loading intervals, shown in Figure 7.1, reveals that their shapes are only slightly concave down. This suggests that the amount of displacement

between test intervals may not have been sufficient enough for the loadpath to return to the static backbone curve (which curve would represent the load-displacement response of the pile cap with backfill if the actuator load had been applied monotonically). It seems that notably more displacement is required to return to the backbone curve upon reloading when the backfill is loosely compacted as compared to when it is densely compacted. Because of this, larger displacement intervals were used during static loadings in later tests performed on other loosely compacted soil types at the site. Unfortunately, the issue was not fully appreciated at the time of the test with loosely compacted clean sand backfill.

7.3 Passive Earth Pressure

Figure 7.2 shows three load-displacement response curves for the pile cap: one for the response with backfill in place (referred to as the total response), one for the response with no backfill present (referred to as the baseline response), and one showing the passive earth response of the backfill (obtained by subtracting the baseline response from the total response. Figure 7.2 shows that after the initial push, the loosely compacted sand backfill provides an additional resistance which is slightly less than the resistance initially provided by the piles and cap acting by themselves. A peak passive force appears to possibly develop by about 37 to 40 mm of displacement which is actually less than the displacement at which the densely compacted sand developed full passive pressure. This is unexpected, given that Clough and Duncan (1991) stated that a loose or medium dense material will require two to four times more displacement to mobilize that a dense material. Although the passive pressure appears to peak at 40 mm,

it is unknown for certain if the passive pressure might have slowly continued to increase had the test continued to a higher displacement levels. Also, a significant amount of this pressure seems to have developed by 6 mm of displacement, after which the earth pressure appears to drop and then later recovers. This behavior is surprising and may be due to the effects of cyclic and dynamic loadings, or possibly even a small error in the baseline response which effects are magnified since the passive resistance of the backfill is also relatively small.

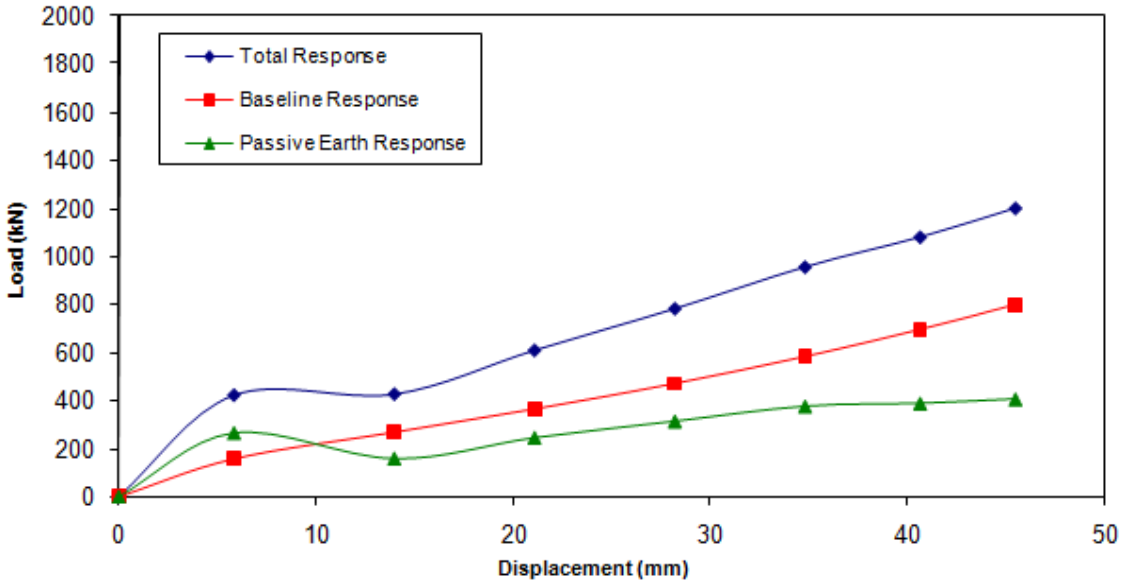

Figure 7.2 Total, baseline and passive earth responses for the pile cap with loosely compacted sand backfill

7.3.1 Measured versus Calculated Passive Earth Pressure

Passive earth pressures were calculated using the modified PYCAP spreadsheet. Table 7.2 summarizes key inputs and outputs for the two cases analyzed while Figure 7.3 shows the measured and the calculated passive earth pressure curves for each case. With the loosely compacted clean sand, the material provided an initial increase in passive

resistance followed by an unexpected drop. The passive resistance again rises following the drop until approximately 40 mm of displacement were the resistance starts to level off to a maximum. As mentioned previously, there was an equipment malfunction during this test, which prematurely ended the test and prevented the collection of data for greater displacement levels.

Table 7.2 Summary of load-displacement analysis using PYCAP for loosely compacted sand backfill

Parameter	Case I	Case II
φ (°)	37	26.5
c (kPa)	0	0
δ (°)	26.1	18
γ_m (kN/m3)	16.5	16.5
E (kPa)	30600	15800
N	0.28	0.28
k (kN/mm)	190	100
Δ_{max} (mm)	40	40
Δ_{max}/H	0.024	0.024
R_f	0.851	0.892
R_{3D}	1.648	1.351
K_p	8.67	3.9

Case I is the best estimate case based on laboratory testing. The ultimate passive resistance from Case I is 174% greater than the measured resistance. The initial modulus value used in Case I is consistent with the preloaded or compacted range given by Mokwa and Duncan (2001). Case II is similar to Case I, except that the initial soil modulus was lowered to match the initial measure slope and the internal friction angle was lowered to 26.5 degrees to better match the ultimate passive resistance. The lowered modulus value is within the normal range suggested by Mokwa and Duncan (2001). The friction angle needed to match the measured pressure is quite a bit lower than what would likely be expected. According to the NAVFAC manual a SW material with a relative

density of 57% would have a friction angle around 34 degrees. This disagreement seems to suggest that a hyperbolic model may be inappropriate to describe the load-displacement response for this backfill with our calculated strength values.

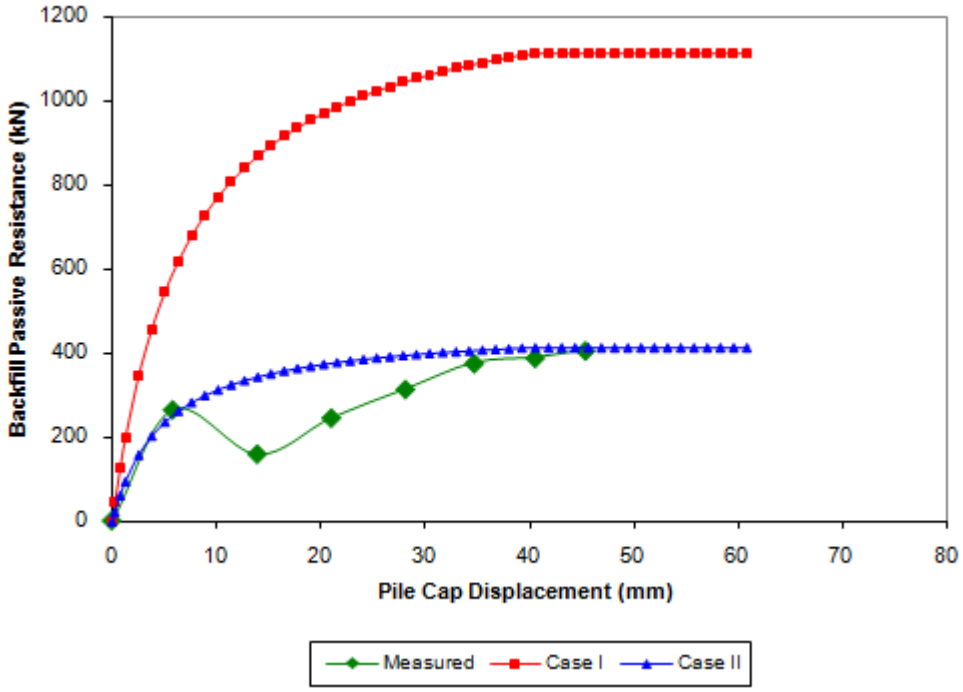

Figure 7.3 Comparison of measured and PYCAP-based calculated passive earth pressure for loosely compacted sand backfill

Passive earth pressures were also calculated using the LSH methodology. Table 7.3 summarizes key inputs and outputs for the cases analyzed while Figure 7.4 Comparison of measured and LSH-based calculated passive earth pressure for loosely compacted sand backfillshows the measured and calculated passive earth pressure curves for each case. Case I is based on the laboratory direct shear test results for ultimate strength, and produces a poor match with the measured earth pressure curve. In Cases II and III, the friction angle has been iteratively reduced to provide a better fit with the data,

and this reduced friction angle is similar to the reduced friction angle used in the PYCAP-based analyses. The interface friction angle has been changed in the two cases to assess the sensitivity of this parameter with the lower friction angle.

Table 7.3 Summary of load-displacement analysis using LSH for loosely compacted sand backfill

Parameter	Case I	Case II	Case III
φ (°)	37	26.5	26.5
c (kPa)	0	0	0.0
δ (°)	26.1	18	19.1
γ_m (kN/m^3)	16.5	16.5	16.5
□$_{50}$	0.003	0.003	0.002
ν	0.28	0.36	0.36
R_f	0.98	0.98	0.98
R_{3D}	1.65	1.35	1.35
K_p	8.1	3.9	3.94

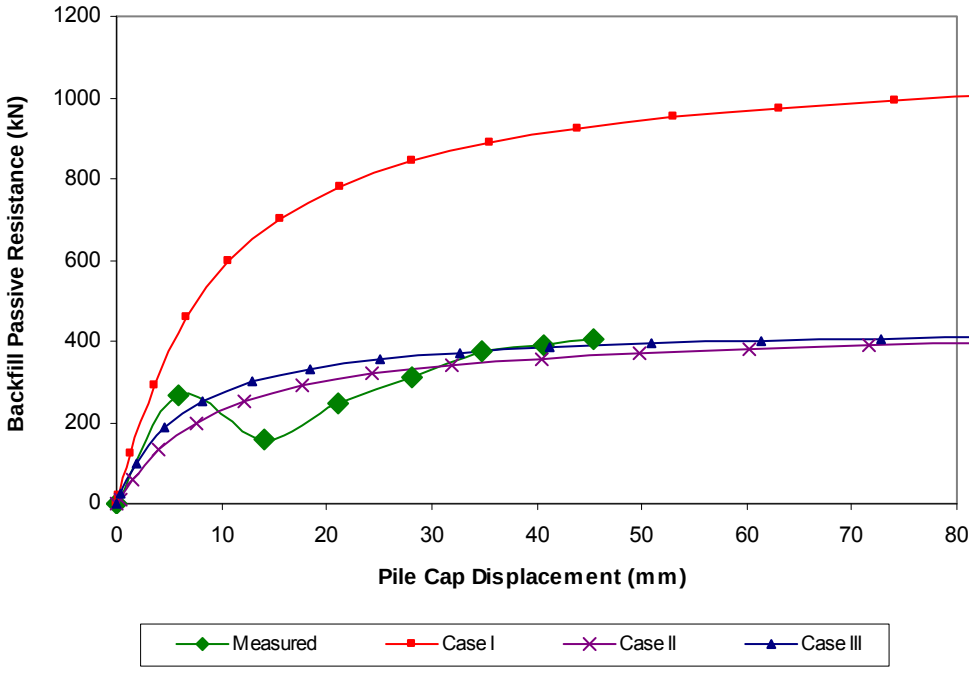

Figure 7.4 Comparison of measured and LSH-based calculated passive earth pressure for loosely compacted sand backfill

Figure 7.5 below shows the measured passive earth pressure compared to the calculated passive earth pressure using the Caltrans method. For the pile cap geometry the initial slope is calculated to be 39.1 kN/mm and the ultimate passive pressure is calculated to be 1381.4 kN. The ultimate passive pressure is over estimated by approximately 240%. The initial slopes of the calculated and measured pressure are comparable, although this assessment is only based on a displacement of 5 mm.

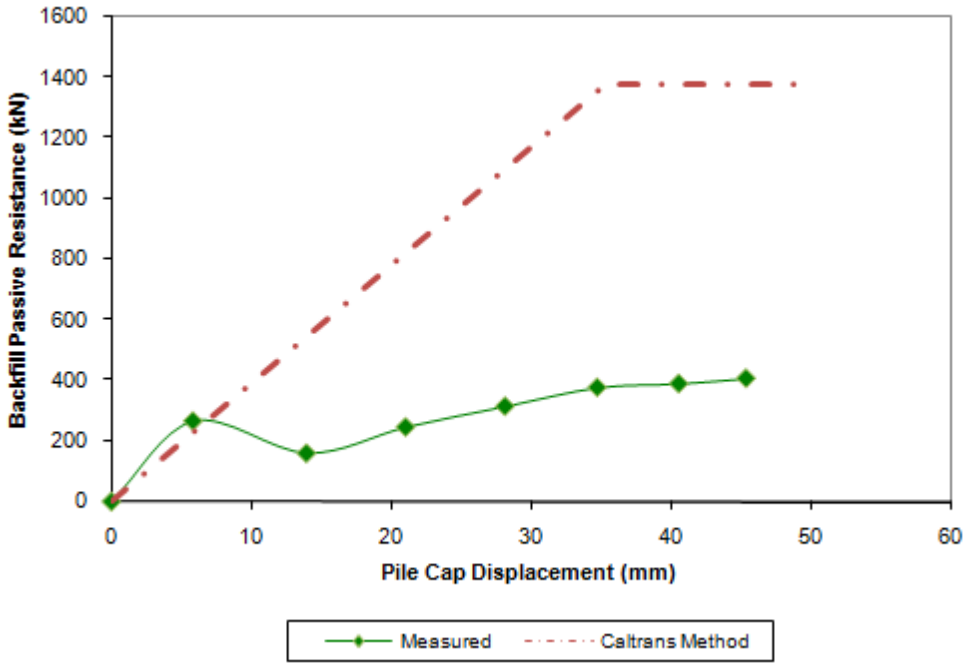

Figure 7.5 Comparison of measured and Caltrans-based calculated passive earth pressure for loosely compacted sand backfill

7.4 Static Actuator Cycle Results

Figure 7.6 shows the loop displacement amplitude, stiffness and damping ratio as a function of cap displacement for the pile cap with backfill in place. Values are based on the median of the 15 low frequency cycles performed at each displacement level The

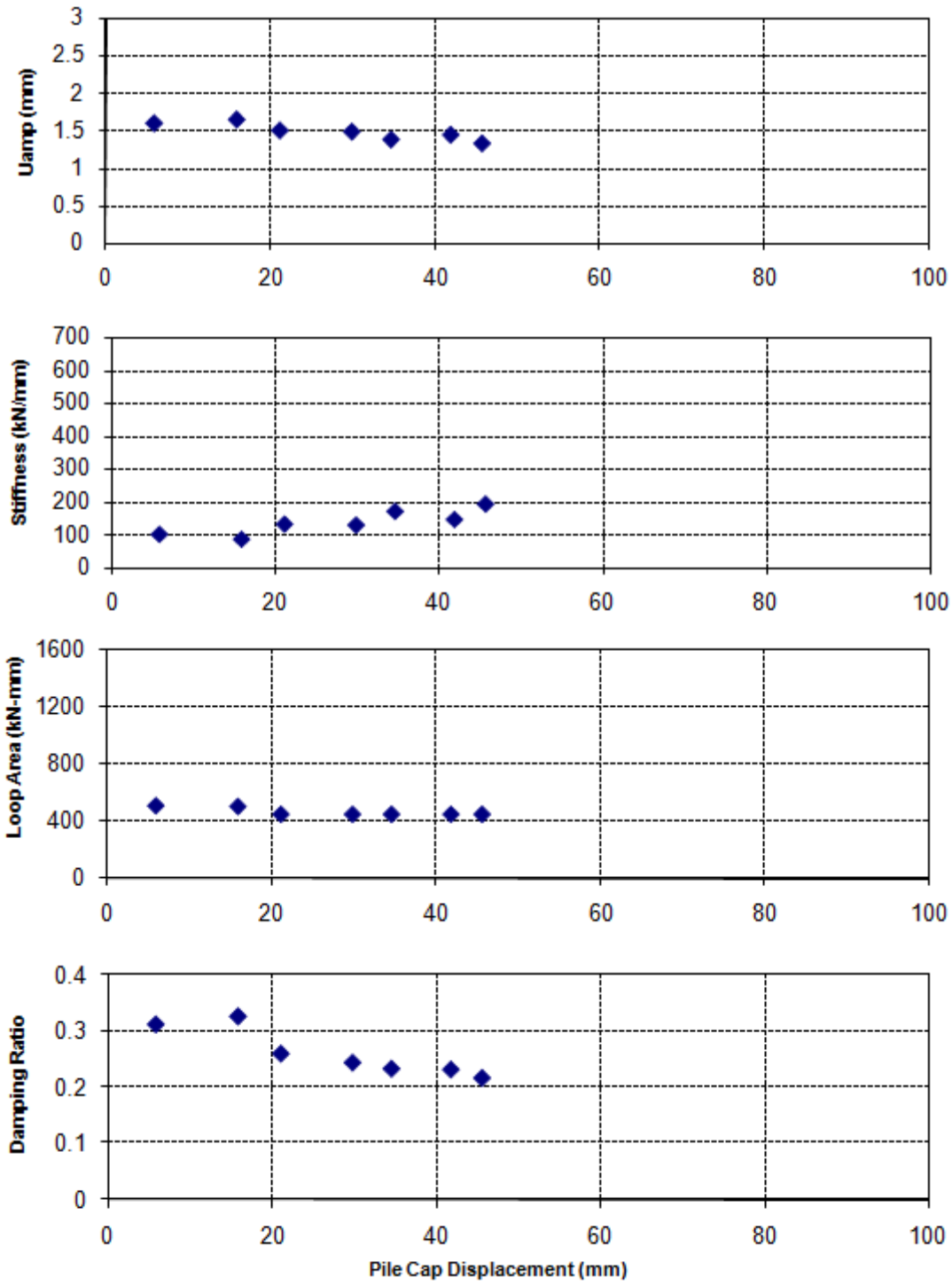

Figure 7.6 Static cycling displacement amplitude, stiffness, loop area and damping ratio for pile cap with loosely compacted sand backfill

displacement amplitude remains fairly constant around 1.5 mm. The stiffness increases from 100 to 200 kN/mm as the cap displacement increases, this appears to be due to greater mobilization of the backfill soil's passive strength and pile stiffness. The stiffness data shows the same sawtooth trend that was observed in the other load tests, due to the order of the static and dynamic cycling phases. The damping ratio decreases fairly linearly from 31% to 21% with an average of approximately 24%. The stiffness and damping values are more similar to those calculated without backfill present than those calculated with the densely compacted sand backfill present.

7.5 Dynamic Shaker Cycle Results

The first row of graphs in Figure 7.7 show loop displacement amplitude as well as loop displacement amplitude normalized by the cyclic amplitude of net applied force from the shaker and actuators as functions of the forcing frequency. The second and third rows of graphs show the calculated reloading stiffness and damping, respectively, of the pile cap system. In the left column, these parameters are shown in terms of forcing frequency. If non-linear behavior is present, these properties will also depend on the displacement amplitude; hence, in the right column, these parameters are shown on terms of the displacement amplitude. Based on the data, it appears that both frequency and displacement amplitude must be considered when interpreting test results. The individual line series shown in all of the graphs correspond to different static displacement levels of the pile cap in which dynamic shaker cycles were applied before the slowly applied actuator cycles.

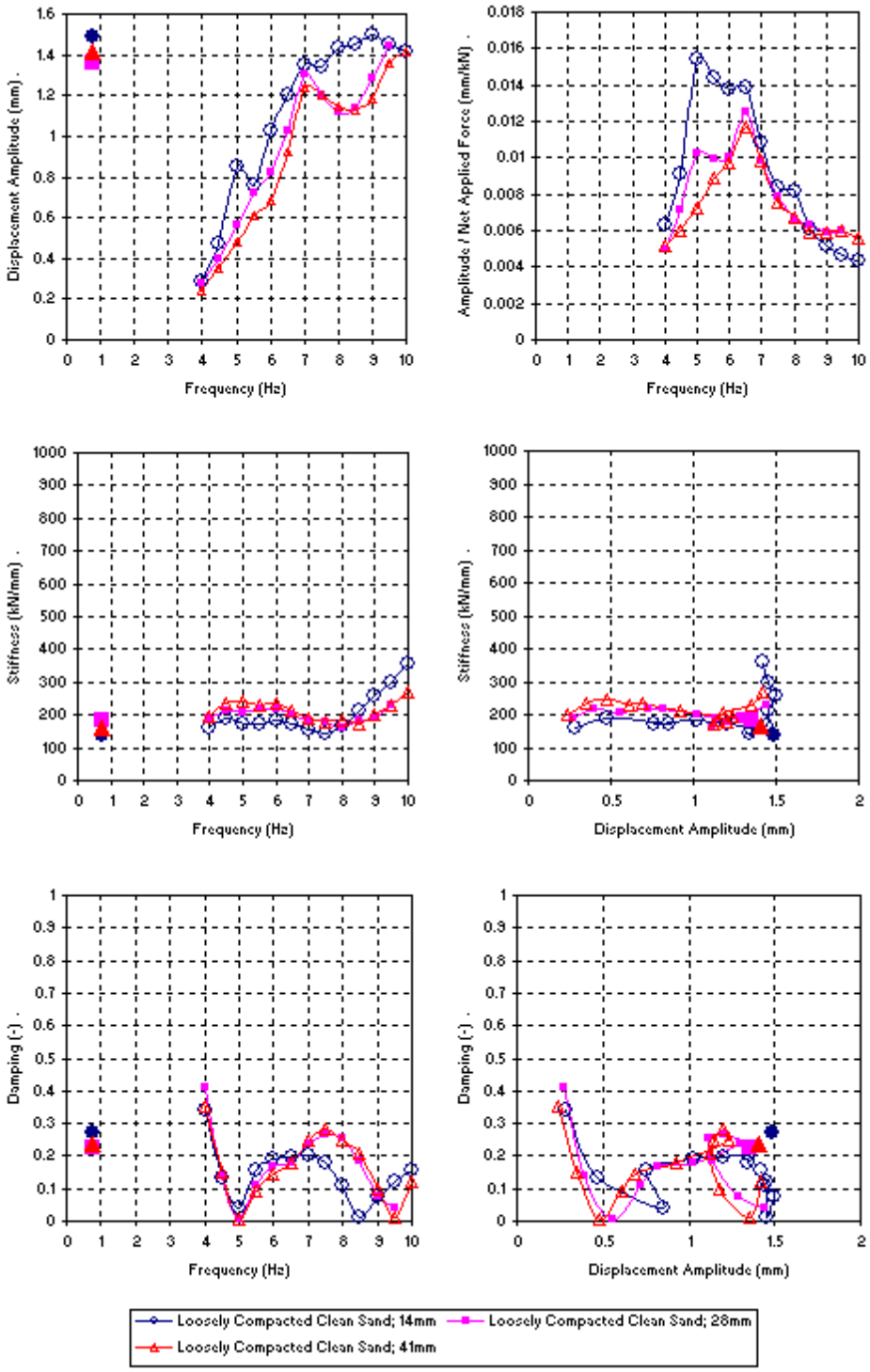

Figure 7.7 Dynamic displacement amplitude, stiffness and damping for pile cap with loosely compacted clean sand backfill

The peaks in the normalized displacement amplitude graph corresponds to the damped natural frequency, which ranges from 5.5 to 6.5 Hz with increasing cap displacement. The displacement amplitudes for the displacement intervals of 28 and 41 mm are close to the same values. Dynamic stiffness ranges from slightly under 200 to over 300 kN/mm as a function of frequency. As a function of displacement amplitude, the stiffness stays close to 200 kN/mm until approximately 1.25 mm of displacement amplitude when the stiffness increases sharply.

Calculated damping values vary greatly with respect to the frequency of the forcing function and displacement amplitude. The minimum damping appears to be approximately 5% at 5 and 9 Hz, and at 0.5 and 1.5 mm of displacement amplitude. At frequencies between 5 and 9 Hz, and displacement amplitudes between 0.5 and 1.5 mm, the damping ratio remains fairly constant at about 20%. Interpreting normalized displacement amplitudes using the half-power bandwidth approach yields damping rations of 25, 21 and 15% for the three pile cap displacement levels shown in Figure 7.7. These damping values are comparable to those reported by Runnels (2007) for similar test with loosely compacted silty sand at another site. His damping ratios varied between 20 and 30% at frequencies between 4 and 9 Hz.

7.6 Comparison of Static and Dynamic Cycle

Included in Figure 7.7 are displacement amplitude, stiffness and damping ratio calculated from the statically applied cycles from the actuators (~ ¾ Hz) at each represented displacement level (solid points). The values presented are averages of the previous and subsequent actuator cycles. An average value is used to represent stiffness

and damping that would have been calculated if the actuator cycles and been performed before the shaker cycles. The dynamic shaker loadings in the range of 7 to 9 Hz resulted in displacement amplitudes on the order of 1.4 mm which are comparable to those produced by the cyclic actuator loadings. Comparing the two test types at similar displacement amplitudes, the dynamic and static values for stiffness and damping ratio have a generally good agreement, being 150 kN/mm and 20% respectively. This similar amount of damping for different ranges of frequency suggests that dynamic loadings do not appreciably increase the apparent resistance of the pile cap relative to slowly applied cyclic loadings.

7.7 Pressure Cell Results

Figure 7.8 shows the pressure measured by the pressure cells with depth at the end of each static push increment. The profiles suggest the pressure is concentrated at a depth near 0.7 m. It is apparent that the measured pressure distribution does not match the normal representation of pressure increasing with depth. However, this may be in part a result of the relatively low pressures being measured and the soil mass being very far from a well defined, ultimate failure state. After the first several pushes, the bottom pressure cell shows a decrease in pressure with increasing displacement, just like what was observed in the case of the densely compacted sand backfill. Also the top pressure cell shows little to no increase in pressure after the third push increment.

Figure 7.9 shows the sum of pressure measured by the pressure cells compared to the backfill responses. This backfill force was calculated by multiplying each pressure by the respective contributory areas of the pile cap face. The pressure cells suggest that the

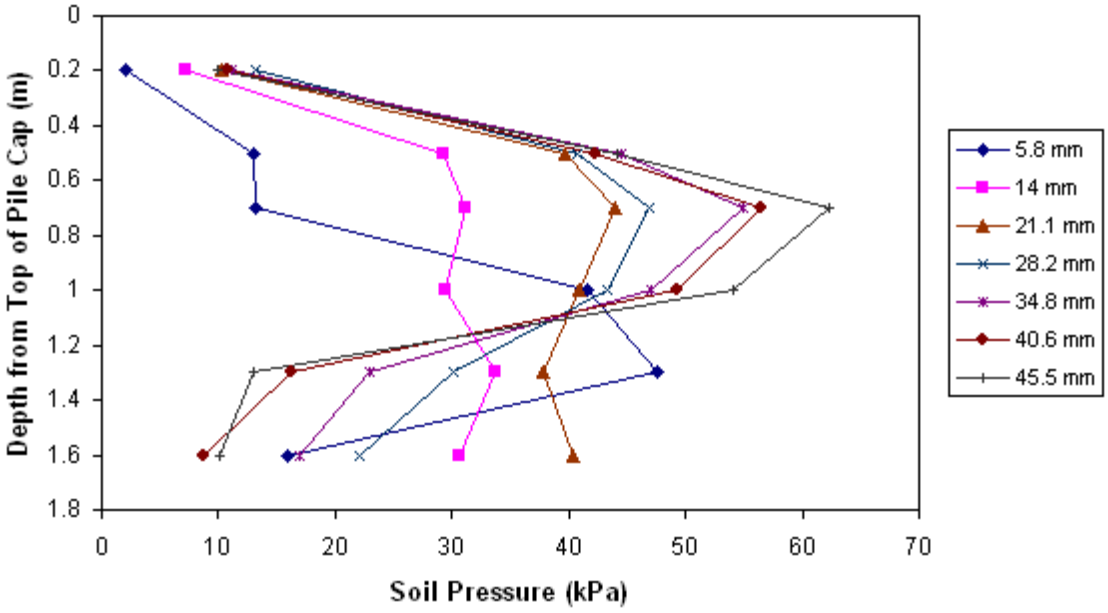

Figure 7.8 Measured pressure on pile cap face with depth at each push interval for loosely compacted sand backfill

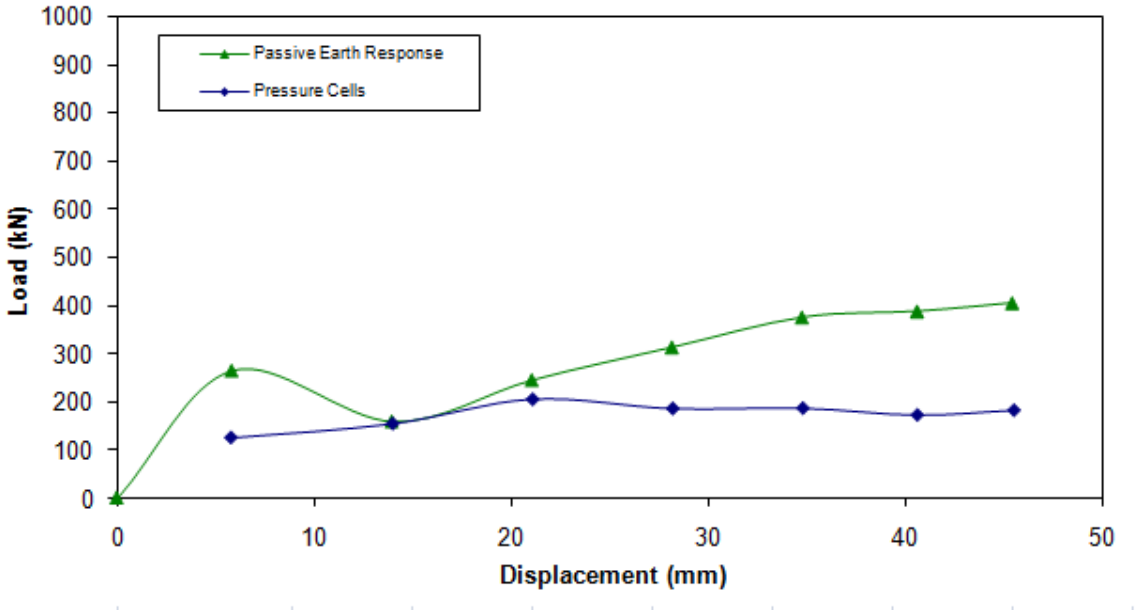

Figure 7.9 Comparison of pressure cell loads to passive earth loads for loosely compacted sand backfill

passive earth force is nearly a constant value of 170 kN with increasing cap displacement, which, like for the densely compacted sand, is consistently less than the earth pressure resistance determined from the applied actuator loading.

7.8 Crack and Elevation Change of Backfill

Figure 7.10 shows visible cracks mapped during the test at each pile cap displacement level. The location of cracks which formed in the backfill material could indicate the presence and location of failure surfaces in the material. The amount and location of cracking in the backfill material was somewhat unexpected and varies considerably from the cracking observed in the densely compacted sand backfill. A large number of cracks were formed during the first push and cycling phases with subsequent displacement intervals producing fewer cracks. These later cracks, however, occur further and further away from the pile cap face. Overall, the cracks form a radial pattern like stress bulbs coming from the face of the pile cap.

Figure 7.11 shows a contour plot of the change in elevation of the backfill material. The maximum elevation change is approximately -10-mm (the negative value representing a decrease or drop in elevation) near the face of the cap. During loading, it appears that the loosely compacted backfill material subsides as it is loaded, causing a decrease in elevation. Some of the previously discussed cracking (particularly near the cap face) looks to be associated with this subsidence and, as such, may not be associated with the development of a passive failure wedges (although those cracks occurring further away where there is little or no subsidence likely are).

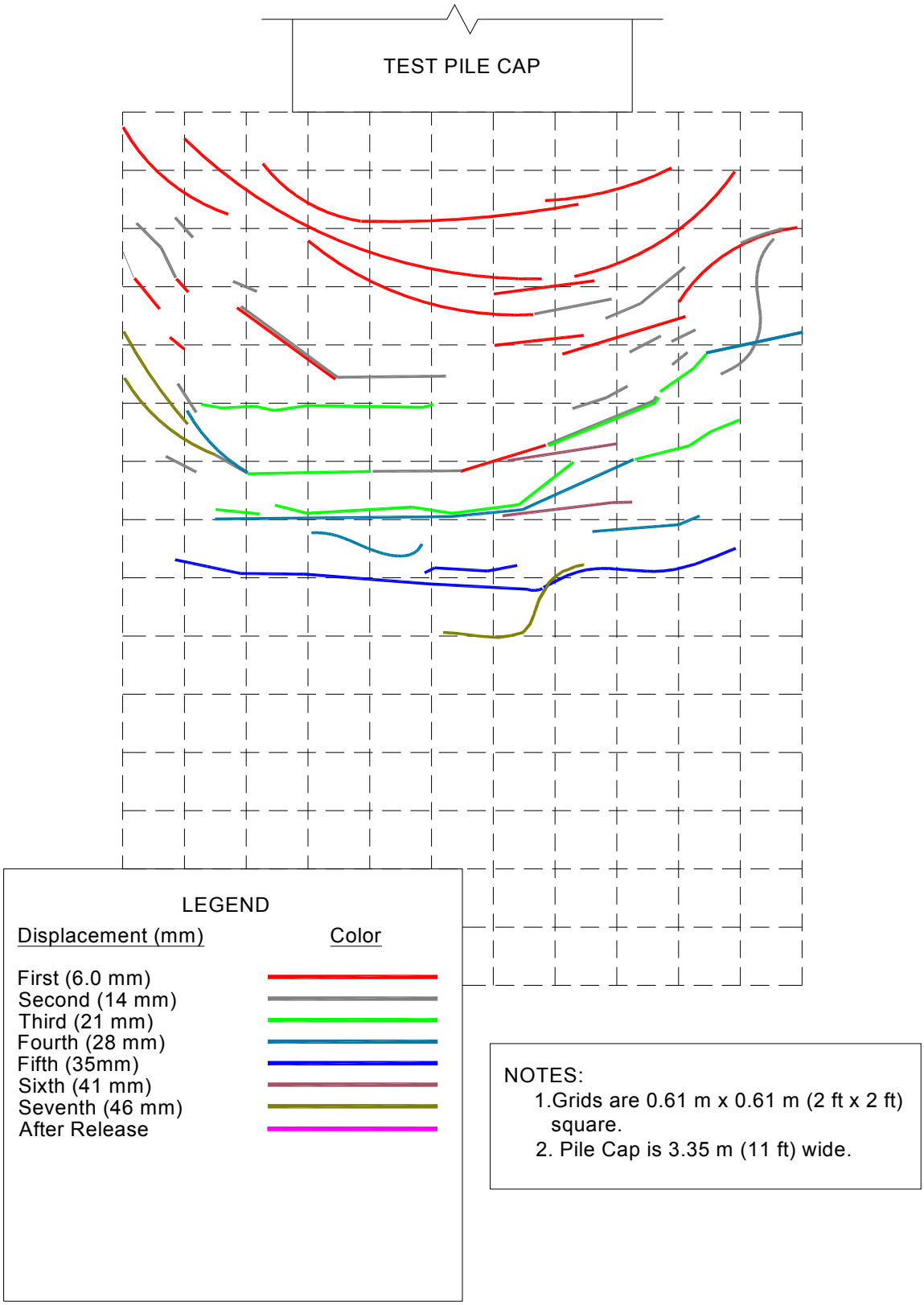

Figure 7.10 Observed cracks in loosely compacted sand backfill

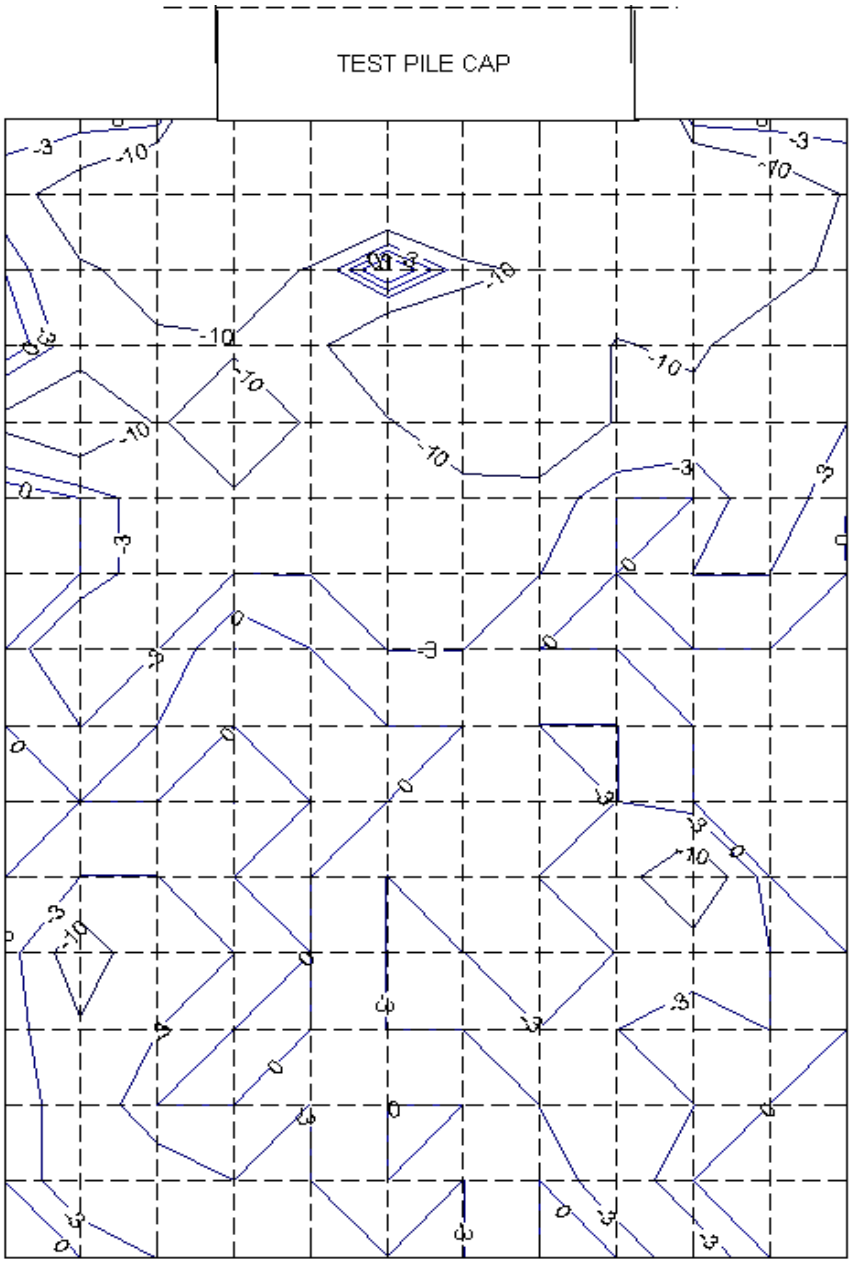

Figure 7.11 Contour plot of elevation change in loosely compacted sand backfill

Figure 7.12 shows a cross section of the pile cap and backfill zone together with the predicted log-spiral failure surface and the mean heave. The heave data has been multiplied by ten so that it can be seen relative to the geometry of the failure surface. The majority of settlement occurs within the first 1m of the backfill zone.

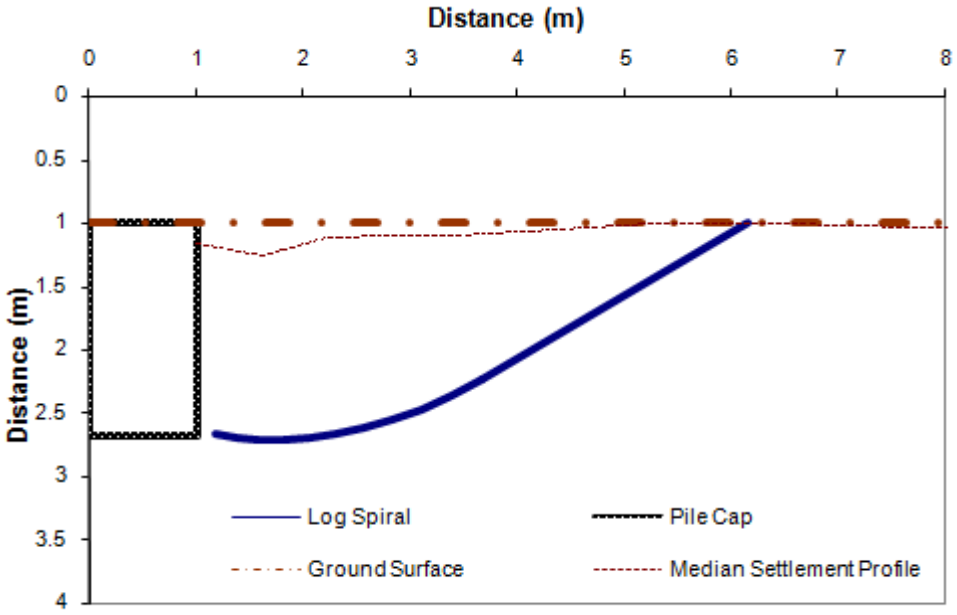

Figure 7.12 Cross section view of pile cap and loosely compacted clean sand backfill

7.9 Horizontal Movement of Backfill Soil

Figure 7.13 and Figure 7.14 show the surficial displacement of the backfill and associated calculated strain, respectively. The backfill displacement ranges from 46 mm at the cap face to 0 mm at 5.5 m from the cap face. The small negative values shown likely result due to the limited precision with which the data could be collected and processed; any tilting of the steel monitoring stakes or differential movement between

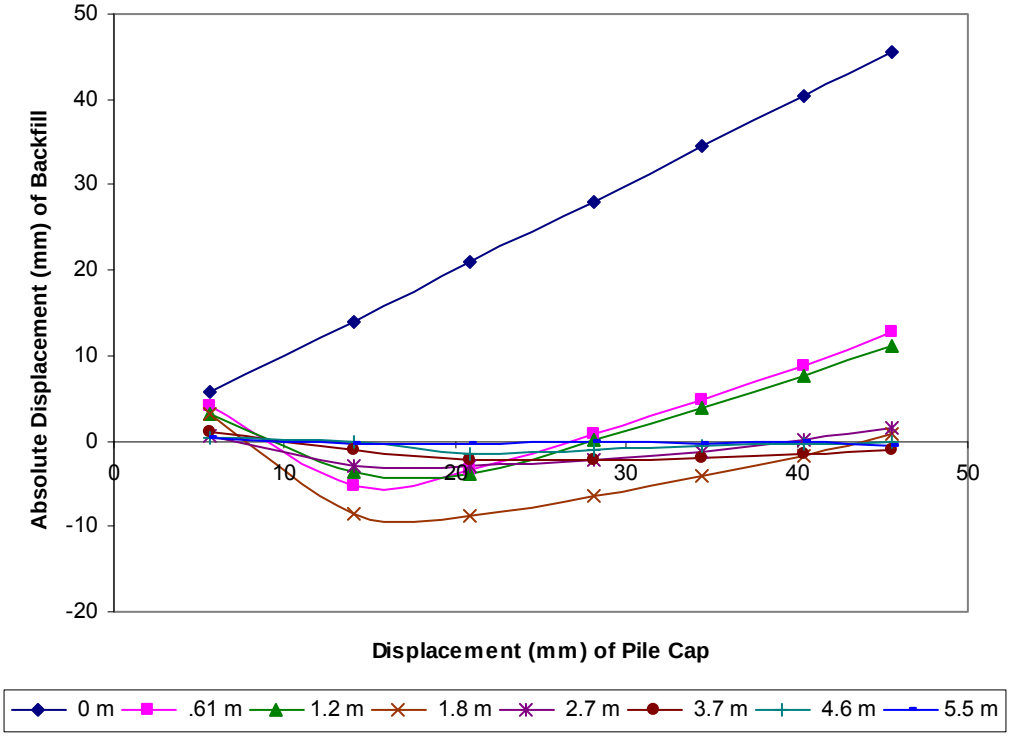

Figure 7.13 Displacement of monitoring points in loosely compacted sand backfill

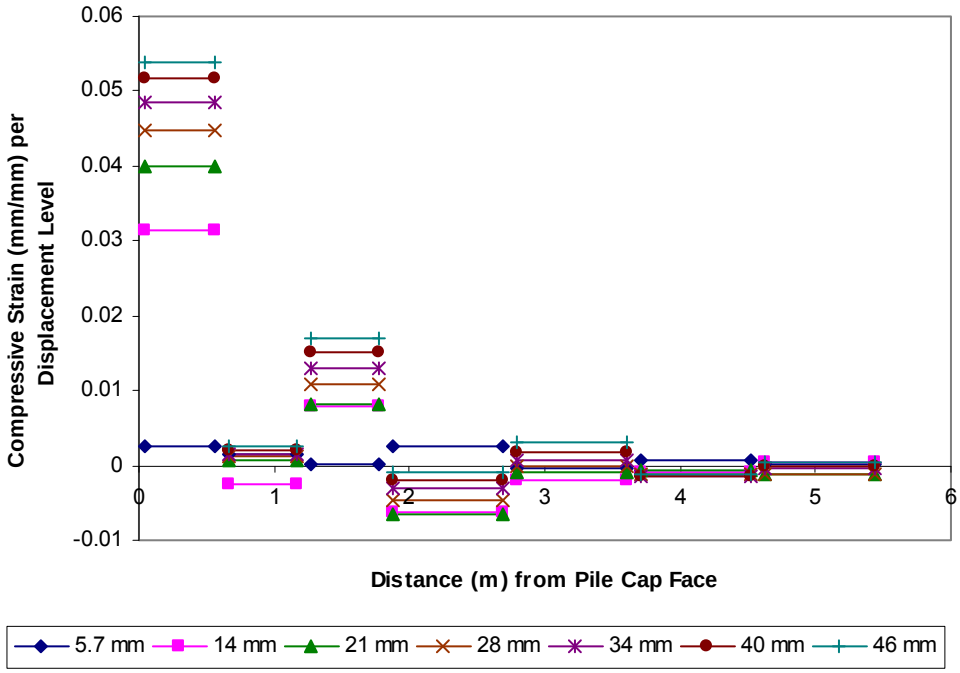

Figure 7.14 Strain per displacement level in loosely compacted sand backfill

the far ends of the pile cap along which the different string potentiometers were mounted would result in small errors in the data. The compressive strain ranges from 0.05 to 0.0 within the backfill zone. The displacement measurements and strain distributions correspond well with the heave patterns, with the majority of movement and therefore strain occurs within the first 2 m of the backfill zone (and the most occurring right at the face of the cap).

8 Comparison of Pile Cap Behaviors with Different Backfill Conditions

8.1 Introduction

This chapter compares the behaviors of the pile cap with the densely compacted and loosely compacted clean sand backfills. In most instances, the behavior of the pile cap with loosely compacted clean sand is relatively similar to that of the pile cap without any backfill present. Details of the individual tests have been presented in the previous chapters.

8.2 Load-Displacement Comparisons

Figure 8.1 shows load-displacement relationships for the pile cap with loosely and densely compacted clean sand backfill, both in terms of the total system load (resistance provided by piles and backfill) and the passive earth load (resistance provided by backfill only). The loosely compacted clean sand backfill had a total resistance of 1201 kN at a displacement of 46 mm while the densely compacted clean sand backfill had a total resistance of 2749 kN at the same displacement level. This is a 130% increase in load capacity due to the backfill sand being compacted into a denser state. In terms of passive earth loads, the loosely compacted clean sand backfill had a passive earth load of 405 kN at a displacement of 46 mm while the densely compacted clean sand backfill had

a passive earth force of 1954 kN at the same displacement level. This is a 380% increase in passive earth force load between the loosely and densely compacted states. This dramatic increase illustrates the significant effect of compaction on the resistance provided backfills, even between soils which are both compacted, but to different degrees (in this case 94% of standard proctor compared to 96% of modified proctor). Normalizing passive earth force by the equivalent plain-strain width of the foundation (which width is the product of the actual foundation width of 3.35 m and the three-dimensional factor), the densely compacted backfill provide a passive earth resistance of 328 kN per meter width for the 1.68 m high pile cap.

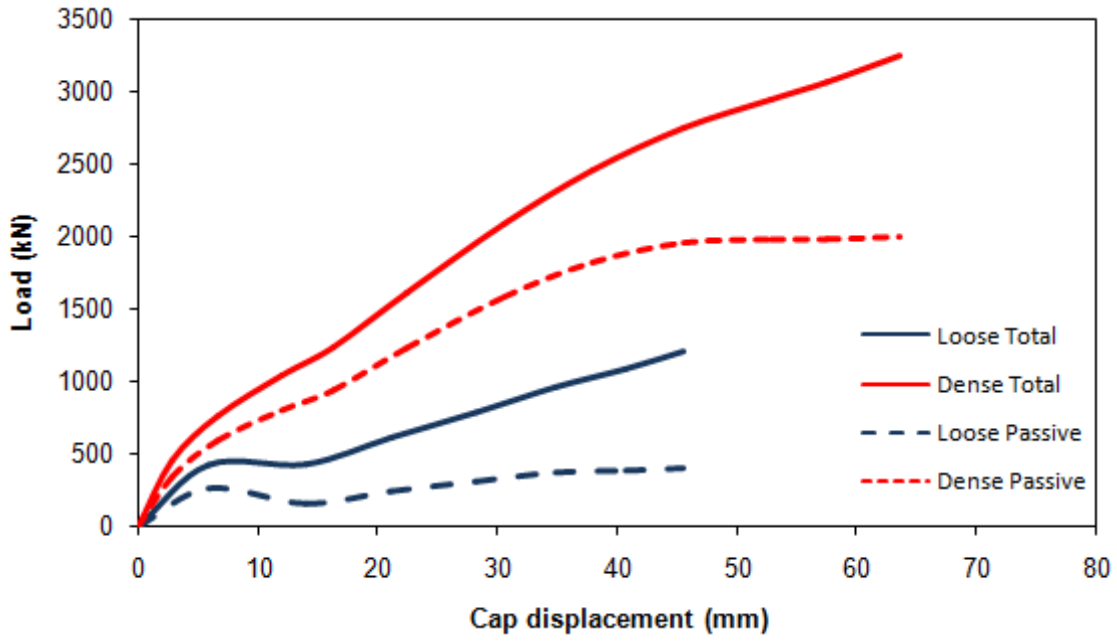

Figure 8.1 Comparison of total and passive earth forces as a function of displacement for the pile cap with densely and loosely compacted sand backfills

8.3 Static Actuator Cycle Comparison

Figure 8.2 shows a comparison of displacement amplitude, stiffness, and damping ratio from the static actuator load cycles for the pile cap without any backfill and with densely and loosely compacted clean sand backfills. Both compacted materials show a fairly consistent value of displacement amplitude with the looser sand being approximately 0.5 mm larger than the denser sand. In general, the stiffness of the pile cap with the densely compacted backfill is two to three times that of the cap with loosely compacted backfill, with the cap and looser sand exhibiting about 200 kN/mm of stiffness and the cap with denser sand exhibiting about 450 kN/mm of stiffness. Correspondingly, damping ratios decrease with increasing stiffness, both with respect to backfill type and pile cap displacement level. After about 20 mm of pile cap displacement, the average damping ratio is about 18% with the looser backfill and about 24% for the denser backfill. As expected, the pile cap without any backfill (the baseline test) shows the lowest stiffness and highest amount of damping.

8.4 Dynamic Shaker Cycle Comparison

Figure 8.3 shows a comparison of displacement amplitude, stiffness, and damping ratio from the dynamic shaker load cycles for the pile cap without any backfill and with densely and loosely compacted clean sand backfills. In looking at the graph of amplitude normalized by applied force, one can see that the damped natural frequency of the pile cap which occurs at the peak of each curve, shifts from around 6 Hz to around 8 Hz as the backfill is placed and is more densely compacted. This is consistent with the increases in stiffness also observed. The stiffness of the more densely compacted material appears to

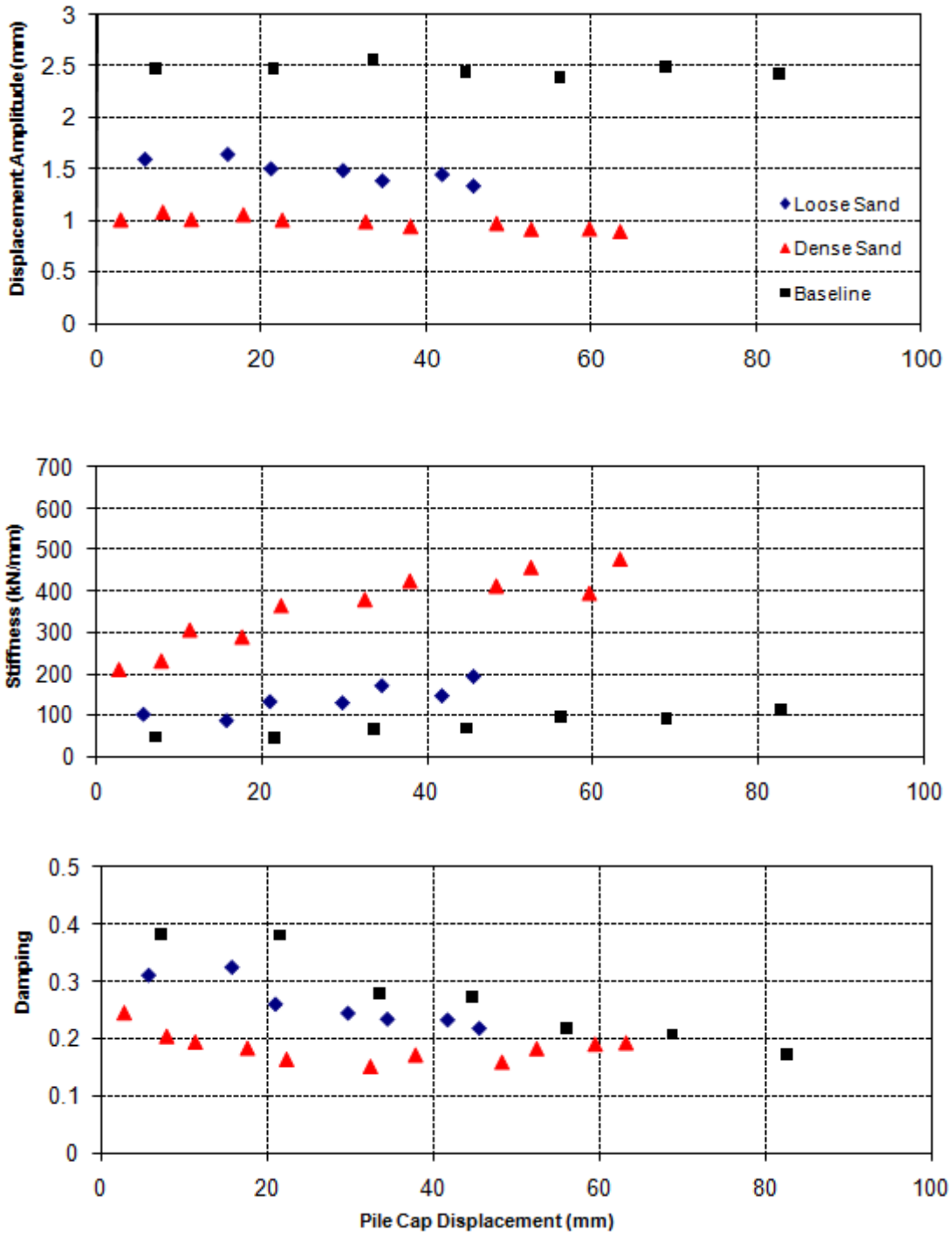

Figure 8.2 Comparison of displacement amplitude, stiffness, and damping ratio from static actuator load cycles for the pile cap without any backfill and with densely and loosely compacted sand backfills

be much more sensitive to the loading rate and/or displacement amplitude than for the other two backfill conditions. The dynamic loading stiffness of the pile cap with the densely compacted clean sand backfill is initially higher in the 4 to 6 Hz frequency range, after which point it decreases, reaching a value of 300 kN/mm at a frequency of 10 Hz and displacement amplitude of 1 mm. On the other hand, the stiffness of the pile cap with loosely compacted clean sand backfill is generally about 200 kN/mm (which is about twice that of the pile cap without backfill), but stiffness increases to nearly that of the pile cap with the denser backfill at a frequency of 10 Hz and displacement amplitude of 1 mm. This suggests that under certain frequencies of dynamic loading, the density of the backfill is not extremely important relative to the passive resistance of the pile cap. This behavior is likely attributable to the backfill responding out of phase with the pile cap. The damping ratios computed from the dynamic load-displacement loops are quite variable and appear to vary with frequency. Damping ratios appear to peak in the vicinity of the natural frequency of the pile cap system for each backfill condition. On the whole, damping ratios tend to range between 10 and 30%, with an average of about 20% for the range of frequencies and displacement amplitudes occurring during the tests.

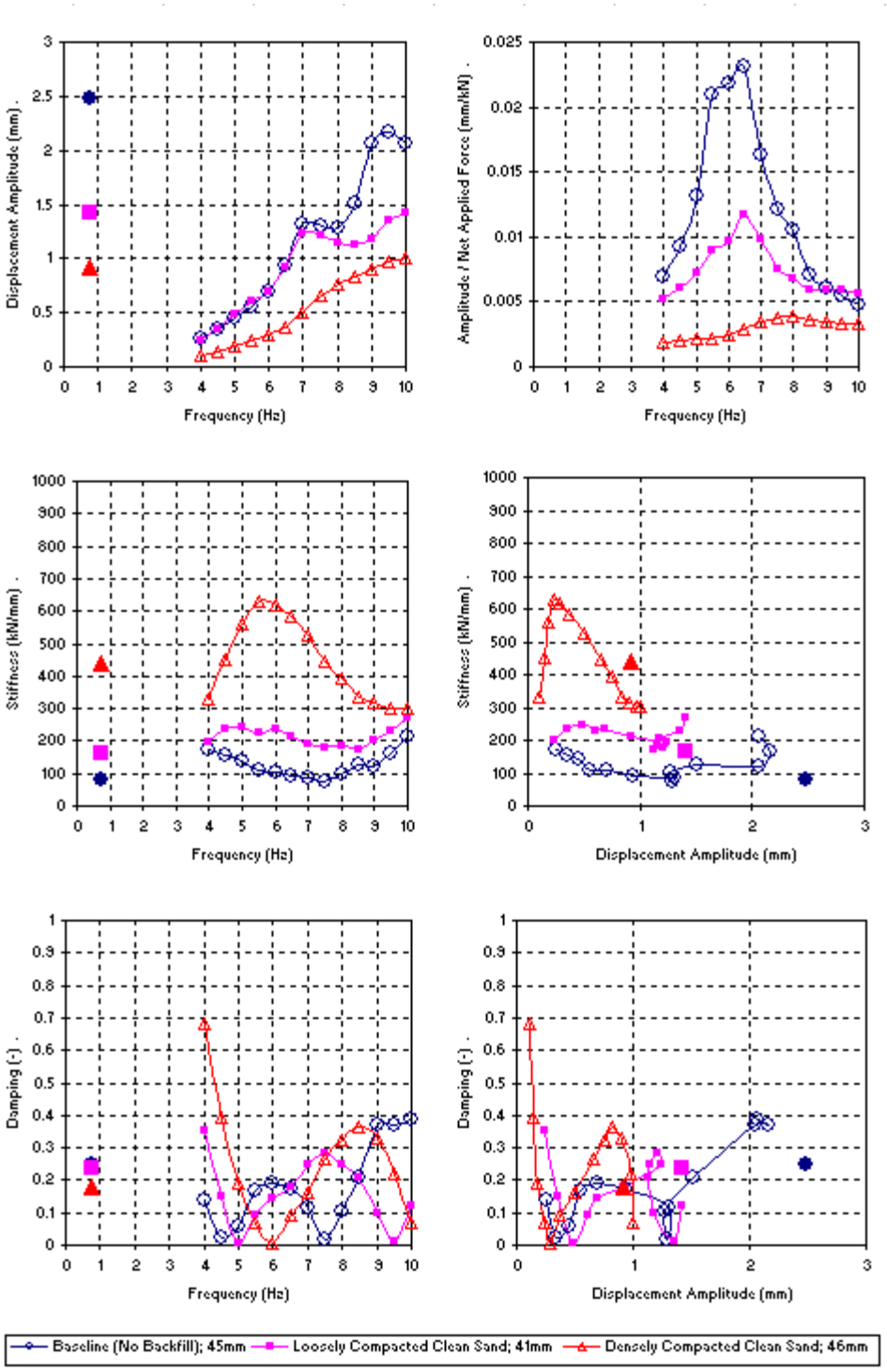

Figure 8.3 Comparison of displacement amplitude, stiffness, and damping ratio from dynamic shaker load cycles for the pile cap without any backfill and with densely and loosely compacted sand backfills

9 Conclusion

This thesis presents results from lateral load tests performed on a full-scale pile cap with three different backfill conditions, namely: with no backfill present, with densely compacted clean sand in place, and with loosely compacted clean sand in place. In addition to being displaced under static loading, the pile cap was subjected to low frequency, small displacement loading cycles and higher frequency, small displacement, dynamic loading cycles. This thesis also presents the analysis and interpretation of the test data. Based on this work, the following conclusions are drawn and recommendation made.

1. The passive earth pressure from the backfill significantly increased the load capacity of the pile cap. At maximum passive earth pressure, the densely compacted backfill accounts for approximately 67% of the total load capacity of the pile cap system.
2. At a displacement of about 46 mm, the loosely and densely compacted backfills increased the capacity of the total resistance of the pile cap otherwise without backfill by 50% and 245%, respectively.
3. The maximum passive earth pressure for the densely compacted backfill occurred at a displacement of approximately 50 mm, which corresponds to a displacement to pile cap height ratio about 0.03. The more poorly defined

peak resistance for the loosely compacted backfill was achieved at displacement of approximately 40 mm.

4. Load-displacement curves calculated using the log-spiral method for determining passive earth pressure coefficients together with three-dimensional loading adjustment factors have good agreement with the measured load-displacement response of the densely compacted backfill.
5. Load-displacement curves calculated using the log-spiral method for determining passive earth pressure coefficients together with three-dimensional loading adjustment factors have poor agreement with the measured load-displacement response of the loosely compacted backfill, using calculated strength parameters.
6. Under low frequency cyclic loadings, the stiffness of the pile cap system increases with the presence of the backfill material. The loosely compacted backfill generally provided double the stiffness of the no backfill case. The densely compacted backfill generally provided double the stiffness of the loosely compacted sand, thus quadrupling the stiffness of the pile cap relative to the case with no backfill present.
7. Under low frequency cyclic loadings, the damping ratio of the pile cap system decreases with cap displacement and with increasing stiffness of backfill material. After about 20 mm of pile cap displacement, the average damping ratio is about 18% with the denser backfill and about 24% for the looser backfill.

8. Under higher frequency cyclic loadings, the stiffness of the pile cap system increases with the presence of the backfill material. The loosely compacted backfill generally provided double the stiffness of the no backfill case. The densely compacted backfill generally provided double the stiffness of the loosely compacted sand, thus quadrupling the stiffness of the pile cap relative to the case with no backfill present.
9. Under higher frequency cyclic loadings, the damping ratio of the pile cap system is quite variable and appears to vary with frequency. Damping ratios appear to peak in the vicinity of the natural frequency of the pile cap system for each backfill condition. On the whole, damping ratios tend to range between 10 and 30%, with an average of about 20% for the range of frequencies and displacement amplitudes occurring during the tests.
10. Comparing stiffness and damping values computed at similar displacement amplitudes for low frequency (~ 0.75 Hz) and higher frequencies (4 to 10 Hz), the dynamic and static values for stiffness and damping ratio have a generally good agreement for the densely compacted backfill, being approximately 150 kN/mm and 20% respectively. This similar amount of damping for different ranges of frequency suggests that dynamic loadings do not appreciably increase the apparent resistance of the pile cap relative to slowly applied cyclic loadings.
11. Measured earth pressure distributions generally increased with depth, except near the bottom of the pile cap. Earth pressure forces, and more particularly the trends in earth pressure forces versus displacement, calculated from these

pressure distributions and adjusted for three-dimensional loading effects are somewhat similar with the passive earth forces calculated from the actuator forces.

12. For the densely compacted backfill, the observed pattern of heave, strain and cracking in the backfill seem to correspond well with each other and the calculated log-spiral failure surface. For the loosely compacted backfill, the observed pattern of settlement, strain, and cracking in the backfill seem to be consistent with the development of resistance due to progressive densification of the backfill with pile cap displacement rather than a well defined log-spiral failure surface.

References

Caltrans (2004). "Seismic design criteria, version 1.3." California Department of Transportation , Sacramento, California.

Christensen, D.S. (2006). "Full scale static lateral load test of a 9 pile group in sand," Thesis (M.S.), Brigham Young University, Department of Civil and Environmental Engineering, Provo, Utah.

Clough, G.W. and Duncan, J.M. (1991). Earth retaining structures, *In Foundation engineering handbook*. 2nd ed. *Edited by* H.Y. Fang. Van Nostrand Reinholdt, New York

Cole, R.T. (2003). "Full-scale effects of passive earth pressure on the lateral resistance of pile caps." Doctor of Philosophy Dissertation, Brigham Young University, Department of Civil and Environmental Engineering, Provo, Utah.

Cole, R.T. and Rollins, K.M. (2006). "Passive earth pressure mobilization during cyclic loading." Journal of Geotechnical and Geoenviromental Engineering, ASCE, Vol. 132, No. 9, pp. 1154-1164.

Dobry, R. and Gazetas, G. (1985). "Dynamic Stiffness and Damping of Foundations by Simple Methods." *Vibration Problems in Geotechnical Engineering*. Symposium proceedings, October 22, 1985.

Douglas, D. J. and Davis, E. H. (1964). "The movements of buried footings due to moment and horizontal load and the movement of anchor plates." Geotechnique, London, 14(2), 115–132.

Duncan, J. M., and Mokwa, R. L. (2001). "Passive earth pressures: theories and tests." Journal of Geotechnical and Geoenviromental Engineering, ASCE Vol. 127, No. 3, pp. 248-257.

Maroney, B.H. (1995). "Large scale bridge abutment tests to determine stiffness and ultimate strength under seismic loading," Ph.D. Dissertation, University of California, Davis

Mokwa, R. L. and, Duncan, J. M. (2001). "Experimental evaluation of lateral-load resistance of pile caps." Journal of Geotechnical and Geoenviromental Engineering, ASCE Vol. 127, No. 2, pp. 185-192.

Peterson, K.T. (1996). "Static and dynamic lateral load testing a full-scale pile group in clay," Thesis (M.S.), Brigham Young University, Department of Civil and Environmental Engineering, Provo, Utah.

Rollins, K.M. and Cole, R.T. (2006). "Cyclic lateral load behavior of a pile cap and backfill." Journal of Geotechnical and Geoenviromental Engineering, ASCE, Vol. 132, No. 9, pp. 1143-1153.

Runnels, I.K. (2007). "Cyclic and dynamic full-scale testing of a pile cap with loose silty sand backfill." Thesis (M.S.), Brigham Young University, Department of Civil and Environmental Engineering, Provo, Utah.

Shamshabadi, A., Rollins, K.M., Kapaskur, M. (2007). "Nonlinear soil-abutment-bridge structure interaction for seismic performance-based design." Journal of Geotechnical and Geoenviromental Engineering., ASCE, Vol. 133 (6), 707-720.

Valentine, T.J. (2007). "Dynamic testing of a full-scale cap with dense silty sand backfill." Thesis (M.S.), Brigham Young University, Department of Civil and Environmental Engineering, Provo, Utah.

Walsh, J. M. (2005). "Full-scale lateral load tests of a 3x5 pile group in sand," Thesis (M.S.), Brigham Young University, Department of Civil and Environmental Engineering, Provo, Utah.